Combinatorial and High-Throughput Screening of Materials Libraries: Review of State of the Art

Radislav Potyrailo*

Chemistry and Chemical Engineering, GE Global Research Center, Niskayuna, New York 12309, United States

Krishna Rajan

Department of Materials Science and Engineering and Institute for Combinatorial Discovery, Iowa State University, Ames, Iowa 50011, United States

Klaus Stoewe

Universität des Saarlandes, Technische Chemie, Campus C4.2, 66123, Saarbruecken, Germany

Ichiro Takeuchi

Department of Materials Science and Engineering, University of Maryland, College Park, Maryland 20742, United States
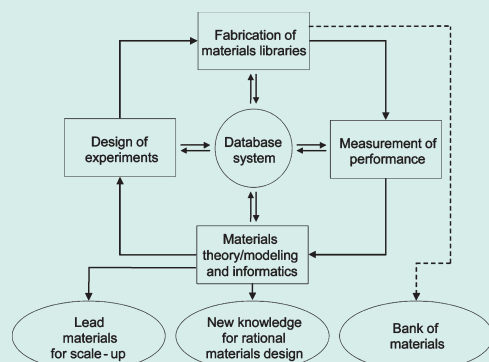
Bret Chisholm

Center for Nanoscale Science and Engineering and Department of Coatings and Polymeric Materials, North Dakota State University, Fargo, North Dakota 58102, United States

Hubert Lam

Chemistry and Chemical Engineering, GE Global Research Center, Niskayuna, New York 12309, United States

ABSTRACT: Rational materials design based on prior knowledge is attractive because it promises to avoid time-consuming synthesis and testing of numerous materials candidates. However with the increase of complexity of materials, the scientific ability for the rational materials design becomes progressively limited. As a result of this complexity, combinatorial and high-throughput (CHT) experimentation in materials science has been recognized as a new scientific approach to generate new knowledge. This review demonstrates the broad applicability of CHT experimentation technologies in discovery and optimization of new materials. We discuss general principles of CHT materials screening, followed by the detailed discussion of high-throughput materials characterization approaches, advances in data analysis/mining, and new materials developments facilitated by CHT experimentation. We critically analyze results of materials development in the areas most impacted by the CHT approaches, such as catalysis, electronic and functional materials, polymer-based industrial coatings, sensing materials, and biomaterials.

KEYWORDS: materials science, combinatorial and high-throughput (CHT) experimentation, electronic and functional materials, polymer-based industrial coatings, sensing materials, biomaterials

■ CONTENTS

1. INTRODUCTION

Rational design and optimization of materials based on prior knowledge is a very attractive approach because it could avoid time-consuming synthesis and testing of numerous materials candidates. However, to be quantitatively successful, rational design requires detailed knowledge regarding relation of intrinsic properties of materials to a set of their performance properties.

This knowledge is typically obtained from extensive experimental and simulation data. However, with the increase of structural and functional complexity of materials, the ability to rationally define the precise requirements that result in a desired set of performance properties becomes increasingly limited.[1] Thus, in addition to limited examples of rational materials design, a variety of materials have been discovered using detailed experimental observations or simply by chance, reflecting a general situation in materials design that is "still too dependent on serendipity".[2,3]

In materials science, the materials properties depend not only on composition, but also on morphology, microstructure, and other parameters that are related to the material-preparation conditions. As a result of this complexity, combinatorial and high-throughput (CHT) experimentation in materials science has been recognized as a new scientific approach to generate significant new knowledge as summarized in recent reviews and books.[4−20]

This review demonstrates the broad applicability of CHT experimentation technologies in discovery and optimization of new materials. We discuss general principles of CHT materials screening, followed by the discussion of the opportunities and new materials developments facilitated by CHT experimentation. We critically analyze results of materials development in the areas most impacted by the CHT approaches, such as catalysis, electronic and functional materials, polymer-based industrial coatings, sensing materials, and biomaterials.

2. GENERAL PRINCIPLES

Combinatorial or high-throughput materials screening is a process that couples the capability for parallel production of large arrays of diverse materials together with different high-throughput measurement techniques for various intrinsic and performance properties followed by the navigation in the collected data for identifying "lead" materials.[4,11,15,21−26] The terms "combinatorial materials screening" and "high-throughput experimentation" are typically interchangeably applied for all types of automated parallel and rapid sequential evaluation processes of materials and process parameters that include truly combinatorial permutations or their selected subsets.

Individual aspects of accelerated materials development have been known for decades. These aspects include combinatorial and factorial experimental designs,[27] parallel synthesis of materials on a single substrate,[28,29] screening of materials for performance properties,[9] and computer data processing.[30,31] In 1970, an integrated materials-development workflow was introduced by Hanak[32] with four key aspects that included (1) complete compositional mapping of a multicomponent system in one experiment, (2) simple rapid nondestructive all-inclusive chemical analysis, (3) testing of properties by a scanning device, and (4) computer data processing. Hanak was truly ahead of his time and "it took 25 years for the world to realize his idea".[21] In 1995, applications of combinatorial methodologies in materials science were reinitiated by Xiang, Schultz, and co-workers.[33] Since then, combinatorial tools have been employed to discover and optimize a wide variety of materials (see Table 1).

A typical combinatorial materials development cycle is outlined in Figure 1. Compared to the initial idea of Hanak[32] (see Figure 1A), the modern workflow (Figure 1B) has several new important aspects, such as design/planning of experiments, materials theory/modeling and informatics, and scale up. In CHT screening of materials, concepts originally thought as

Table 1. Examples of Materials Explored Using Combinatorial and High-Throughput Experimentation Techniques

materials examples	ref	materials examples	ref
superconductor materials	33	zeolites	473
ferroelectric materials	474	polymers	475
magnetoresistive materials	476	metal alloys	477
luminescent materials	478	materials for methanol fuel cells	479
structural materials	480	materials for solid oxide fuel cells	481
hydrogen storage materials	482	materials for solar cells	483
organic light-emitting materials	484	automotive coatings	247
ferromagnetic shape-memory alloys	485	waterborne coatings	486
thermoelastic shape-memory alloys	487	vapor−barrier coatings	269
heterogeneous catalysts	488	marine coatings	263
homogeneous catalysts	489	fouling-release coatings	490
polymerization catalysts	491	organic dyes	492
electrochemical catalysts	164	polymeric sensing materials	389
electrocatalysts for hydrogen evolution	493	metal oxide sensing materials	494
fuel cell anode catalysts	495	formulated sensing materials	332
enantioselective catalysts	496	agricultural materials	497

highly automated, have been recently refined to have more human input, with only an appropriate level of automation. For the throughput of 50−100 materials formulations per day, it is acceptable to perform certain aspects of the process manually.[34,35] While it is attractive to produce multiple small-scale samples of materials at once using combinatorial tools, it is important to validate the performance of the combinatorial system by reproducing materials with good performance in laboratory scale synthesis and performance testing under conventional test conditions. In a reliable combinatorial workflow, relative materials performances correlate well with those reproduced by traditional scale fabrication and testing. Thus, a correlation between performance of materials fabricated on the traditional and combinatorial scales is established using known materials.

2.1. Experimental Planning. Searching for "a needle in the haystack" has been popular in the early days of combinatorial materials science.[4,36,37] It was estimated that 2^{86} of chemical systems needed to be potentially investigated for their new materials properties (see Figure 2A) however with only the unary and binary chemical systems investigated so far.[38] Taking into the account not only the properties of starting materials but also the needed variable levels of process conditions, rapidly brings the number of experimental runs in CHT screening of simple catalytic materials up to several million (see Figure 2B).[39] It was also shown that a theoretical dimensionality of the hyperspace of independent materials response features could be 10^{21} by including the permutations of varying materials, measurement principles, and modes of operation for each material/measurement combination in chemical sensors (see Figure 2C).[40]

It was realized further that screening of the whole materials and process parameters space is still too costly and time prohibitive even with the availability of existing tools.[38] Instead, designing the CHT experiments to discover relevant descriptors
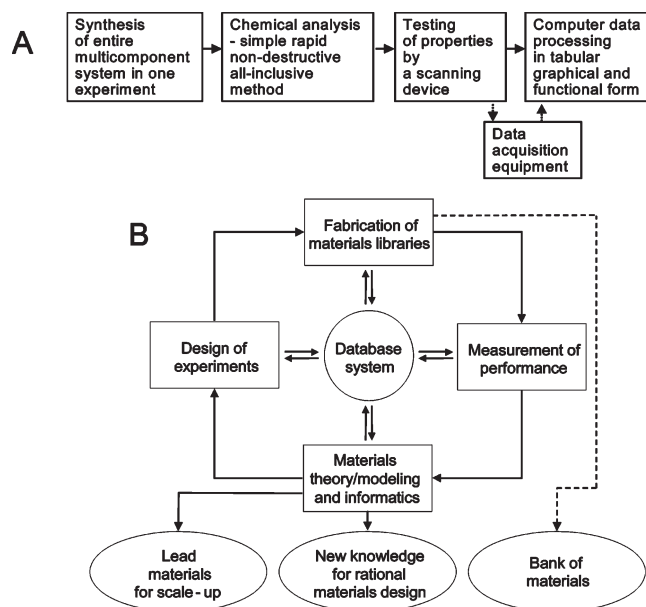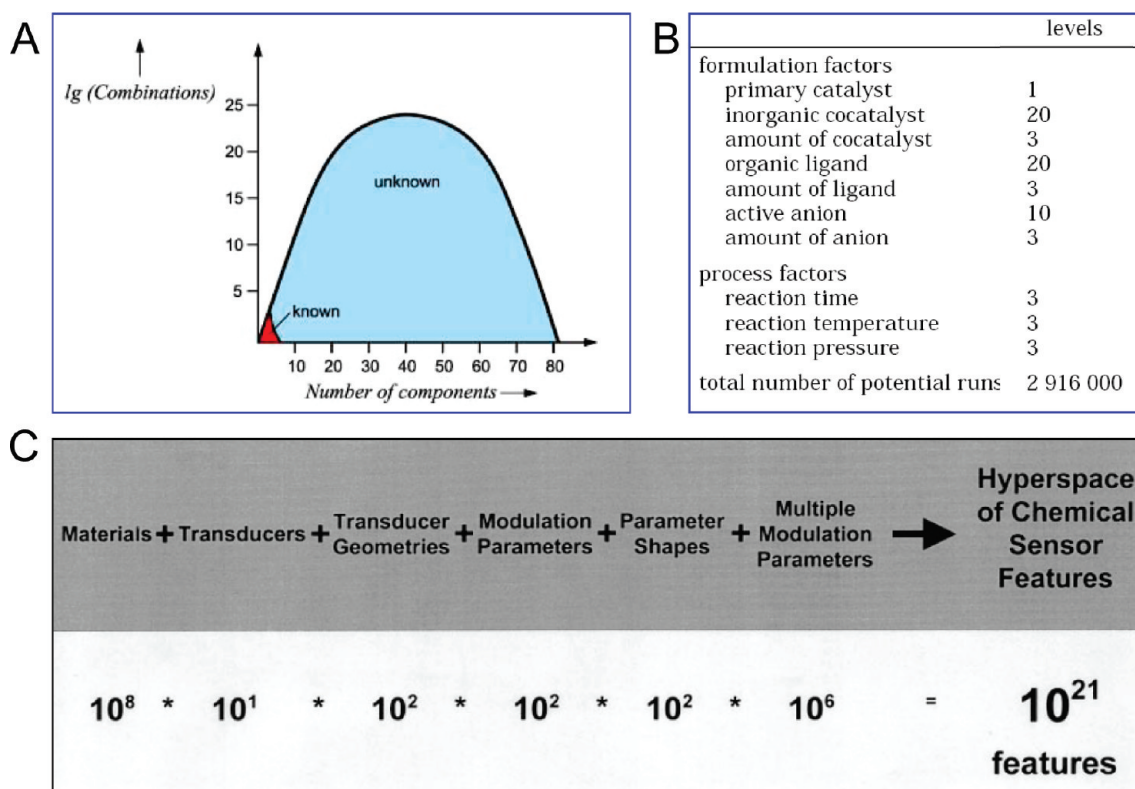

Figure 1. Concepts of the combinatorial materials-development workflow. (A) Initial concept proposed by Hanak in 1970.[32] (B) Modern "combinatorial materials cycle".[19]

became more attractive.[37] At present, methods for CHT experiment planning can be summarized as four general classes that include (1) traditional statistical design-of-experiments approaches, such as factorial or fractional factorial designs that are intended to generate statistically reliable conclusions from a limited number of experiments; (2) "diversity" methods to cover a space of interest using various measures to characterize ensembles of experimental samples; (3) "search" methods to intelligently navigate through the experiment space in a succession of experiments; and (4) hierarchical or hybrid methods to develop a series of experiments with increasing focus.[41−45]

2.2. Materials Synthesis. Specific aspects of CHT techniques for the synthesis, formulation, and preparation of materials are provided in respective sections 3.1−3.5.

2.3. Materials Characterization. To address quantitation needs of numerous materials-specific intrinsic and performance properties, a variety of high-throughput characterization tools are required for rapid and automated assessment of single or multiple properties of the large number of samples fabricated together as a combinatorial array or "library".[24,46,47] Typical library layouts can be discrete[27,29,33] and gradient.[28,32,48−52] A specific type of library layout will depend on the required density of space to be explored, available library-fabrication capabilities, and capabilities of high-throughput characterization tools.

As indicated in *Technology Roadmap for Combinatorial Methods, Vision 2020*,[53] an integration of analytical equipment with the combinatorial reactors is of critical importance for characterization of combinatorial libraries. Thus, significant part of research efforts in the area of CHT materials science has been dedicated to the development of methods for in situ quantitative monitoring of combinatorial reactions in both discovery and optimization phases. In situ monitoring of combinatorial reactions provides several attractive options for high-throughput screening. Real-time observation of the reaction progress in combinatorial reactors can tremendously speed up the materials discovery process by providing previously unavailable information about

A

lg (Combinations)

unknown

known

Number of components →

B

	levels
formulation factors	
primary catalyst	1
inorganic cocatalyst	20
amount of cocatalyst	3
organic ligand	20
amount of ligand	3
active anion	10
amount of anion	3
process factors	
reaction time	3
reaction temperature	3
reaction pressure	3
total number of potential runs	2 916 000

C

Materials + Transducers + Transducer Geometries + Modulation Parameters + Parameter Shapes + Multiple Modulation Parameters → Hyperspace of Chemical Sensor Features

10^8 * 10^1 * 10^2 * 10^2 * 10^2 * 10^6 = 10^{21} features

Figure 2. Examples of diversity of materials compositions, process factors, and operation conditions applicable for combinatorial screening. (A) Dependence of the number of possible systems on the number of components. Red: systems investigated up to now.[38] (B) Factors and their levels for one-step synthesis of diphenylcarbonate.[39] (C) Hyperspace of features of materials and measurements in chemical sensors.[40]

the starting reaction components evolving into the reaction and the dynamics of progress of multiple reactions at once at each reaction phase. Monitoring of reaction components can provide valuable feedback information to control and rapidly optimize reaction parameters. Overall, in situ monitoring of combinatorial reactions includes all of the attractive features of in-line detection methods, such as automation, no sample removal or preparation steps and, thus, reduced number of contamination sources. It has been statistically demonstrated that in situ measurement systems, in principle, are capable of making quality determinations to a substantially higher order of precision than the traditional off-line laboratory systems.[54–56]

Optical, chromatographic, electrochemical, and mass-spectrometric techniques are evolving as the most widely used analytical methodologies for direct in situ monitoring and optimization of combinatorial reactions.[57–61] A representative list of applications of analytical techniques recently reported for the in situ monitoring of combinatorial reactions and processes is compiled in Table 2.

When an analytical instrument collects quantitative data from a combinatorial experiment, the accuracy of determinations often depends on the ability to provide an interference-free response. The interferences can arise from a variety of sources and can include chemical and environmental interferences. The ability to provide accurate quantitative data improves with the increase of the information content or dimensionality of the collected data per combinatorial sample. Analytical instruments can be classified according to the dimensionality of data that they provide such as zero-, first-, second-, and higher order instruments. Such classification of analytical instruments is well accepted[62] and can

be applied for description of capabilities of instruments for real time monitoring and optimization of combinatorial reactions. The classification principles are illustrated in Figure 3. A measurement system that generates a single data point per combinatorial sample is a zero-order instrument (see Figure 3A). First-order measurement systems generate a string of multiple measurements per combinatorial sample (see Figure 3B). Measurements provided by the first-order measurement system are of the same nature, for example, temporal, spectral, or sensor array responses. Second-order measurement systems generate a matrix of an instrument response upon the change of two independent types of variables per sample (see Figure 3C). Depending on the particular need in the combinatorial screening, higher-order measurement systems are also possible.[63]

Examples of performance of zero-, first-, and second-order instruments in combinatorial screening of materials are presented in Figure 4. A zero-order measurement approach is illustrated in Figure 4A and B where abrasion resistance of organic protective coatings was determined from measurements of scattered light from each coating in a 48-element array.[34] A simple zero-order measurement approach was useful because it provided the required information about the end-use performance of the protective coatings after an abrasion test (see Figure 4A). Measurements of the abrasion-induced increase in the amount of light scatter were performed at a single wavelength as shown in Figure 4B. A single-wavelength measurement was adequate for the correlation between the high-throughput and traditional evaluation of abrasion resistance of coatings.[34]

A first-order measurement approach is illustrated in Figure 4C and D where measurements of fluorescence spectra of solid

Table 2. Selected Examples of Real-Time Monitoring of Combinatorial Reactions: Instrumentation and New Knowledge

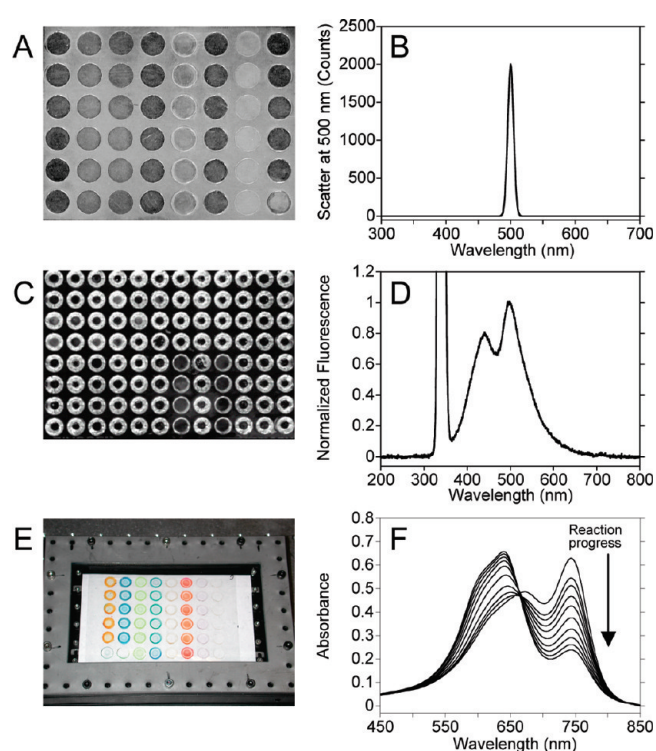| materials system	instrumentation	knowledge	ref
solid-phase synthesis of trisubstituted amines	five-step reaction sequence on resin is followed the reaction step-by-step using the sequence of five analytical tools as a function of experiment time: single bead IR, ^{1}H MAS NMR, 2D MAS COSY, MAS HMQC, ^{13}C MAS NMR	generation of a protocol of analytical tools that allows a chemist to decisively evaluate synthetic steps, verify new building blocks, and detect possible side reactions prior to or during actual library construction	498
metal alloys catalyst candidates	serial MS screening of a $15 \times 15 \times 15$ libraries with 120 different compositions	kinetics of catalytic reactions	499
96-capillary array for palladium-catalyzed annulation	nonaqueous multiplexed capillary electrophoresis	rapid determination of catalytic activity, selectivity and kinetics of the various combinations	59
solid-phase organic synthesis products	single-bead FTIR	reaction kinetics, conversion yield	93
resin-bead supported combinatorial libraries	hyperspectral IR imaging for monitoring of catalytic reactions with the screening time independent of the number of elements in the library	kinetics of catalytic reactions	500
solid-phase peptide synthesis products	near-IR multispectral imaging based on scanning acousto-optic tunable filter	simultaneous determination of kinetics of multiple reactions	501
catalytic dehydrogenation of cyclohexane to benzene	resonance-enhanced multiphoton ionization for low parts per billion and high parts per trillion detection capability	determination of activities of catalyst sites by monitoring of a single reaction product; possibility for monitoring of multiple reaction products to determine catalyst selectivity	502
amorphous microporous mixed oxide catalysts	IR thermography for gas-phase screening of catalyst candidates (sample size 200 μg)	kinetics of catalytic reactions	488
bead-bound catalysts	IR thermography for solution-phase screening of 3150 potential catalysts bound to 300—500 μm diameter polymer beads	kinetics of catalytic reactions	503
styrene-polymerization catalysis	IR thermographic imaging of organometallic catalysts	reaction kinetics from the time dependence of the heat generation	504
catalytic activity of V_2O_5 in oxidation of naphthalene to naphthoquinone by O_2	fluorescence and thermographic imaging for monitoring of catalytic reactions	determination of nonspecific temperature increase by thermography and species-specific concentration maps by fluorescence	505
48 element array of epoxy formulations	automated large sample array differential scanning calorimeter for process optimization for screening studies of multivariable arrays	cure kinetics	506
discrete array of inorganic oxide films	pulsed laser deposition with in situ monitoring of growth surface with reflection high energy electron diffraction (RHEED).	one-lot optimization of epitaxial growth process by using a carrousel type masking plate. Variable growth conditions include pressure, temperature, laser energy and laser repetition rate	507
electrochemical catalysts	fluorescence imaging of catalysts for oxidation of methanol using a pH indicator in discovery and focus libraries	kinetics of catalytic reactions	164
catalytic hydrogen-producing materials	near-IR reflection sensor array for 2-D mapping of H_2 from catalytic hydrogen-producing materials	kinetics of catalytic reactions	508
organic coating formulations	optimization of processing conditions (curing parameters) in fabrication of UV-cured automotive organic protective coatings. Fluorescence of a viscosity-sensitive molecular probe monitored during curing of coatings.	rapid decoupling of temperature and radiation effects in curing of UV curable coating formulations by using multiple coatings and process conditions at once	509
chemical and biochemical catalysts	96-thermistor array for detection of temperature changes with a 0.1 mK resolution	correlation of catalysts concentration and time-dependent recorded maximum temperature	510
libraries of polymer/pigment compositions	fluorescence spectroscopy and imaging for the evaluation of oxidative stability (weathering) of polymer/pigment compositions under conventional test conditions	multiple levels of end-use testing conditions provide more reliable ranking of performance of materials. Similar kinetic rates of weathering of polymers with quite different pigments were found	511

Table 2. Continued

materials system	instrumentation	knowledge	ref
one-dimensional coiled libraries of polymer/UV absorber compositions	fluorescence spectroscopy and imaging for the evaluation of oxidative stability (weathering) of polymer/UV absorber compositions under accelerated test conditions. Environmental stress is applied to only local regions, followed by high-sensitivity spatially resolved characterization.	ranking of polymer/UV absorber compositions equivalent to traditional weathering data while achieved 20 times faster	333
polyphasic fluid reactions	microreactor for liquid/liquid isomerization and gas/liquid asymmetric hydrogenation based on dynamic sequential operation	reaction rate is proportional to the catalyst concentration; the rate decreases with increasing surfactant concentration, no change in the enantiomeric excess was observed	512
polymer synthesis	on-line GPC for reaction optimization	determination of activation energy of polymerization	513
siloxane rubber/ carbon black nanocomposites	automated scanning probe microscope	study of curing rate of siloxane rubber matrix on roughness and conductivity of composites	514
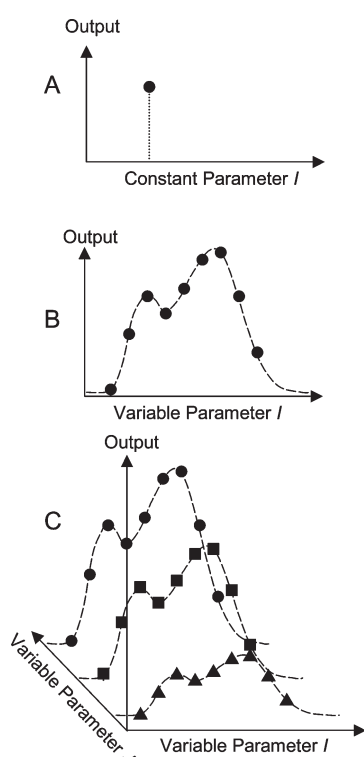
Figure 3. Schematic of (A) zero-, (B) first-, and (C) second-order analytical measurements for high-throughput materials characterization.

Figure 4. Typical examples of zero-, first, and second-order analytical measurements for high-throughput materials characterization: (A, B) Zero-order measurements of scattered light from each organic coating in a 48-element array at a single wavelength upon an abrasion resistance test. A, reflected-light image of the coatings array. B, representative reflected light intensity from a single coating in the array. (C, D) First-order measurements of fluorescence spectra from each polycarbonate material in a 96-element microreactor array at a single excitation wavelength. C, reflected-light image of the microreactor array. D, representative fluorescence spectrum from a single polymer material in the array. (E, F) Second-order measurements of color changes in colorimetric sensing materials in a 48-element array. E, general view of the sensor materials array in a gas flow-through cell. F, representative absorption spectra from a single material in the array collected over a period of time of reaction of this sensor material with a vapor of interest.

polymeric materials upon their melt polymerization were performed directly in individual microreactors. A view of the 96-microreactor array is shown in Figure 4C. From these measurements, several chemical parameters in the combinatorial samples were identified. The spectral shape of the fluorescence emission with an excitation at 340 nm provided the information about the concentration of the branched product in the polycarbonate polymer and the selectivity of a catalyst used for the melt polymerization.[60,64,65] A representative fluorescence spectrum (along with an excitation line at 340 nm) from a single microreactor in the array is illustrated in Figure 4D.

When measurements are done with a first-order instrument and there is another independent variable involved, this constitutes a second-order measurement approach (see Figure 4E and F). This type of screening was used for the evaluation of sensing materials.

Table 3. Functions of Data Management System

function	current capabilities	needs
experimental planning		
	• composition parameters	• iterative intelligent experimental planning based on results from
	• process parameters	virtual or experimental libraries
	• library design	
database		
	• entry and search of composition and process variables	• storage and manipulation (search) of large amounts (tera/peta bytes
	• operation with heterogeneous data	and more) of data
	• unification of numerical data between different instruments,	• development of advanced query systems to databases that can be
	databases, individual computers	adapted to machine learning algorithms
instrument control	operation of diverse instruments	
		• interinstrument calibration
		• full instrument diagnostics
		• plug-'n'-play multiple instrument configurations
data processing		
	• visualization of compositions and process conditions	• advanced data compression
	of library elements	• processing of large amounts (terabytes and more) of data
	• visualization of measured parameters	• linking of physical base computational tools to data processing
	• matrix algebra	• scientific visualization tools
	• cluster analysis	
	• quantification	
	• outlier detection	
	• multivariate processing of steady-state and time-resolved	
	data	
	• third party statistical packages	
data mining		
	• prediction of properties of new materials	• establishment of nonlinear and hybrid data mining tools
	• virtual libraries	• "smart" data mining algorithms that can identify the right type
	• cluster analysis	of tools simply based on the survey of the data available
	• molecular modeling	
	• QSAR	
	• identification of appropriate descriptors on different levels	
	(atomic, molecular, process, etc.)	

Figure 4E shows a 48-element array of sensor materials positioned in a gas flow-cell for the monitoring of the materials response upon exposure to vapors of interest. For the evaluation of sensing materials, absorption spectra were collected over a period of time of reaction of these sensing materials with a vapor of interest. Results of these measurements are illustrated in Figure 4F. Other examples of second-order systems applied for high-throughput materials characterization are excitation–emission luminescence measurement systems,[65,66] GC-MS,[67,68] and others.

The increase in the measurement dimensionality (i.e., the order of analytical instrumentation) improves the analytical capabilities of the screening systems and makes possible their use for reaction monitoring and optimization. These capabilities include increased analyte selectivity, more simple approach to reject contributions from interferences, multicomponent analysis, and outlier detection. Importantly, second- and higher-order measurement approaches benefit from the improved performance even in presence of unknown interferences.[69]

2.4. Data Analysis and Mining. The CHT experiments create significant amount of data, generating challenges in data management. The issues range from managing work flows in experiments, to tracking multivariate measurements, to storing the data, to be able to query and retrieve information from databases, and to mine the appropriate descriptors to predict materials properties. In an ideal CHT workflow, one should "analyze in a day what is made in a day".[70] Such performance depends on the adequate data management capabilities of the CHT workflow. Table 3 illustrates important functions of the data management system and demonstrates aspects that have been already developed and that are under development. Data management strategies for different applications were summarized by Koinuma and co-workers.[71,72] The aspects of information processing that focus on the scientific interpretation of data generated from CHT screening have been extensively discussed.[72–78]

Data mining techniques have two primary functions such as pattern recognition and prediction, both of which form the foundations for understanding materials behavior. Following the treatment of Tan et.al.[79–81] *pattern recognition* serves as a basis for deriving correlations, trends, clusters, trajectory and anomalies among disparate data. The interpretation of these patterns is intrinsically tied to an understanding of materials physics and chemistry. In many ways this role of data mining is similar to the phenomenological structure–property paradigms that play a central role in the study of engineering materials. It is

possible to recognize these relationships with far greater speed and not necessarily depending on a priori models, provided the availability of the relevant data. The *predictive aspect* of data mining tasks can serve for both classification and regression operations. Data mining, which is an interdisciplinary blend of statistics, machine learning, artificial intelligence, and pattern recognition, is viewed to have four core tasks:

Cluster analysis seeks to find groups of closely related observations and is valuable in targeting groups of data that may have well behaved correlations and can form the basis of physics-based as well statistically based models. Cluster analysis when integrated with CHT experimentation, can serve as a powerful tool for rapidly screening combinatorial libraries.

Predictive modeling helps build models for targeted objectives (e.g., a specific materials property) as a function of input or exploratory variables. The success of these models also helps refine the relevance of the input parameters.

Association analysis is used to discover patterns that describe strongly associated features in data (for instance the frequency of association of a specific materials property to materials chemistry). Such an analysis over extremely large data sets is made possible with the development of very high-speed search algorithms and can help to develop heuristic rules for materials behavior governed by many factors.

Anomaly detection does the opposite by identifying data or observations significantly different from the norm. To be able to identify such anomalies or outliers are critical in CHT experiments and high throughput screening especially to quantitatively assess uncertainty and accuracy of results and distinguish between true "discoveries" and false positives.

Massive data generated from high-troughput characterization tools leads to the need for effective data analysis and interpretation to identify the trends and relationships in the data.[9] Advanced mathematical and statistical techniques are used in CHT screening to determine, often by indirect means, the properties of substances that otherwise would be very difficult to measure directly.[82,83] These techniques have been successfully applied for visualization and pattern recognition,[84,85] lead identification and optimization,[86,87] process optimization,[66,88] and development of predictive models and quantitative structure—activity relationships (QSARs) and quantitative structure—property relationships (QSPRs).[85,89,90] The implementation of multivariate calibration improves analysis selectivity when spectroscopic or any other types of measurements are performed with relatively low resolution instruments.[91,92]

Multivariate data analysis techniques are essential analytical tools for in combinatorial materials science. The attractiveness of partial least-squares (PLS) method has been demonstrated for in situ monitoring of combinatorial reactions using single-bead FTIR spectroscopy.[93] Using these tools, quantitative and qualitative analysis of combinatorial samples was performed with IR spectra with severely overlapped bands. A limitation of PLS method is in the ability to reveal only the changes due to reaction but it cannot provide spectra for pure components.[93] This limitation can be overcome by using other multivariate analysis tools such as evolving factor analysis and multivariate curve resolution methods.[8]

In combinatorial materials science, pattern recognition techniques find similarities and differences between samples of combinatorial libraries, serve as a powerful visualization and descriptor-identification tool, and can warn of the occurrence of abnormalities in the measured data.[84] These techniques can reveal correlated patterns in large data sets obtained from combinatorial experiments, large databases or simulations, can determine the structural relationship among screening hits, and can significantly reduce data dimensionality to make it more manageable in the database with the minimal loss of information.[79−81,94] Methods of pattern recognition include principal components analysis (PCA), hierarchical cluster analysis (HCA), soft independent modeling of class analogies (SIMCA), neural networks, and some others.[95,96]

PCA is a widely used approach to search for patterns by seeking to reduce the dimensionality of data because it provides an unsupervised and robust way for analysis of multivariate data. PCA projects the data set onto a subspace of lower dimensionality with removed collinearity. PCA achieves this objective by explaining the variance of the data matrix in terms of the weighted sums of the original variables without significant loss of information. These weighted sums of the original variables are called principal components (PCs). Each PC is a suitable linear combination of all the original variables. The first PC accounts for the maximum variance (eigenvalue) in the original data set. The second PC is orthogonal (uncorrelated) to the first and accounts for most of the remaining variance. Thus, the mth PC is orthogonal to all others and has the mth largest variance in the set of PCs. Once the N PCs have been calculated using eigenvalue/eigenvector matrix operations, only M PCs with variances above a critical level are retained. This M-dimensional PC space has retained most of the information from the initial N-dimensional variable space, by projecting it into orthogonal axes of high variance and forming a suitable PCA model.[18]

In PCA, the scores plots show the relations between analyzed samples, while the loadings plots show the relations between analyzed variables. To ensure the quality of the data analyzed using PCA, several statistical tools are also available. Multivariate control charts use two statistical indicators of the PCA model such as Hotelling's T^2 and Q values plotted as a function of combinatorial sample or time. The significant principal components of the PCA model are used to develop the T^2-chart and the remaining PCs contribute to the Q-chart. The Hotelling's T^2 statistic is the sum of normalized squared scores and is a measure of the variation in each sample within the PCA model. The T^2 contributions describe how individual variables contribute to the Hotelling's T^2 value for a given sample. The Q residual is the squared prediction error and describes how well the PCA model fits each sample. It is a measure of the amount of variation in each sample not captured by principal components retained in the model. The graphical representation of PCA with T^2 and Q statistics for multiple samples in the PCA model is illustrated in Figure 5.

It is important not only to discover a target feature in a combinatorial library but also to glean from these combinatorial experiments the variations in the library. An illustrative example can be provided from combinatorial polymer libraries of polyanhydrides (see Figure 6), which are important biomaterials for biomedical applications and drug delivery because of their degradation and erosion properties.[97] For drug delivery applications, the choice of correct chemistry and management of various degradation factors (for example, kinetics of drug release and polymer-drug interaction) are essential for proper drug stabilization. High throughput FTIR screening has been shown to be an appropriate tool for screening compositional libraries of polyanhydride copolymers. FTIR spectra (see Figure 6A, B) and images (see Figure 6C) were utilized for the PCA-based tracking of the subtle changes in chemistry of polyanhydride copolymers.[98]

The PCA model has been developed to track how critical changes in dominant spectral regions occur at polymer chemistry blends that could not be detected by a simple direct observation of the FTIR spectra associated with each chemistry in the combinatorial library. Figure 6D shows a scores plot of the developed PCA model
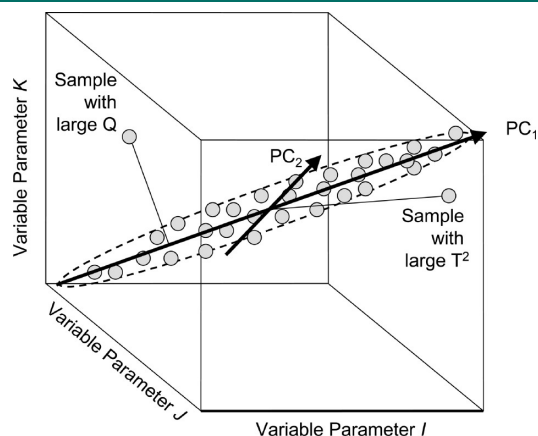

Figure 5. Graphical representation of of PCA with T^2 and Q statistics for multiple samples in the PCA model.

of the FTIR spectra. Two inflection points in the scores plot that corresponded to compositions #19 and #53 are clearly seen, signifying effects of chemistries of #19 and #53 samples on the molecular structure that influences target properties.[18,98] This example showed that the merging of informatics techniques with combinatorial experiments provided a significant "value added" level of interpretation to the analysis of results from combinatorial libraries. The use of such data mining techniques is becoming an integral part of high throughput screening methods in combinatorial experimentation.

Data analysis comes in many forms, and scientific visualization is a powerful tool to aid in the interpretation of CHT experiments and especially in identifying targeted information from large data sets resulting from these CHT experiments. A representative example can be provided from the field of mixed-metal oxides that play an increasingly important role in many areas of chemistry, physics, and materials science originating from the opportunities for tailoring of chemical composition, microstructure, porosity, and surface properties. In principle, the combination of several metals in an oxide matrix can produce materials with novel physical and chemical properties that can lead to a superior performance in technological applications ranging from catalysis to sensing.[19,99−101] The metals can behave as "isolated units" that bring their intrinsic properties to the system or their
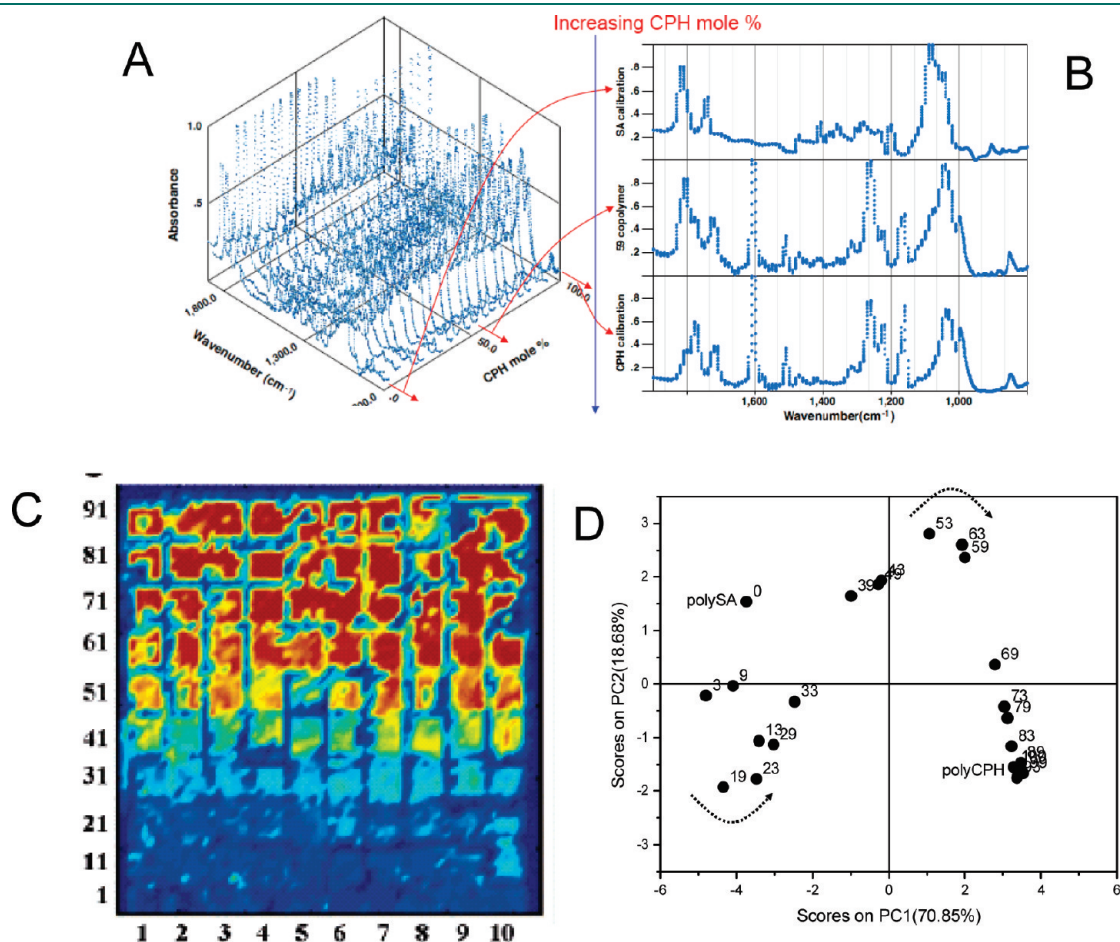
Figure 6. Integration of informatics with high throughput materials characterization to extract data trends that are not easily visualized from simple inspection of FTIR spectra and images from combinatorial experiments with polyanhydride copolymers (CPHs). A and B are FTIR spectra, and C is the corresponding FTIR chemical imaging map for a 10 × 10 array of CPHs mixtures. (D) The scores plot of the PCA model of the FTIR spectra. Numbers represent compositions of CPH (e.g., for sample 3, it contains 3 mol % of CPH and 97% of SA (SA= sebacic anhydride).[103]
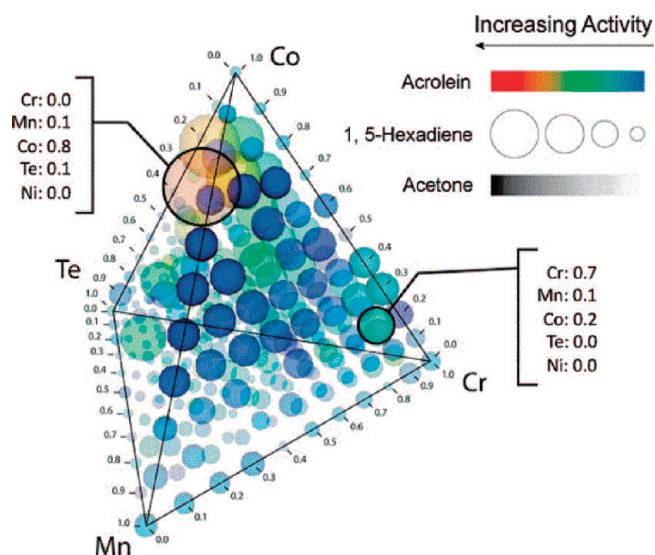
Figure 7. D-Glyph plot of a catalyst library data. Four elements (Cr, Mn, Co, and Te) are plotted on a 3D quaternary mixtures plot, while three activities are mapped to three graphical attributes of a sphere glyph: color is mapped to activities for acrolein, size is mapped to activities for 1, 5-hexadiene, and intensity is mapped to activities for acetone. The intensity of the glyphs is adjusted on the left plot to accentuate the levels of acetone.[13]


Figure 8. Loadings plot of the developed PCA model derived from a combinatorial library of multicomponent oxides (Mo, Ni, Mn, Cr, and Co) and the selectivity of chemical products (acetone, propionic adelhyde, acreolein, and 1,5-hexadiene).[18,97,103]

behavior can be modified by the effects of metal/metal or metal/oxygen/metal interactions. In this respect, it is important to know how to choose the "right" combination of metals. Just to consider which combination is appropriate and why is in itself a challenge, and hence when one considers mixed metal catalysts with 4, 5, and more metals, we clearly have, what appears to be a prohibitive problem on exploring in a reasonably timely manner the catalytic behavior of such a vast array of chemistries.

The groups of Maier and Rajan[13,102,103] addressed this issue through a study of 10^3 combinatorial catalyst library. The chemistries sampled the complete composition spread of a five dimensional search space containing the elements Cr, Co, Mn, Mo, and Ni prepared by a sol—gel recipe and tested by the high-throughput screening reactor. To unravel the complexity of these materials compositions, a visualization approach shown in Figure 7 has been utilized to track the raw data from combinatorial experiments. This visualization approach facilitated the establishment of the framework on how data mining techniques can be applied to unravel the complexity of combinatorial experiments.

The further application of data mining techniques addressed two questions, such as (1) the selectivity of a given metal to catalytic activity (i.e., a reaction product) and (2) the relative influence between metal chemistry and catalytic activity. The loading plot of the developed PCA model provided the correlations between the presence of a specific metal species and the selectivity of a given reaction product (see Figure 8). The relative correlations of different chemistries and their influence on the selectivity of chemical reactions can be visualized through the screening of the geometrical relationships between variables represented in this loadings plot. In this case Mo or the pair (Mo, Co) has positive correlations with acetone formation, while Ni and Mn are tend to inhibit the formation of all the reaction products, especially acetone. This example has shown that the data mining techniques can not only help to identify the relative
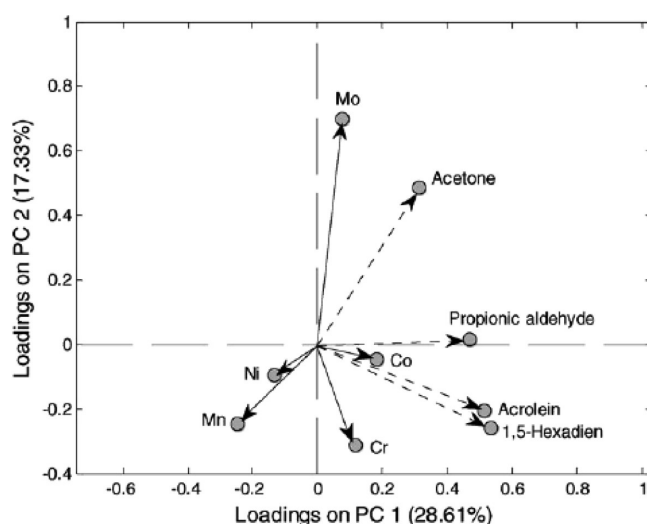
selectivity of metal ions on catalytic products but also can help to assess the relative impact of these elements.

Importantly, while PCA and other pattern recognition tools are helpful in assessing the relative impact of multiple parameters on materials properties, they are not predictive tools. For predicting of materials properties, other methods should be applied.[97] Just as informatics can aid in searching and discovering critical data from combinatorial experiments,[71−76] it can also serve as a predictive modeling tool based on CHT experimentation. For instance, Li et al. have shown,[104] a new approach involving a hybrid data mining to determine which aspects of a polymeric molecular structure have the most impact on the release kinetics behavior for drug delivery (see Figure 9). They used these molecular descriptors to model the release profile of proteins from a combinatorial library of biodegradable polymers. The mathematical approach for modeling the release profile was based on a combination of genetic algorithms (GA) and support vector regression methods. The polymers explored from the combinatorial libraries included linearly varying molar compositions of binary formulations of copolymers, with the protein release rate found to increase with decreasing polymer hydrophobicity. From the new attribute selection approach, it was determined that number of nonconjugated backbone −COO− bonds, number of aromatic rings, and number of −CH$_2$− bonds were most important for accurately modeling the release kinetics behavior. This work introduces a new approach for understanding which factors control drug release and has important implications for the rational design of new polymeric carriers for drug delivery

In addition to materials composition, materials microstructure and processing parameters play equally important effects. Unraveling the interactions between these effects is critical. Thus, informatics techniques is applied to high-throughput screening data from combinatorial synthesis methods. In one representative example, the ability of a polymer system to both modulate its effect on the immune response and to deliver a drug or antigen in a controlled fashion provides an ideal platform for both vaccine adjuvants and multicomponent implants. Many factors influence the innate and adaptive immune responses, including the activation
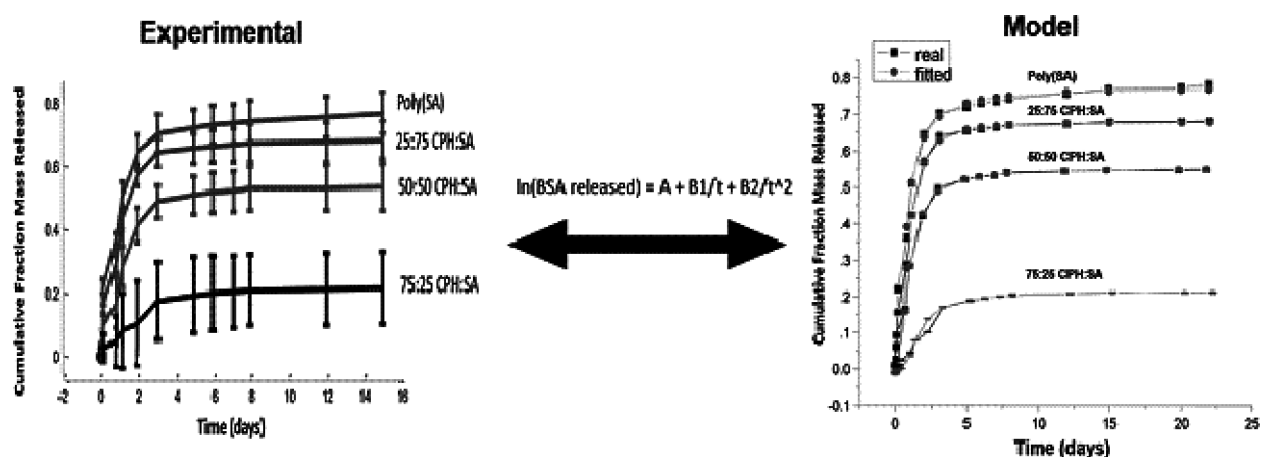
Figure 9. Cumulative mass fraction of released BSA from polymer film libraries polymer release kinetics demonstrated chemistry dependent trends of decreasing protein release with increasing polymer hydrophobicity (CPH content). The informatics based models show a robust level of agreement with experiments (CPH, carboxyphenoxy hexane; SA, sebacic anhydride).[104]

of dendritic cells (DCs). Petersen et al.[105] have built combinatorial libraries that utilized the known measures of DC activation as a means to more rationally design biodegradable adjuvants for vaccine development. Adjuvant properties, such as enhancing immunogenicity have been investigated by developing a multiplexed polyanhydride library, that also explored the role of polymer films and nanospheres using a novel method for high-throughput nanosphere fabrication.

The concomitant use of this multiplexed technique and the informatics analysis have permitted rapid optimization of the CPH:SA polyanhydride system for use in tissue engineering (where biocompatibility is desirable) or vaccine delivery (where enhanced innate immune responses are desirable). The developed multiplexed method was able to clearly demonstrate that the chemistry of the polymer played a major role in up-regulating cell surface marker expression and cytokine production when films or nanospheres were used to stimulate DCs. The informatics analysis employed in this study defined the clear differences between these two effects (chemistry and device geometry) and showed that the CPH:SA system has immunomodulatory capabilities to regulate both cellular expression of surface markers and production of cytokines. This rapid and multiplexed investigation of the adjuvant effect (five different polymer film chemistries and six different nanosphere chemistries with multiple replicates) was made possible by the use of a novel multiplexed approach to fabricate nanospheres and films and screen their interactions with immune cells. This generality of the technique paved the path for rational design and development of biomaterials for specific applications in drug/vaccine delivery and tissue engineering. The use of data dimensionality reduction methods on combinatorially derived data provides a very powerful means to uncover structure-processing-property relationships that otherwise may be difficult to detect. Figure 10 shows an example of a clear discrimination in the behavior of polymers in for the form of nanoparticles versus flat films in terms of their efficacy for drug delivery. This example serves to highlight the value of informatics in linking information across length scales.

3. MATERIALS DEVELOPMENT EXAMPLES

The CHT experimentation technologies have the broad applicability in discovery and optimization of new materials.
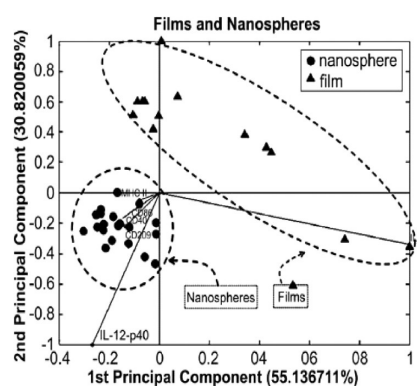
Figure 10. PCA biplot comparing the polyanhydride nanosphere and film systems showing inverse correlations with clusters in opposite quadrants. The IL-12 production is strongly associated with the nanospheres while the IL-6 production is more associated with the film geometry. IL-2 and IL-6 are terms associated with different types of cytokines which are chemical messengers capable of mediating several facets of the immune response.[105]

The areas that are most impacted by the CHT approaches include catalysis, electronic and functional materials, polymer-based industrial coatings, sensing materials, and biomaterials. The CHT experimentation advances in these areas are reviewed in sections 3.1−3.5.

3.1. Catalysis. Catalyzed reactions range from fine chemicals to bulk chemicals, to pharmaceuticals, and to refinery chemicals. In general, about 90% of all chemical processes are catalyzed.[106] A classical compartmentation of catalysis is into heterogeneous and homogeneous catalysis (see Figure 11). In practical industrial applications, 80% of all catalysts are heterogeneous catalysts and 15% are homogeneous catalysts. The remaining 5% are biocatalysts.[107,108] The figures of merit of catalysts performance include sensitivity, cost, separation from products, selectivity, and catalyst design.[109] The design of a catalyst − coming from the Latin word *designare*, which means identifying − describes the process of finding a new catalyst for a special reaction or the improvement of an existing reaction in order to make the whole process more effective (for example, more economic). It is the starting point of a series of subsequent items including synthesis
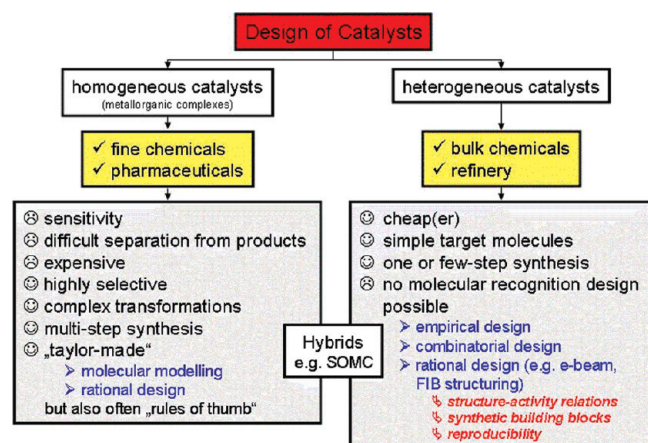
Figure 11. Homogeneous vs heterogeneous catalyst design.

Figure 12. Self-assembled metal complex catalyst library based on the aminopyridine — isoquinolone complex ($D_{X,Y}$ = donor groups such as for instance PPh_2; $D_{X,Y}$ and R are to be varied to form the library with ($m \times n$) members).[515]

and testing of possible candidates in an iterative process. Often the superiority of homogeneous over heterogeneous catalysis is attributed to the fact that transition-metal complexes can be identified by rational instead of empirical design. Although computational techniques have evolved enormously, at present, the necessary accuracy is still not high enough to predict selectivity of catalysts. Therefore, in homogeneous and heterogeneous catalysis, researches oftern rely on empirical design strategies and are confronted with the challenge of performing tests on a large number of possible catalyst candidates. As a result of this significant number of catalyst candidates, CHT screening has been identified as an indispensable tool for catalysis research.[110] The state of the art of combinatorial research on catalysis up to 2006 has been reviewed earlier.[17]

3.1.1. Homogeneous Catalysts. Independent, whether homogeneous or heterogeneous systems are used, high-throughput synthesis and screening rely on structurally diverse catalyst libraries. In the case of homogeneous catalysis, either molecular, metal—organic or enzymatic catalysis, library members have to be prepared by multistep syntheses, thus having to presynthesize all the candidates to be tested renders this method far too time-consuming. However, an easy synthetic access to structurally diverse libraries is to use of dynamic or reversible chemistry approaches for the construction of catalysts. In this approach the synthesis is restricted to building blocks and diversity is simply generated by mixing. By self-assembly and self-selection processes the best catalyst outperforms all other library members in a specific target reaction. Gasparini et al.[111] described the possibilities of dynamic approaches toward catalyst discovery. They discussed three classes of catalysts, such as (1) self-assembled catalysts, which are formed through noncovalent interactions between molecular subunits, (2) self-selected catalysts, which are identified by their ability to stabilize the transition-state of the reaction of interest — similar to the strategy used for the development of antibodies, and (3) self-evolving catalysts, which are defined to describe complex dynamic networks of molecules with catalytic properties. The most intriguing effect of the third class is that these ensembles of molecules have properties that cannot be tracked back to a single component. For all three classes Gasparini et al.[111] gave examples originating from metal—organic and organic chemistry. The advantages of self-assembled ligand libraries, for instance, are clear, as structural variation is introduced in the monomeric components and the structural diversity of libraries is generated by mixing the ligand in
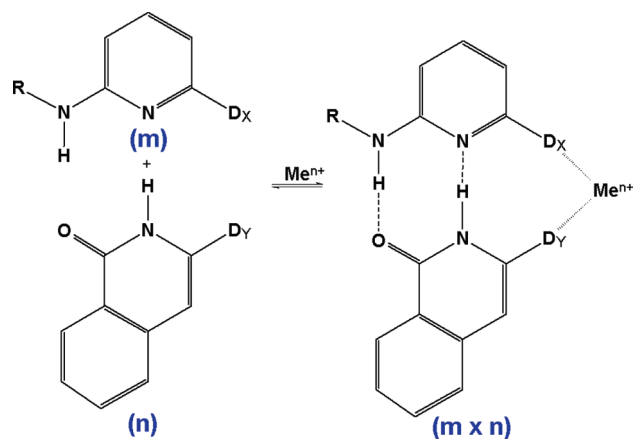
different combinations, as shown in Figure 12 using ligand sets based on aminopyridine and isoquinolone.

Despite numerous advantages, these methods also revealed some disadvantages.[112] For example, in palladium complexes identified from catalyst screening, numerous ligand—metal combinations revealed products resulting from unexpected chemistry such as C—H bond activation, C—P bond cleavage, and an addition of solvent molecules leading to further assembly into oligomeric structures with unusual interconnections unlikely to function as effective catalysts.

A simulated evolution of library design was explored by Vriamont and co-workers[113] to build a library of chiral catalysts that have been used in asymmetric hydride transfer for reduction of ketones to chiral alcohols. From six metal precursors and 330 chiral β-amino-alcohol ligands as building blocks a library of all 1980 possible combinations was generated by CHT experimentation, followed by the application of a GA to a small part of the library with systematic variation of the adjustable parameters. Simulated evolutions were performed to evaluate the ability of the algorithm to find the best catalysts without testing the entire library. As optimization of two parameters is required in this approach, enantiomeric excess and conversion rate, but GA are usually designed for the optimization of a single parameter, the value of a normalized performance factor was calculated. It was shown that is was sufficient to test about 10% of the whole library to get the best catalyst. For asymmetric hydrogenation,[114] combinatorial screening was implemented as cost-effective tool to find a scalable catalyst to be used after scale up in the kilogram production of a desired bulky amide. Target of this development was a sterically demanding aryl enamide as an intermediate toward a new potent melanocortin receptor agonist useful in the treatment of obesity. Testing of a first library of 96 chiral monodendate phosphoramidites led to the design of a second focused library of 16 chiral ligands, allowing the discovery of a new efficient catalyst. Combinatorial screening was the key success factor for the discovery of an efficient catalyst within a short time as summarized in Figure 13.

In the long-lasting discussion, whether mono- or bidendate phosphorus ligands give a higher asymmetric induction, Goudriaan et al.[115] presented three different approaches for the design of chiral bidendate phosphorus ligands and their application as ligands in

590

dx.doi.org/10.1021/co200007w |*ACS Comb. Sci.* 2011, 13, 579–633
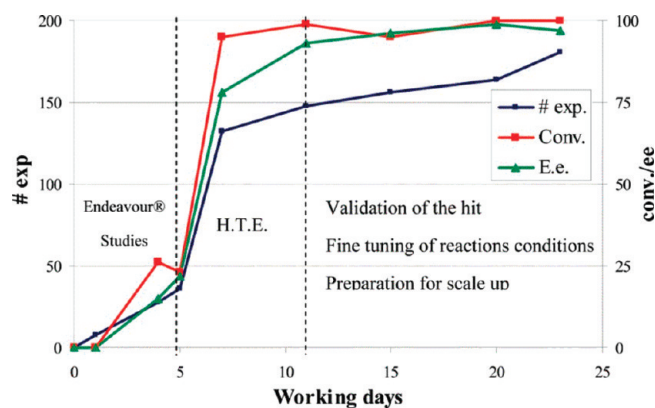
Figure 13. Typical timeline of a combinatorial catalyst discovery project of an asymmetric hydrogenation[114] with the indication of activity, enantiomeric excess (ee/E.e.) of the best catalytic systems, and the cumulated number of experiments performed.

transition-metal complexes for homogeneous asymmetric catalysts: (1) modular synthesis of bidendate ligands, (2) the solid support synthesis of bidendate ligands, and (3) the self-assembly of ligand building blocks into bidendate ligands. It was concluded that the divergent or modular synthesis leads to a series of structurally related ligands, which can be used for fine-tuning or optimization of catalysts, and the libraries are generally rather small, as the library members have to be prepared serially, whereas the application of solid-phase synthesis has the potential for larger libraries, but which has not been used in the past. The highest potential for large libraries has the formation of ligands by self-assembly, as the number of bidendate ligands grows exponentially with the number of building blocks used. Also the degree of diversity of such a ligand library may be very high. Future strategies may also include a combination of the approaches mentioned above and efforts in this direction are currently pursued in the laboratory of the authors.

A key challenge for the synthesis of large and diverse libraries is the development of high-throughput amenable chemical reactions that allow rapid synthesis with a small number of individual steps. One method that has received much attention in recent years is the Cu(I) catalyzed 1,3-dipolar (Huisgen) cycloaddition between an azide and an alkyne at room temperature also known as "click chemistry", introduced by Sharpless in 2001[116] and which describes chemical reactions tailored to generate substances quickly and reliably by joining small units together. The most frequently cited reaction within click chemistry is the 1,3-dipolar cycloaddition discovered by groups of Sharpless[116] and Meldal.[117] Srinivasan et al.[118] reported the high-throughput synthesis of a 325-member azide library with the subsequent "click" synthesis of bidendate enzyme inhibitors. Coupling reagent in this high-throughput enzymology study was an alkyne-modified isoxazole, whose choice was guided by computational modeling. The spectrum of different possibilities in high-throughput enzyme, also called "catalomic", profiling of the click chemistry approach within a fragment-based assembly concept was reviewed by Uttamchandani and co-workers.[119] Such strategies will inspire future innovation in the systematic investigation of novel chemical entities and chemical proteomics tools that target various other enzyme classes.

3.1.2. Homogeneous—Heterogeneous Hybrid Approaches. A hybrid between homogeneous and heterogeneous catalysis is the surface organo-metallic chemistry (SOMC) approach, where for

asymmetric induction chiral metal—organic complexes are covalently bonded to a support surface. Immobilisation of catalysts and their high-throughput screening are brought together in the so-called split-and-pool (S&P), split-and-mix, split-and-combine, and "one bead—one compound" (OBOC) concepts, all synonyms of the same principle. Based on the pioneering work of Houghton[120] and Geysen[121] on multiple peptide synthesis, a concept was introduced by Furka et al.[122] merging some characteristics of these known methods. The S&P method has been developed to achieve very high-throughput of highly diverse materials libraries in the range of $10^3 - 10^8$ samples with a simple workflow, for example, to realize combinatorial chemistry in its intrinsic meaning, that is, the combinatorial permutation of element combinations or synthesis parameters. Immobilization of chiral catalysts on the surface of polymer beads within an OBOC concept rises the question, whether the solid support influences the asymmetric induction ability of the chiral center. Whereas Arai et al.[123] argue that the origin of chirality is restricted by the solid support and thus no asymmetric induction occurs, the results of Broussy and Waldmann[124] on the solid phase synthesis of highly substituted tetrahydropyrans by tandem ene-reaction and intramolecular Sakurai cyclization clearly revealed that asymmetric induction is possible on solid phase and that enantiomerically pure tetrahydropyrans containing up to four stereocenters can be effectively synthesized with this method. In their approach the compounds were covalently bound to a p-bromophenylpoly styrene resin, which were loaded in IRORI MacroKans enabling handling of the resin beads during synthesis because of their porosity. Support influence on enantioselectivity was also reported by Thomas and Raja[125] exploiting nanospace for asymmetric catalysis by combinatorial chemistry. By confinement of an immobilized, single-site chiral catalyst within the cavity of a chirally modified mesoporous host an enhancement of enantioselectivity was observed. This was because of the deliberate restriction of the special freedom in the vicinity of an active center tethered to the inner wall of a nanopore in such a manner that a prochiral molecule approaching it and its chiral ligands would additionally interact with the pore wall (see Figure 14). This idea, originally suggested to John Meurig Thomas by this postdoctoral colleague Thomas Maschmeyer[126] in 1995, offers novel opportunities for improving enantioselectivities in chiral conversions. Any quantitative analysis has been made to provide insight into these steric effects, only molecular dynamics simulations by Malek et al.[127,128] on anchored Mn(III) salen complexes in mesoporous silica have led to a deeper understanding of the detailed contributions that enhance enantioselectivities. Recently this topic was reviewed by Fraile and co-workers.[129]

Some other obstacles are associated with combinatorial catalyst synthesis on resin beads. If in an OBOC library peptide structures have to be identified, the peptide sequence is usually analyzed by Edman degradation,[130] which is expensive and time-consuming. An efficient alternative can be the ladder peptide synthesis method.[131] In this method a small portion of the peptides are N-terminally capped during each coupling cycle in the synthesis of peptides on the polymer beads. For structure identification the peptide ladders are later cleaved off and analyzed by mass spectrometry. Gel-type resin beads have a porous structure so that photolytic cleavage in the analysis of a peptide-encoded combinatorial small molecule library on TentaGel resin gives a poor photocleavage yield.[132] This problem is avoided by using a core—shell-type resin like the HiCore resin, the structure of which is segregated into two regions, a rigid core cross-linked
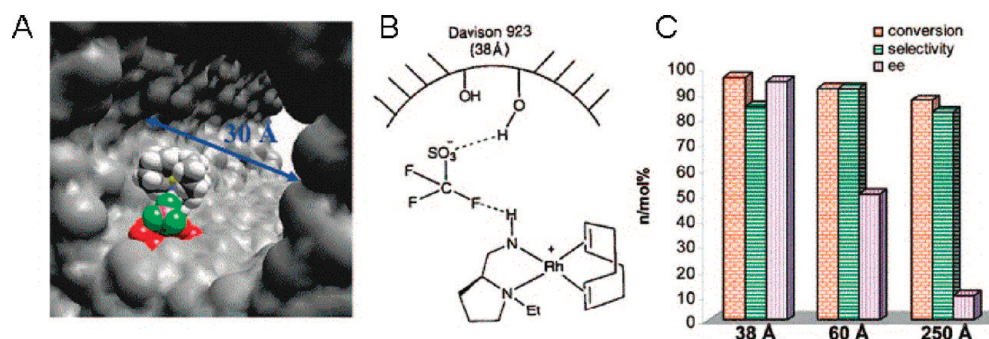
Figure 14. Effect of surface curvature and concavity of the support in facilitating the asymmetric hydrogenation of methyl benzoylformate to methyl mandelate using $[Rh(COD)-(S)-(+)-1-(2-pyrrolidinylmethyl)-pyrrolidine] CF_3SO_3$ anchored onto mesoporous silicas of varying pore dimensions. (A) computational model; (B) chemical structure of the complex; (C) effect of pore radius on conversion, selectivity, and ee.[125]

by 2,4,6-trichloro-1,3,5-triazine and a flexible shell functionalized by diamino PEG. Thus, the photoelution of peptides on the HiCore resin was two times more efficient than on TentaGel resin when irradiated with UV light for 30 min.[133]

Another obstacle of OBOC libraries is the question whether the activity of "on-bead" assays, in which the library is tested by a staining reaction while the compounds are linked to the synthesis beads are really predictive of the activity of the compound as free molecule in solution. For that reason the group of Maillard[134] developed a simple and practical "off-bead" screening protocol for catalysis that allows one to assay OBOC libraries as free molecules in solution on the surface of silica gel plates. Their combinatorial library of up to 65,536 peptide dendrimers prepared on a photocleavable TentaGel resin was screened for ester hydrolysis activity and a fluorescent halo appeared after photocleavage from the beads around some of the beads on the silica plate, which were identified as hits. Using this "off-bead" assay they report that the catalysis of the ester hydrolysis comes from core-active sites of the peptide dendrimers and depends on the presence of histidine residues at the dendritic core, but is also controlled by the outer dendritic branches, whereby anionic residues in these branches inhibit catalysis.

A new method for screening S&P combinatorial libraries for catalytic activity was also reported by Stanton and co-workers[135] using a spatial separation of resin-bound catalyst on an adhesive array on a microscope slide for catalytic Knoevenagel condensation screening. A visible absorption difference between reactands and products was used to site-selectively detect product formation in and around the catalytic beads. The method can be extended for colorless products by application of pH-sensitive indicators for array-based screening. Organic—inorganic hybrid catalysts prepared by the coupling of 3-(triethoxysilyl)propyl-triphenyl-phosphonium bromide and mesoporous silica enabled Sakai et al.[136] to prepare cyclic carbonates from carbon dioxide and epoxides. The pore size of silica was found to be important for catalysis. Organic and inorganic moieties had a synergistic effect on the catalytic activity, both the phosphonium bromide but also the OH group participating in catalysis.
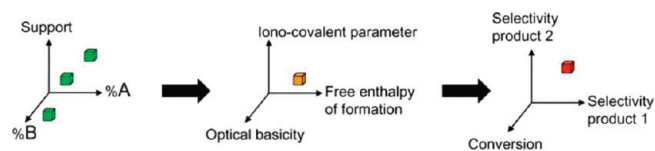
3.1.3. Heterogeneous Catalysts. Heterogeneous catalysis utilizing the S&P method relies on solid supports. For the design of heterogeneous catalyst libraries numerous strategies have been developed (see, for instance, refs 137 and 138) Fundamental problem in the application of combinatorial or high-throughput methods in the development and optimization of heterogeneous catalysts is the number of possible elements of the periodic

system. The combinatorial number of screenable element combinations scales with the number of components and generated the need of very high throughput methods, such as the S&P concept of solid support bead impregnation mentioned above. Solids are even more complex and to specify them completely, not only the composition has to be given but also crystallinity, polymorphic form, defect type and concentration, domain, and interface characteristics, and much more information is needed for a single solid catalyst.

To reduce the efforts and costs necessary to screen all possible catalyst candidates, computational methods have been introduced for the prediction of solid catalyst performance including an electronic infrastructure as informatics toolbox for high-throughput kinetic studies and virtual screening. The latter was developed by Farrusseng, Mirodatos and co-workers for the TOPCOMBI research project funded by the European Commission for Nanotechnology and Nanoscience.[139] It represents a collection of modules dealing with laboratory analytics, robotics, data handling and analytics, optimization, in-database processing and visualization generated collegially by the partners of a consortium. It was developed for large or contract research organizations to control cost, build or strengthen their competitive advantages and disseminate knowledge from centers of expertise of scattered or not interacting groups within the company. Knowledge generally is regarded to reduce screening efforts as quantitative structure—activity relations (QSAR) correlate the characteristics of heterogeneous catalysts and their experimentally measured performances for certain reactions.

As stated by Schüth et al.,[140] unfortunately, the classical QSAR approach cannot be directly transferred to the discovery of materials, especially of heterogeneous catalysts, because of the complexity of solid materials, that can hardly be characterized on atomic scale as a fingerprint signature similar to molecular fingerprint signatures. For molecules, a similarity principle holds according to which the similarity between two molecules can be assessed by measuring a distance between them. The quantification of distances between molecules is the key issue in the QSAR approach. Unfortunately, this similarity principle is not valid for solid catalysts. For materials, physicochemical properties encoded in a descriptor vector have to be used instead of distances. The key descriptors are usually not known or can hardly be measured in the case of diverse libraries.

The principle of the advanced QSAR approach in heterogeneous catalysis is illustrated in Figure 15.[140] A minimal set of attributes is defined that can correctly classify a data set into its

Figure 15. Advanced QSAR approach in heterogeneous catalysis. Composition space (left), physicochemical descriptor space (middle) and performance space (right).[140]

performance categories. By a preprocessing procedure variables with a significant projection onto the response space can be identified, irrelevance eliminated, as well as redundancy and multicollinearity addressed. Afterward the data-driven selection strategies have been applied to obtain an estimate of the differences in variance and information content of various attributes including a comparison of relative importance. Using probabilistic neural networks various semiempirical QSAR models have been created. Machine learning models as neural networks and classification trees have been used by Corma et al. for comparison of the fitting performance to that of support vector machines for the modeling and prediction of zeolite synthesis, when the gel molar ratios are used as synthesis descriptors.[141] It was found that support vector machines models show very good prediction performances and generalization capacity in zeolite synthesis prediction. Overfitting problems sometimes observed for neural networks may be overcome by this method. The efficiencies of several global optimization algorithms comparing methods such as GA, evolutionary strategies, simulated annealing, taboo search and GA hybridized with knowledge discovery procedures have been compared using the Selox benchmark by Farrusseng, Maschmeyer, and co-workers.[142] Selox stands for the selective catalytic oxidation reaction of carbon monoxide in the presence of hydrogen and is investigated for fuel cell applications to relate catalyst composition and reaction temperature effects on the conversion and selectivity of CO oxidation. In taboo search, the word taboo originally coming from the Polynesian language Tongan and indicating things, which cannot be touched, because they are sacred, a list of taboo candidate solutions are not repeated in the subsequent iteration of a global optimization algorithm and are updated in each iterative step. The authors find that an adjustment of the size of parameter space during different Design of Experiment (DoE) stages on the iterations through the high-throughput optimization cycle bear the risk that synergistic variables are discarded at an early stage, because their interactions were not detected. Thus becoming rapidly trapped on a local optimum or performing too lengthy an optimization may occur. If a certain number of necessary experiments are performed, with the global optimization algorithms mentioned above the final (global) optimum is more efficiently achieved and guaranteed, but only a poor understanding of the chemical system in the form of knowledge is obtained. On the other hand, the search space has to have a certain minimum size to apply global optimization algorithms, so that they are not appropriate for every problem.

A completely different approach for DoE has been suggested by Schunk, Sundermann, and Hibst.[143,144] This is the structure oriented library design, which was tested with regard to their usefulness and applicability in catalyst screening in two different research projects with different degree of exploratory character, namely the ammonoxidation reaction for the conversion of C_6 feedstocks to adiponitrile intermediates and the oxidation of acrolein and methacrolein to the corresponding acids. Compared

to descriptor-based approaches here the additional information taken into account for discrimination of the catalyst candidates is limited to structural parameters estimated by X-ray diffraction techniques prior to and after catalytic testing. In this case the choice of the target structure is regarded as crucial to the success of the program. In the first step an initial library was set up mainly consisting of candidates structurally well characterized and known to be catalytically active and selective in the reactions given above. From this initial phase, a lead candidate of highly complex structure was identified by testing. Despite the identification of a high amorphous oxide content with crystalline portions in this lead composition, again a structure-based approach was chosen to develop this candidate further. After deconvolution of the lead compound into binary, ternary and quaternary oxides and inclusion of other element combinations from structural databases forming the same structure types these potential candidates of less complex nature were taken as reference points of compositional designs to build a multidimensional grid of highly crystalline multinary candidate materials. A variation in stoichiometry, phase composition and crystalline nature increases the diversity of the library constituents further on a systematic basis. Classical DoE elements such as composite designs facilitate the evaluation of the results and the approach may be combined with even more complex methods as artificial neural networks (ANN) or GA. Problem in this approach may arise from differences between bulk and surface structure, as the catalytic activity is exclusively related to the latter, but the crystal (bulk) structure has been here the decisive design parameter. Perhaps one can argue that both are related, that a certain bulk structure enables a specific surface structure, which gives the catalytic activity.

Another general problem in catalytic studies is that not only a single objective function has to be optimized, a common scenario is the evaluation of response surfaces for conversion as well as selectivity to a number of alternative products. A GA based multiobjective DoE aided a high-throughput approach to optimize the combinations and concentrations of a noble metal-free catalyst system active in the selective catalytic reduction of NO by propene.[145] A direct comparison of single- and multiobjective design of combinatorial experiments was also performed for the optimization of a solid catalyst system active in the selective oxidative dehydrogenation (ODH) of propane.[146] The basis of the multiobjective optimization was a strength Pareto evolutionary algorithm (SPEA-2), that is, a Pareto-based algorithm operating toward two objectives, minimization of the distance toward the Pareto-optimal set and maximization of the diversity within this set. Elitism is implemented in SPEA-2 by an additional archive population composed of the best 24 nondominated individuals during the search, which is used in combination with the regular population as mating pool. Due to the SPEA-2 features it is not surprising that in a Pareto plot of selectivity versus conversion (Figure 16) the SPEA-2 solutions are well distributed over Pareto space. The most important element combinations found in the high conversion and high selectivity region are highlighted. To have a fair comparison, a new population has been created, denoted as the archive population of the single objective approach. Similar to the way the multiobjective archive population was created, the single objective archive population consisted of the 24 best catalysts found so far. The major difference compared to the SPEA-2 archive is that no Pareto-selection was performed and the catalysts were only selected with respect to their yield. For the single objective approach

593

dx.doi.org/10.1021/co200007w |*ACS Comb. Sci.* 2011, 13, 579–633
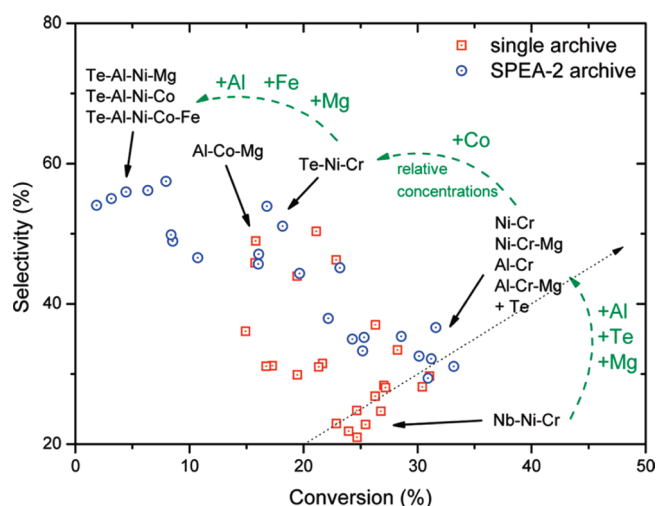
Figure 16. Visualization of the development of 6-generation archive populations for ODH of propane in Pareto space in a direct comparison of single- and multiobjective design of combinatorial experiments. The single objective archive population consisted of the 24 best catalysts found so far with respect to yield. The basis of the multiobjective optimization was a strength Pareto evolutionary algorithm (SPEA-2), that is, a Pareto-based algorithm operating toward two objectives, minimization of the distance toward the Pareto-optimal set and maximization of the diversity within this set.[146]

the strongest attraction is toward the product of selectivity and conversion, marked by a dotted arrow in Figure 16.

The multiobjective optimization performs better compared to the single objective approach with respect to the optimization of yield, which is not explicitly calculated during this procedure and, therefore, not directly optimized. Consequently the multiobjective algorithm was able to find catalysts in extreme regions of the Pareto space, which were not found by the single objective approach. As selectivity and conversion are optimized simultaneously, it is more likely to find interesting possible combinations with a multiobjective approach. Not selectivity and conversion of a single target molecule, but the conversion rates of a multicomponent feed gas monitored in a parallel manner in a multichannel monolith reactor have been in the focus of a multicriteria optimization procedure based on a GA carried out in the search of an advanced heterogeneous catalyst for total oxidation performed by the group of Claus.[147] In this case the search space consisted of more than 150 000 individuals including mono-, bi-, and trimetallic compositions assembled out of 49 different metals and impregnated onto alumina supports in 9 different amount levels.

Heterogeneous catalysts are used for a wide range of transformations going from small to medium-sized molecules. They also include materials used as photo- or electrocatalysts. Within the discussion of peak oil production, which might be reached according to the International Energy Agency (IEA) at the end of the next decade,[148] the search for new environmentally friendly energy sources such as fuel cells attracted much research attention. In the field of CHT experimentation, especially the direct methanol fuel cell (DMFC) using an easy available and storable high density fuel alternative for hydrogen has been considered intensely in the past few years. Whereas at the anode side methanol is consumed, oxygen is catalytically reduced at the cathode side, the latter reaction representing also the electrode reaction in other fuel cells as the proton exchange membrane fuel

cells (PEMFC). The conditions of an aqueous acidic environment together with high electrode potentials turn especially stability considerations in the identification of improved electrocatalysts into a crucial point. So it is not surprising that almost exclusively alloys containing platinum or palladium, materials that are known to be kinetically stable in electrochemical systems over relatively long periods of operation, are screened.

Combinatorial high-throughput techniques aiding the search for new oxygen electroreduction (OER) or oxygen reduction reaction (ORR) catalysts were reported by He and co-workers of the Honda Research Institute in several papers using multisource physical vapor deposition (M-PVD) capable of depositing up to 81 consecutive samples for the preparation of thin alloy films by plasma cosputtering. After analysis of the morphology, composition, and phase content of the samples prior to electrochemical stability testing, the catalytic OER activity screening has been performed on a multichannel rotating disk electrode (M-RDE) system. At the end of the screening process the final compositions were analyzed to determine if any corrosion occurred during the electrochemical testing.[149] Among the alloys studied several binary ones such as PtCo, PtNi, Pt_3Ni, and PtW_2,[150−152] as well as several ternary ones such as PtTiNi, PtNiCu and PtTiY beyond alloys of general formula PtTiMe (Me = Co, Cr, Cu, Fe, Mn, Mo, Ni, Pd, Ta, V, W)[149] were identified as candidates with enhanced catalytic activities and reasonable stabilities. Additionally, organometallic synthesis methods have been studied by this group to synthesize carbon supported alloy nanoparticles.[151] In DMFCs, the crossover of methanol results in a reduced ORR activity because of simultaneous competing reactions of the crossed-over methanol and oxygen at the cathode. Solutions for this problem are either the development of new low methanol crossover rate membrane materials or to improve cathode performance by developing methanol tolerant ORR catalysts. The advances on this field have recently been reviewed by McGinn, Woo, and co-workers.[153] The group also reports on a combinatorial library with 645 different compositions containing combinations of 1−4 different metals among Pt, Ru, Fe, Mo, and Se prepared by dispensing of precursor solutions on a PTFE-treated carbon paper using a microdispensing system. For electrochemical analysis via optical screening the synthesized library served as working electrode, Pt foil and an Ag/AgCl electrode as counter and reference electrode, respectively. As protons are consumed during the ORR fluorescein was applied as pH indicator to evaluate the ORR activity of the library in the presence of methanol. Later, the most active library member of composition $Pt_{50}Ru_{10}Fe_{20}Se_{10}$ was synthesized as powder and examined for the ORR both, with and without the presence of methanol. The addition of methanol caused a decrease in ORR current, but this decrease was much lower than for a Pt/C reference catalyst illustrating the high methanol tolerance of this new catalyst.

Cyclic voltammetry in a multichannel electrochemical cell instead of optical screening was used by McGinn and co-workers for the screening of thin film Pt alloy systems, including some ternary combinations of Pt, Ru, Co, Fe, Ni, Ta, W, C, Ti, Cu, and Cr.[154,155] A similar approach was used by Strasser et al. in the study of catalyst materials for lowering the necessary input power of electrochemical water splitting devices in acidic environments as proton exchange membrane fuel cell electrolyzers.[156] After production of catalysts by automated liquid-precursor impregnation using robotic liquid dispensing, these were tested by a high-throughput combinatorial electrochemical screening

platform consisting of 16 individually addressable, three-electrode chambers. It was shown that Ru-rich materials are better suited for the use as oxygen evolution reaction catalysts than Pt-, Ir-, Pd-, or Re-rich materials. A first example of the use of computational, density functional theory (DFT) based approaches to screen for improved electrocatalyst for the ORR has also been reported.[157] A descriptor-based approach based on binding energies, activation barriers, etc. applied to a database of DFT calculations on nearly 750 binary transition metal surface alloys was used to estimate the ORR activity of these alloys. The calculations include rigorous, potential-dependent computational tests of the alloy stability in aqueous, acidic environments. For this purpose potential-dependent free energies of oxygen adsorption were introduced. Addition of a water bilayer had no effect on the binding energy of atomic oxygen and therefore was neglected in this study, but appropriate zero-point energy and entropy correction were applied. The results of these calculations suggest that only very few surface alloys are likely to possess sufficient stability over extended periods of operation to serve as ORR catalysts. Among the 10 candidates with the highest stability 9 alloys have more than 2/3 Pt or Pd atoms in the surface layer, thus revealing that binary surface alloys without these elements are not likely to be suitable candidates for long-term use as ORR catalysts unless additional mechanisms can be identified to stabilize these materials. In alloys with more alloying components the probability to find more promising catalysts is even higher, especially those showing a high tendency of Pt to segregate to the surface and thus passivating the alloy.

A very similar situation with regard to preparation and screening techniques as well as element combinations is observed for the methanol electrooxidation side of the DMFC. HT syntheses of electrocatalyst libraries were performed either by thin film magnetron cosputtering with the help of shadow masks in the form of discrete samples,[158,159] in the form of continuous composition spreads,[160,161] by the $NaBH_4$ reduction method of metal precursor solutions on carbon paper,[162] or in a slurry of solvent and carbon powder.[158,163] HT screening of the resulting libraries supported on conducting substrates (glassy carbon or metal coated electrode wafers) was achieved either by cycling the potential in a multielectrode potentiostat system[158,159] exposed to the electrolyte at the same time[161] or separated by Teflon masks[162] or by a parallel-screening fluorescence assay initially developed by Reddington et al.[164] and adapted for the evaluation of continuous composition-spread thin film libraries.[160,165] The latter method was also applied by Welsch et al. for rapid optical DMFC electrocatalyst screening in a variant that allows also the quantification of the fluorescence development of up to 60 materials.[166] Only those materials were electrochemically tested, that brought along the required stability of the electrode catalysts toward acidic polymer membrane conditions. This was tested by an optical prescreening method with a commercial scanner and data acquisition software. Based on four elimination criteria, about 90% of the materials out of a test set of 1300 noble metal-free samples prepared by a sol–gel method and partially reduced in hydrogen were identified as acid instable and thus not electrochemically tested. All stable candidates were brought onto electrode spots of structured graphite plates and tested using quinine as a fluorescent reagent and a high-resolution CCD camera. Validation of hits was done by cyclic voltammetry (CV) measurements in a standard three-electrode cell. A comparison of the methanol oxidation current density and fluorescence intensity of a reference material $Pt_{50}Ru_{50}$ revealed that the onset of current density measured in a conventional CV setup shows a shift of about 60 mV to lower potentials compared with the optical

fluorescence intensity onset. This is due to pH differences in both electrolytes, whereas the pH of the electrolyte used in the fluorescence measurement had to be adjusted to pH = 6 to get no initial fluorescence signal. A review of reported elemental compositions of DMFC catalysts was also given,[166] based on the established system PtRu and classified into binary up to quaternary systems with and without Ru together with the associated references.

Several other identified fuel cell problems as cross-contaminations between half-cells or catalyst stability issues have been addressed in a number of papers. A complete electrochemical cell array containing a common air electrode and 16 microanodes for CHT screening of complete fuel cells using water-based electrolytes and polymer electrolyte membranes (micro-MEAs) with the possibility of cross-contaminations absent in single half-cell consideration was tested by Jiang.[167] The cell array was used to study 16 micro-DMFCs simultaneously including catalyst screening and determination of optimum operating conditions. Parameters as methanol concentration and composition of Pt/Ru black mixtures have been studied revealing a maximum in discharge performance at a methanol concentration of 1.5 M and highest catalytic activity at 98% Pt content for the current range between 0.2 and 3.0 mA. Another problem is the significant loss of electrochemical surface area (ECSA) over time during fuel cell operating as a result of an electrochemically driven dissolution of Pt metal at high potentials. Most significant at the cathode of PEMFCs this results in an agglomeration and growth of Pt nanoparticles on the carbonaceous support material termed as Ostwald ripening. Additionally dissolved Pt ions diffuse into the ion-exchange membrane and subsequently precipitate because of permeating hydrogen reduction inside the ionomer phase or at the interface of cathode and membrane.

A nanostructured thin film (NSTF) catalyst was developed by 3 M Company to overcome limitations in durability and specific activity by supporting Pt nanoparticles onto oriented, nanometer-sized crystalline organic wiskers, which are synthesized by sublimation and annealing of an organic pigment material based on a perylene dicarboximide compound.[168] The wiskers (see Figure 17) with a rectangular cross section have a density greater than 3 billion/cm^2 and loaded with catalysts by physical vapor deposition (PVD) methods. The surface structure of the crystalline whiskers facilitates metal nucleation resulting in whiskerettes increasing the surface roughness of a factor of 6 and maximizing the amount of Pt [111] surface facets. Significant advantages of the NSTF catalysts are their durability and specific activity in comparison to conventional carbon-supported dispersed Pt catalysts. Debe, Dahn, and co-workers[169] deposited a series of Pt-coated underlayer materials by a HT magnetron sputtering method on NSTF support wiskers for FC testing. Electrochemical testing of the composition spreads showed that Au and $TiSi_2$ underlayers and supports caused a loss of Pt ECSA during PEMFC operation with hydrogen and air in contrast to Al_2O_3 and TiC, which are promising underlayer materials on NSTF wiskers, because the Pt ECSA is stable through normal FC operation.[170]

Another field of heterogeneous catalysis, in which thin film deposition techniques for HT library preparation are applied, is photocatalysis. Kafizas and Parkin used combinatorial atmospheric pressure chemical vapor deposition (cAPCVD) to synthesize films with grating nitrogen dopant concentration and anatase–rutile phase mixtures on a single film.[171] The photocatalytic activities were screened using a novel high-throughput digital image color analysis method based on an "intelligent ink" formulated by

595

dx.doi.org/10.1021/co200007w |ACS Comb. Sci. 2011, 13, 579–633
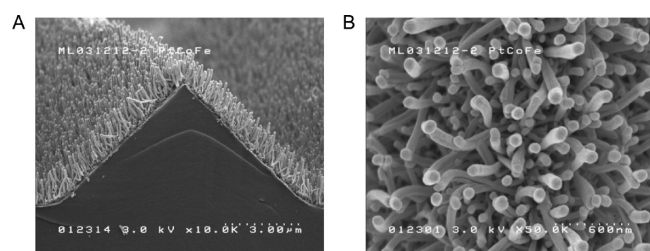
Figure 17. SEM images (A) NSTF whiskers coated/grown onto a microstructured substrate, which aids processing and increases surface area by a factor of $2^{0.5}$. (B) Top-view with increased magnification.[516]

Mills et al.[172] with the blue redox dye Resazurin and the sacrificial electron donor glycerol as components. A 13×19 grid was drawn with such ink on the prephotocatalytically charged combinatorial film. Photocatalytic reduction of the ink under 365 nm UV irradiation was monitored by a commercial photo scanner and software. After extraction of the red-green-blue values of 100 pixel areas centered on the grid positions plotting of the green component of digital color versus time revealed a minimum, which signifies maximum pink Resorufin intermediate formation and is directly related to the rate of photocatalysis. While N-doping of titania improved the electrical conductivity and stabilized the rutile phase, the photocatalytic activity under UVA light illumination correlated with the anatase content and film crystallinity.

A high vacuum combinatorial laser MBE system using PVD instead of CVD methods for thin film library deposition was used by Koinuma and co-workers.[173] The group investigated TiO_2 thin films gradually increasing in thickness to discover new phenomena indicating quantum size effects in titania photocatalysts. They observed an anomalously high activity at a film thickness of 5 nm indicative of a quantum size effect as the peak position changes depending on the wavelength of the UV irradiation. An overview on CHT approaches toward photocatalytic hydrogen production from water is also given by Seyler et al.[174] with details of sol—gel recipes that were tested for automated library synthesis of diverse binary oxides, bismuth oxides and aluminum—bismuth—lead ternary oxides. Starting with these diverse libraries and applying doping and preparation of composition spreads as tools of combinatorial chemistry, several new multicomponent photocatalysts for the production of hydrogen from aqueous methanol solutions have been discovered.

According to the European Technology Platform for Sustainable Chemistry (SusChem), alternative energy and fuels generation, effective energy transmission and distribution, high capacity energy storage and efficient energy management are all areas in which sustainable chemistry will bring viable solutions.[175] Catalysis and process intensification are regarded to efficiently harness energy resources, fields in which the application of CHT experimentation could dramatically improve performance and reduce costs in the discovery and study of new catalysts. The conversion of natural gas to syngas by autothermal reforming can be regarded as alternative route for the production of high value compounds, such as synthetic liquid fuels and oxygenated compounds. Alternative reforming processes are steam reforming and partial oxidation (non catalytic or catalytic), but the autothermal reforming reaction is revealing the advantage that it occurs at uniform temperature by balancing exothermic partial oxidation and endothermic steam reforming. Thus, external heating is reduced, hot spot formation in the catalyst bed is avoided and the risk of catalyst deactivation minimized. On the other side the needed thermal reversibility leads to strict limits on the maximum methane conversion and the control of H_2/CO ratio of the synthesis gas. The development of new catalysts by HTS became focus by Woo and co-workers, who investigated highest activity catalysts among 30 catalyst candidates consisting of Ni—M (M = Co, Fe, Ce) metal combinations impregnated on γ-Al_2O_3.[176] The screening was performed in a newly designed 32-channel reactor revealing Co and Fe not to be efficient promoters. After successful validation in a conventional single bed reactor 13.3 wt % CeO_2 and 5.54 wt % Ni supported on alumina was found to show highest activity for autothermal reforming of methane.

Triggered by the development of stationary, as well as mobile FC systems, as alternative energy sources renewed interest in the water gas shift (WGS) reaction and the demand for more efficient WGS catalysts emerged. For the conversion of gasoline into a hydrogen-rich gas for automotive PEMFCs the WGS reaction is commonly used to adjust the CO/H_2 ratio in syngas in order to remove CO from gas streams and to generate pure hydrogen. An overview of the present situation in this field has just been given by Yaccato et al.[177] summarizing applied catalysts and focusing also on the Partnership for a New Generation of Vehicle (PNGV) cost target of 150\$, which will be met with reactors of less than 6 L of volume and 3 kg in weight with cost/weight/volume modeling of WGS reactors based on ceramic monoliths washcoated with Pt on Ceria catalysts. By scanning mass spectrometry version 2 (SMS-II) primary screening and data analysis by mass balance plots the same group found that using supported noble metals as catalysts WGS and methanation compete with each other and hence the selectivity of the WGS reaction strongly depends on the temperature of the reaction, the type of noble metal used, as well as the noble metal dispersion. A new advanced noble metal WGS catalyst has been discovered, paramount for this being the development of time efficient and reliable combinatorial technologies for discovery and exploration of these novel materials. The screening method has also been used in the search for new NO_x abatement, low-temperature CO oxidation, VOC removal, and CO_x methanation catalysts.[178]

For the combinatorial discovery of active catalyst for CO oxidation also cataluminescence-based array imaging was reported for CHT screening.[179] Cataluminescence (CTL) is a form of chemoluminescence emitted during catalytic oxidation of combustible gases on the surface of solid catalysts in an atmosphere containing oxygen, which was discovered by Breysse et al. catalytically oxidizing CO on thoria.[180] There are two types of mechanisms for the CTL emission.[181] One is the recombinant radiation and the other is radiation from excited species in the gas phase. In the oxidation of CO on thoria, for instance, CO can be regarded as chemisorbed at the surface as CO^+ and O_2 as O^-. Both species generate at the surface a corresponding electron and hole, respectively (see Figure 18). After migration of the two species at the surface to each other, the desorption of a CO_2 molecule as product of the CO^+/O^- recombination is accompanied by the annihilation of the surface exciton and luminescence is emitted by recombination of electron and hole. For a broad application of CTL-based array imaging as HTS method important criteria for supported metal catalysts are independence from support material as well as independence from metal species deposited on the support. Both criteria seem to be fulfilled, as CTL emission is reported on various nanomaterials including TiO_2, Y_2O_3, Al_2O_3, $SrCO_3$, ZrO_2, ZnO, MgO, Fe_2O_3,

596

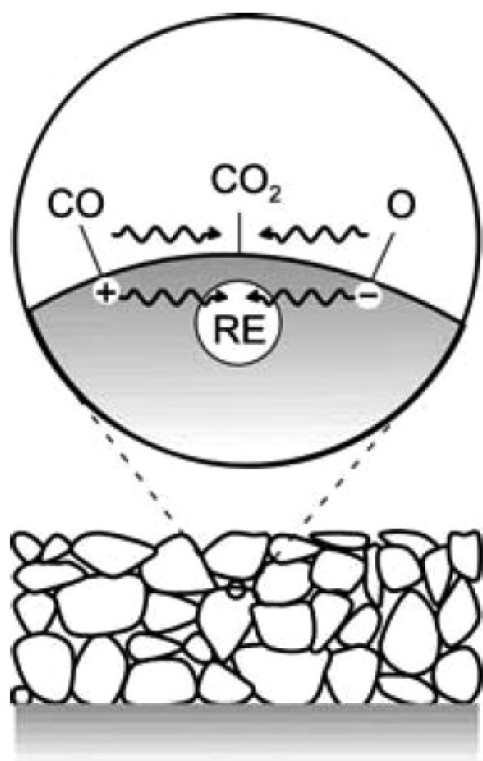dx.doi.org/10.1021/co200007w |*ACS Comb. Sci.* 2011, 13, 579–633

Figure 18. Schematic illustration of recombinant radiation CTL.[181]

and others (see ref 179) and different metals as Au, Pt, and bimetallic Au–Pt nanoparticles.[179] The 4 × 4 arrays of deposited nanosized catalysts with different metal loadings and atomic ratios on a ceramic chip were evaluated parallel to another by both CTL imaging and gas chromatography (GC) as active catalysts for CO oxidation. The correlation coefficient of these two techniques was 0.914 indicating that the CTL imaging method can be applied for the evaluation of catalytic activities. Just recently the sensitivity of the CTL reaction has been enhanced by plasma assistance.[182]

A comparison of literature data accumulated by HTS methods and validations experiments in single fixed bed reactor were also the purpose of an investigation by Oh and Woo in the field of NO selective catalytic reduction (SCR).[183] The catalytic reduction of NO_x in the presence of excess oxygen can be achieved either by lean reduction with hydrocarbons (HC-SCR) on Pt or Cu-based catalysts revealing useful NO_x conversion over broad temperature ranges or by ammonia addition (NH_3–SCR) with V_2O_5–WO_3 /TiO_2 or Fe exchanged zeolites as reduction catalysts and connected upstream or downstream Pt based oxidation catalysts for NO to NO_2 or NH_3 to N_2 oxidation. Pt as noble metal has not only the disadvantage of high expense but additionally produces between 200 and 300 °C significant amounts of the green house gas N_2O. Cu ion exchanges zeolites, especially Cu/ZSM-5, are also active in $deNO_x$ reactions, both the decomposition and SCR by hydrocarbons, but their commercial applications suffers from their low thermal stability, hydrocarbon slip, undesired selectivity toward CO, and low activity in the presence of H_2O and SO_2.

Earlier work by Ozturk and Senkan searching for new HC-SCR catalysts by screening single, binary, ternary, and quaternary combinations of 41 active elements on 13 different support materials showed that the combination of Cu and Os, in

particular 10% Cu and 1% Os on 13X zeolite, exhibited a high NO conversion at 250–600 °C even in the presence of 10% water vapor.[184] The conventional validation experiments by Oh and Woo[183] revealed that the catalytic performance of CuOs-13X without water presence agrees well with the literature, however addition of water lowers drastically the catalytic NO decomposition. According to TPD data this activity decrease was not reversible indicating that this effect was because of reaction inhibition, as well as catalyst deactivation. So the authors conclude that the observed differences in activity might be due to different kinetic properties and preparation as well as experimental conditions. Nevertheless, combinatorial high-throughput screening does not absolve from responsibility to perform validation experiments and further improvement will be required to determine accurate properties of catalysts from HTS.

The development of a technology platform for the investigation of NH_3–SCR and NO oxidation catalyst poisoning with combinatorial as well as rational methods has been described by the group of Claus.[185] This platform consists of a new HT screening method for SCR catalysts allowing fast discrimination of catalyst poisons under realistic conditions as well as a poisoning test possibility of monolithic segments of industrial series-production catalysts by passing inorganic aerosols over them. Thus a direct possibility for verification of high-throughput results in scales close to reality is given by the Claus group.

NO oxidation catalysts are also applied in automobile exhaust gas treatment systems to produce NO_2 for soot oxidation in continuous regenerating trap (CRT) systems of Diesel engines. Diesel engines are operated under lean conditions with an oxygen excess so that conventional 3-way catalysts optimized for an oxygen to fuel ratio $\lambda = 1$ are not working properly. Usually a Diesel particle filter (DPF) has an upstream oxidation catalyst system converting NO to NO_2, which combusts soot particles produced because of fuel properties and combustion mechanism.[186] Since particle and NO_x emission in a Diesel engine are inversely related to each other and future emission regulations will restrict the NO_x emissions drastically, Diesel engines in the near future will be adjusted to low NO_x/high soot emission, as soot combustion and SCR of NO_x together require rather costly additional exhaust gas treatment components.[187] With soot combustion alone these costs are reduced, but on the other side the need for new soot combustion catalysts operating at low temperatures even in the absence of NO_x is generated.

A combinatorial approach for the discovery of low temperature soot oxidation calalysts is presented by Olong and co-workers.[188] It was found that alkali mixed oxides have the potential to decrease the soot oxidation temperature to realistic Diesel exhaust temperatures below 400 °C. CHT screening hits were successfully confirmed by thermogravimetric analysis (TGA). Hensgen et al.[189] emphasized that combustion temperatures of particulate matter of Diesel automobile engines under lean conditions in laboratory experiments depend on a number of parameters such as model gas composition, gas flow rate, catalyst composition, catalyst micro structure, soot/catalyst ratio, model soot type (composition, particle size, and size distribution), and contact type. It seems that the last two factors are often underestimated. Thus, Hensgen et al.[189] investigated the influence of these factors. They also focused on finding a preparation technique for the soot-catalyst contact, which fulfills the criteria of high reproducibility, high comparability to real conditions, and facile automation. The last criterion has been the

basis for its use in CHT screening for parallelized discovery and optimization studies of new combustion catalysts.[189]

A vast number of heterogeneously catalyzed reactions have been also used for the synthesis of industrial mass products. Combinatorial screening has been applied to investigate the catalytic activity and selectivity of quaternary Mo—V—Te—Nb mixed oxide catalysts for the selective oxidation of propane to acrylic acid.[190] By treatment of salt solutions during preparation of catalyst libraries with various substances such as H_2O_2, I_2, V_2O_5, N_2H_4, $NaBH_4$, etc., instead of nitric acid and calcination of the resulting mixtures under nitrogen atmosphere final $Mo_1V_{0.33}$-$Te_{0.22}M_{0.11}O_x$ (M = Nb, Ni, Fe, Ce, Cu, and Co) catalysts were obtained. A computer-controlled 32-channel tubular reactor system developed for high temperature (>500 °C) catalytic reactions connected to a quadrupole mass spectrometer (QMS) was used for library screening. Only the first generation library catalyst containing Nb showed a catalytic activity toward acrylic acid. Chemical treatment with I_2 during preparation of the second generation library gave highest selectivity performance and acrylic acid yield. After scale-up this hit was validated in a conventional gas flow reactor. To optimize the preparation conditions the iodine species, its concentration and the pH value were varied in a third generation library. Good catalytic performance was observed for samples treated with 0.4 g I_2, 0.3 g HIO_3, and pH 6 during preparation. Characterization of the lead compound by XRD and XPS revealed a high degree of crystallinity compared to that of a reference catalyst and a Nb and Te enrichment at the surface of the catalyst resulting from the I-species treatment.

Synergetic effects in multimetallic systems were also reported by the group of Senkan[191] resulting from HT sol—gel synthesis and also HTS investigations of catalysts for the direct oxidation propylene with oxygen to propylene oxide. Focusing on the effects of metal loading, support material, and metal—metal interactions they found Cu on silica as support material prepared with dodecylamine as template at low Cu^{2+} loadings together with large metallic Ag particles to be responsible for propylene oxide gas phase formation. Further studies on the Ag—Cu and Cu—Mn systems to fully explore their potential are still necessary to optimize both catalyst preparation and reactor operation conditions. By the same preparation method several libraries containing about 600 ternary and quaternary mixed oxide samples were generated by Maier, Woo, and co-workers and screened for propane to acrolein selective oxidation reaction.[190] After directed evolution, it came clear that each system has its own optimum composition were acrolein formation is highest.

3.1.4. Influences of Preparation Effects. A comparative study of the WO_x dispersion on Mn-promoted tungstated zirconia isomerization catalysts prepared by conventional and CHT methods was presented by Hernández—Pichardo et al.[192] By isomerization of C5 and C6 light paraffin feedstocks to branched species aromatic hydrocarbons in gasoline pools can be substituted because of the high octane number of the branched species. Earlier studies on the isomerization of hydrocarbons[193] showed tungstated zirconia catalysts despite a low surface area to be active but their catalytic performance depending on the dispersion of the WO_x phase on the support. Because of a strong WO_x—ZrO_2 interaction the WO_x species are difficult to reduce, but this tendency is diminished as tungsten loading increases and nanostructures of polytungstates are converted into WO_3 crystallites. But in this case the accessibility of the WO_x species is reduced and less active catalysts are resulting. The addition of

hydrogen leads only in the case of intermediate-sized WO_x clusters to a reformation of active species, because for large WO_3 crystallites again high temperatures for reduction are needed. Whereas using a conventional coprecipitation method for preparation resulted in less-active catalysts because of low WO_x dispersion, a HTE approach gave Mn—WO_x—ZrO_2 oxides with a well-dispersed surface WO_x phase and an enhanced activity. Tungsten segregation at the surface and the mesoporous nature of the support both increase the catalytic activity improving the accessibility and probably the reduction of the polytungstate domains with intermediate size.

The influence of catalyst preparation conditions such as metal oxide loading, catalyst calcination conditions, catalyst pretreatment, as well as the reaction temperature and contact time on catalyst performance with the metathesis reaction of ethane and but-2-ene to propene as example were also discussed by Rodemerck et al.[194] It was concluded that the applied HT tools and methodology allowed a quick and reproducible synthesis of downscaled industrial catalysts as shown for the system Re_2O_7 on γ-Al_2O_3. The parallel tests revealed for these quite different catalysts reliable data under identical reaction conditions. Too low, as well as too high calcination temperatures and too long calcination duration, lowered the catalyst activity and resulted in fast deactivation by carbon deposition. It was found that Lewis acid sites are involved in the start of the metathesis reaction. By rising the Re content the Lewis acidity is increased, whereas Brønstedt acid sites were not detected.

3.1.5. Kinetic Studies. Data acquisition is not restricted to the determination of conversion and selectivity as function of several influencing parameters during catalyst preparation, as just discussed above, especially in later stages of the screening process during the development and optimization process of a new catalyst accurate kinetic data have to be accumulated to get quantitative information describing some catalyst features. In combination with CHT methodology the question arises whether this approach is adequate for the problem of kinetic modeling of diverse catalysts on a library with the ability to tackle apart from catalyst formulation parameters also deactivation phenomena such as carbon deposits, particle growth, metal—support interaction, alloy formation or demixing, catalyst poisoning, etc. During a CHT investigation using a parallel reactor assembly in particular the later issue may get critical, if the assembly allows only serially switching between the different samples, as during test of one sample the others may not be flushed by the reaction mixture and thus not allowed to deactivate. On the other side enabling a truly parallel operation of all reactors at the same time rises the problem of handling the different flow resistances of the various catalyst samples and generates the need also for a truly parallel or ultrafast analysis system.

Using a 16-channel multitubular reactor enabling the test of catalysts at the sample time-on-stream was presented by Morra et al.[195] For accessing intrinsic kinetic parameters for the hydrogenation of *o*-xylene they used a library of 80 diverse bimetallic catalysts and developed an adapted screening strategy to correct observed data from deactivation phenomena for the calculation of kinetic parameters. Analyzing effects of metal nature, dopants and supports on deactivation rate by a statistical approach they were able to give a tentative classification of the deactivation processes. Especially the coke formation rate on aged materials was the key parameter for this classification. Considering the whole studied library it was not obvious to determine which

598

dx.doi.org/10.1021/co200007w |*ACS Comb. Sci.* 2011, 13, 579–633

metal, dopant or support led significantly to a certain deactivation profile, whereas a tentative simplified classification between Ni-based and noble metal-based systems was still possible. But to combine catalysts features that direct the deactivation to either a linear or an exponential profile was not straightforward.

Another approach for CHT kinetic studies of hydrogenations with a combination of reaction and analysis was given by Trapp and co-workers.[196] The chromatographic techniques they used have the advantage that even complex reaction mixtures can be separated and quantified without any tagging of the analyte with marker molecules. Microfluidic devices combining chemical synthesis and analysis on one chip represent a clear enhancement in the field of parallelized kinetic measurements with minute material consumption. Unfortunately, at present they often suffer from the same limitation as commonly used batch reactors of studying only one reaction per run with consecutive steps of reaction, separation and quantification of starting materials and products to determine conversions thus leading to indefinable reaction kinetics in the case of competing reactions. Trapṕs group reported a strategy that allows the synchronous combination of heterogeneous catalysis and product separation as well as speciation in capillaries to perform HT reaction rate measurements of reactant libraries with an average frequency of 147 reactions per hour.[197] Microstructured reaction systems as GC columns have intrinsically a high specific interfacial area thus reducing the problem of an apparent reaction rate composing of intrinsic reaction rates and diffusion coefficients inherent in multiphase catalytic systems (gas—liquid—solid) typically used in industrial applications. Trapp et al. performed the hydrogenations with Pd nanoparticles as stationary phases between 60 and 100 °C at various contact times by on-column GC to determine temperature reaction rate constants and to obtain other activation parameters with a kinetic model based on the Langmuir—Hinshelwood mechanism with different Pd loadings. Additionally coefficients of molecular diffusion in the mobile and stationary phases have been determined by von Deemter plots for four substrates with precisely 2400 cm fused-silica columns of 250 μm inner diameter. This approach has recently been extended to Ullmann-type C—C cross coupling reactions.[198] Peak deconvolution of overlapping gas chromatographic elution profiles of constitutional isomers by multiple-reaction-monitoring mass spectrometry was described in detail.[199]

Additional examples of successful application of combinatorial and high-throughput methods in catalysis are also provided in recent reviews by Farrusseng[200] and by Yan et al.[201] Advances in combinatorial computational chemistry (CCC) have been recently reviewed by Koyama et al.[202] More and more CHT methods for synthesis and screening of catalysts became standard tools, they are integrated into the workflows and are not explicitly stated in publications anymore. Thus, many success stories, especially those from industry, may be found in patent literature or even remain unidentified.

3.2. Electronic and Functional Materials. In the area of electronic and functional materials, progress in combinatorial materials science over the last ten years is marked by the diversity in topics where CHT experimentation was successfully implemented and by significant advances in library fabrication and characterization techniques. Thin film libraries consisting of high quality epitaxial thin films are now routinely used to explore large compositional landscapes in search of compounds with enhanced physical properties. By far the most popular library design scheme is the composition spread or the phase spread approach, where composition regions of (pseudo)binary or (pseudo)ternary compositional phase diagrams are recreated and mapped in a continuous manner on a library chip or a wafer. This trend reflects the fact that it is relatively easy to design a composition spread library and that there are several thin film deposition techniques which are readily available for creating composition gradients. They include cosputtering, which can be used to generate natural composition gradients and the use of moving shutters to create thickness gradients. This trend also reflects the fact that more and more scientists are relying on the combinatorial strategy to investigate detailed composition dependent properties of materials as a function of continuously changing stoichiometry, rather than to explore hundreds to thousands of very different and discrete compositions at a time. This is also consistent with the fact that the general combinatorial approach is now accepted in the materials science community, not just as a tool of rapid search, but also as a tool for rapid delineation of composition-structure—property relationships.[11,203] In this section, we highlight some recent experiments where the composition spread was particularly instrumental in swiftly mapping how different functional properties vary against complex composition landscapes.

3.2.1. Combinatorial Investigation of Lead-Free Piezoelectric Materials. Among materials and chemicals designated as environmentally harmful, lead-containing compounds have been targeted by the community for removal and replacement. One area where replacement has been slow in being introduced is piezoelecrics, and Pb-based compounds, such as $Pb(Zr,Ti)O_3$ (PZT) still account for majority of the materials being used. The problem arises from the fact that there are very few compounds which possess the same high piezoelectric coefficient needed for important applications such as sonars, ultrasonic transducers, and airbag sensors.[204] To this end, the piezoelectric materials community has had a concerted effort in finding suitable replacements for PZT. Of particular challenge has been to find materials systems, which exhibit the morphotropic phase broundary (MPB) behavior displayed by PZT. At the MPB composition of $PbZr_{0.52}Ti_{0.48}O_3$, the material undergoes a structural transition from rhombohedral to tetragonal, and it shows a significant enhancement in piezoelectric properties. Because piezoelectric properties inherently arise from mechanical displacement at the unitcell level, the structural transition naturally plays a critical role in giving rise to the high value of the piezoelectric coefficient. Thus, it is of significant interest to find other materials systems, which may exhibit similar property enhancing structural transitions.[205]

In one study, as a starting compound to search for a novel lead-free piezoelectric material at an MPB, $BiFeO_3$ (BFO) was selected.[206] BFO is a multiferroic material with rich and intricate physical and chemical properties.[207,208] There are some guidelines which predict the presence of MPBs,[209−211] and one can explore novel compositions by systematically searching for similar structural transitions. In this study, composition spread techniques were applied to systematically look for MPBs. A series of pseudobinary composition spread epitaxial thin film libraries (200 nm thick) were fabricated on $SrTiO_3$ (STO) (100) substrates 6 mm long by the combinatorial pulsed laser deposition (PLD) system (Pascal, Inc.) at 600 °C, where a pseudobinary compositional phase diagram of $Bi_{1-x}(RE)_xFeO_3$ was continuously mapped on each chip, where RE denotes rare-earth.[206]

The PLD composition spread technique based on repeated alternating gradient deposition was adopted where gradient

599

dx.doi.org/10.1021/co200007w |*ACS Comb. Sci.* 2011, 13, 579–633
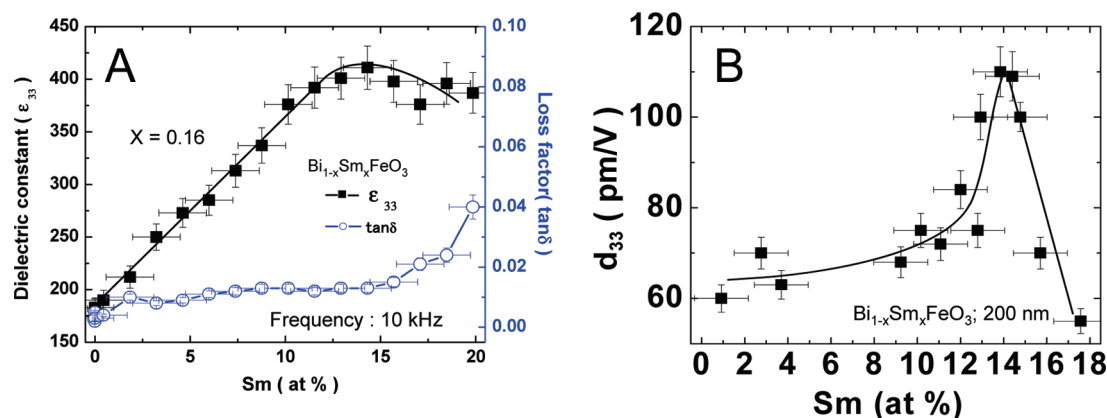
Figure 19. Discovery of a lead-free morhotropic phase boundary using the combinatorial approach. (A) Dielectric constant and tan δ measured for Sm substituted $BiFeO_3$. The dielectric constant shows enhancement at ~14% substituted composition; (B) Piezoelectric coefficient measured as a function of substitution composition. A sharp peak is observed at the same composition.[206]

thickness thin films of two targets are deposited whose compositions correspond to two end compositions of the spread.[212] Automated moving shutters are used to create the gradient thin films deposited under the epitaxial growth condition at an elevated temperature. To ensure uniform composition at each spot and a well controlled composition variation across the spread length, the thickness of thick end of each gradient is controlled to be less than a unitcell (~0.4 nm), and depositions are repeated hundreds of times in order to attain the total uniform thickness of ~200 nm across the spread. Composition variation across the spreads is confirmed by an electron probe (JEOL JXA-8900), and the uncertainty in the composition at each point on the spread is ±1.5%. This method was previously used to perform combinatorial mapping of a variety of materials systems.[213−216] This method is most effective in investigation of solid solution systems, where two end compositions are isostructural. For electrical characterization, an epitaxial $SrRuO_3$ (SRO) layer (50 nm) was used as the bottom electrode, and a sputter-deposited top Pd layer (50 nm) was patterned into 50 μm capacitor dots. Ferroelectric (FE) polarization hysteresis loops were obtained using the Radiant Precision LC. Quantitative piezoresponse force microscopy (PFM) was used to measure the out-of-plane piezoresponse. Initial PFM scans of a $Bi_{1-x}Sm_xFeO_3$ (BSFO) spread indicated significant enhancement of piezoresponse near $Bi_{0.8-0.85}Sm_{0.2-0.15}FeO_3$, where the structure undergoes substantial change in the out-of-plane lattice constant as detected by X-ray diffraction (XRD) mapping. In Figure 19 **A**, the out-of-plane dielectric constant (ε_{33}) and loss tangent measured at 10 kHz as a function of increasing Sm concentration are plotted. The dielectric constant reaches a maximum at $x = 0.14$ in agreement with the structural transition taking place at the composition. The loss tangent at this composition is relatively low (~0.01). These are characteristic properties of a high-quality dielectric material. The piezoelectric properties of BSFO were measured via quantitative PFM.[217] The effective piezoelectric coefficient d_{33} values were mapped across the composition spread (see Figure 19B). Around $x = 0.13−0.15$, the effective d_{33} displays a rapid increase peaking at $x = 0.14$ with 110 pm/V. Beyond this value, it rapidly decreases to ~55 pm/V for $Bi_{0.83}Sm_{0.17}FeO_3$. The measured remanent and high field d_{33} here are comparable to values previously reported for epitaxial thin films of Pb-based compounds such as PZT and $PbMg_{1/3}Nb_{2/3}O_3$—$PbTiO_3$. In comparing nominally similar thin film samples of the same thickness, the MPB discovered here

exhibits intrinsic piezoelectric properties which are among the best. The added advantage of the present system is a simpler crystal chemistry than some of the reported Pb-free compounds, as well as ease of processing.[205] High resolution planar transmission electron microscopy (A JEOL 2100 F operating at 200 kV) of an individual composition sample at $x \approx 0.14$ revealed presence of unusual nanoscale twined triclinic domains 20−50 nm in size displaying three different epitaxial orientations. The occurrence of nanosized twins and concomitant stress accommodation is known as a signature of an adaptive FE phase at the MPB, which could result in a high piezoelectric coefficient.[218]

These results had indicated that it is the chemical pressure effect due to the RE substitution into the Bi site, which induces a structural transition and the observed enhancement in dielectric and piezoelectric properties. Since the ferroelectric polarization mainly results from the 6s lone pair of the Bi ion in the A-site, introduction of dopants into B-site (Fe site) is expected to improve ferroelectric and dielectric properties without losing fundamental structural and ferroelectric properties of $BiFeO_3$. Thus, in the follow up study, the B-site substitution effect on the ferroelectric properties in $(Bi,Sm)FeO_3$ was investigated. In particular, to systematically track the relative effects of A-site and B-site doping, a combinatorial codoping investigation was carried out. Sc was chosen as the substitutional dopant for the B-site.[219] A Sc ion has a robust 3+ valence state which is unlikely to cause an increase in leakage current. The ionic radius of Sc^{3+} in 8-coordination is 0.0745 nm which is larger than the one for Fe^{3+}, 0.0645 nm. To make this library, the same moving shutter technique described above was implemented in pulsed laser deposition. To create the composition layout which contains continuous doping of both A and B-sites, the pseudoternary library design was used. In this design, concentration of the each dopant (A- or B-site dopant) varies along one of the sides of the triangle (Figure 20). This can be used to separate the A-site and B-site substitution effect. Ceramic sintered pellets of $Bi_{1.1}FeO_3$, $SmFeO_3$, and $BiScO_3$ were used as starting materials. The shutter mask design for generating appropriate thickness gradient films to fabricate the epitaxial ternary (pseudoternary) epitaxial composition spread was described by Koinuma and co-workers.[220] In Figure 20, all room-temperature FE hysteresis loops taken across the library are displayed at the positions of the top electrodes. For each loop, the horizontal axis spans −500 to 500 kV/cm for electric field, and the vertical axis is from −120 to +120 $\mu C/cm^2$
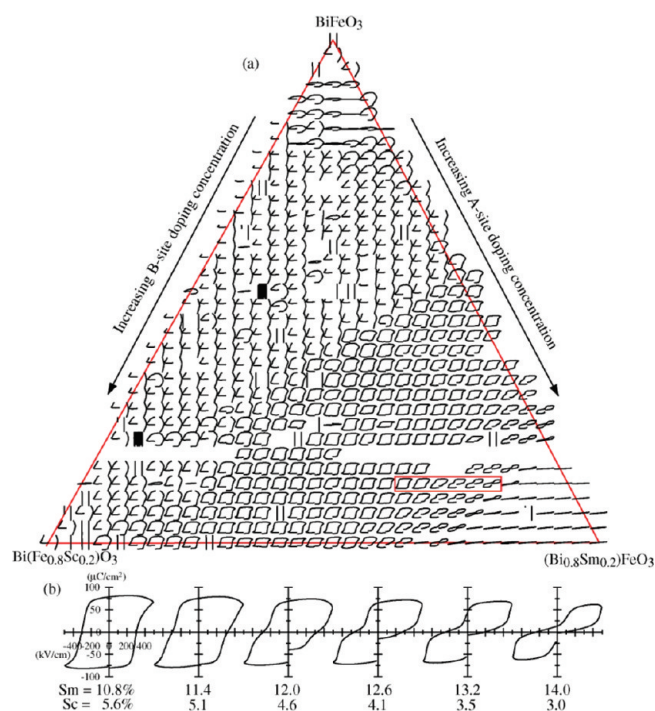
Figure 20. Pseudoternary codoping investigation of BiFeO₃. The library was designed to map (Bi,Sm)(Fe,Sc)O₃ compositions. Resulting ferroelectric polarization hysteresis loops measured at each spot are plotted. The zoom-up of the red highlighted region is plotted below.[219]

for polarization. Ferroelectric properties exhibit clear changes in response to the structural evolution induced by the substitution. In the region with lower dopant compositions, the unclosed loops are observed indicating that leakage current is too high. As the substitution of Sm and Sc is increased, the square-shaped ferroelectric hysteresis loop with the saturation polarization of about 70 μC/cm^2 begins to appear. This indicates that the substitution helps to reduce the leakage current. The fact that in the composition region where only Sc is substituted, the hysteresis loops are characteristic of leaky ferroelectrics suggests that the Sm doping is effective in reducing the leakage current as compared to Sc doping. As the Sm substitution reaches 14%, the ferroelectric hysteresis loops undergo a transition to double-hysteresis loops. This transition from the single to the double-hysteresis loop is clearly seen in Figure 20 where the FE hysteresis loops in the red box are separately plotted underneath. The FE hysteresis loop becomes distorted and the double-hysteresis behavior begins to appear as the Sm composition approaches 14%. Beyond this composition, the fully developed double-hysteresis loops are observed. The observed behavior is in a good agreement with previous observations for Sm-doped BiFeO₃ thin films.[206,221,222] These results imply that the B-site substitution does not affect this transition. As in the case of the structural transition, the evolution in the ferroelectric properties also takes place along the Sm composition axis and confirms that the substitution on A-site plays the main role on the both structural and ferroelectric properties. These series of discoveries have led to a number of groups around the world now investigating materials with similar compositions in bulk and in thin film forms.[223]

For many applications of piezoelectrics, the materials need to be in bulk forms. Thus, it is important to carry out the bulk scale-up experiments of discovered compositions in bulk. It is worthwhile to note that there are *bulk* composition spread

techniques.[203,224] Jones et al. have developed techniques which are effective in investigating how microstructural properties change as a function of composition in bulk diffusion couple samples where two end member composition samples are hydrostatically pressed together and then sintered to induce diffusion leading to occurrence composition gradient. While the composition gradient is not as extensive as in thin film spreads, important properties for bulk applications can be directly measured from such samples.

3.2.2. Thermoelectric Materials and Gate Stack Materials. Because of the recent surge in energy demand, the field of thermoelectric materials has seen much increased activities in research exploring novel thermoelectric materials. The efficiency of thermoelectric materials is defined by the dimensionless figure of merit ZT given by ZT = $S^2\sigma T/\kappa$. Here, T is the absolute temperature, S is the Seebeck coefficient, σ is the electrical conductivity, and k is the thermal conductivity. ZT is a direct measure of efficacy of thermoelectric power generation. There are only a handful of materials which are currently used for practical applications, and they generally have relatively low ZT values. They include Bi₂Te₃ and Bi₂Se₃, and the typical values of ZT are around 1. There have been a number of reports of combinatorial mapping of the Seebeck coefficient and electrical conductivity. Previously, pulsed laser deposition has been used to fabricate composition spreads of (Zn,Al)O and (Ca$_{1-x-y}$Sr$_x$La$_y$)Co₄O₉ systems.[225,226] In one recent experiment, a Ce—Co—Sn ternary composition-spread was fabricated using RF magnetron cosputtering.[227] The 50-nm-thick thin film spread was annealed at 325 °C. Ohtani et al. were able to use their new high-throughput screening system to map the electrical conductivity and the Seebeck coefficient across the ternary phase space as shown in Figure 21 where power factor ($S^2\sigma$) is plotted in the right-hand panel. In the conductivity map, the highest values of conductivity (10^5 Ω^{-1}cm^{-1}) were observed in the Co-rich composition region, while moderately high values were observed near the binary Co—Sn region. The Seebeck coefficient displays larger values in the pure elemental regions, and they are lower in the binary and ternary regions. Room temperature Seebeck values are negative cross the entire wafer, reflecting the fact that electrons are the main the charge carriers generating the thermal voltage. The power factor, although relatively small ($\sim10^{-3}$ W K^{-2} m^{-1}) shows maximum near the Co-region consistent with the fact that this is the region with highest electrical conductivity coupled with in moderately large Seebeck values in this composition range. Future studies will involve investigation of libraries annealed at different temperatures and mapping of thermal conductivity. Accurate quantative mapping of thermal conductivity mapping of thin film libraries has been a major challenge to the community. The difficulty arises from the fact that it is nontrivial to separate thermal conductivity of small volumes of thin films from that of the substrate. Accurate mapping of thermal conductivity combined with the other characterization tools will enable one to attain combinatorial mapping of ZT, the central figure of merit for thermoelectric materials.

Within the microelectronics industry, there is a perennial need to improve the gate stack (gate dielectric and the gate electrode) because of the continuous demands for higher performance field-effect transistors. While there have been many reports of combinatorial exploration of the gate dielectrics,[228,229] Chang et al. have focused their efforts on investigation of metal gate electrodes to replace the polycrystalline Si which suffers from excessive leakage current density.[230,231] Ni—Ti—Pt ternary
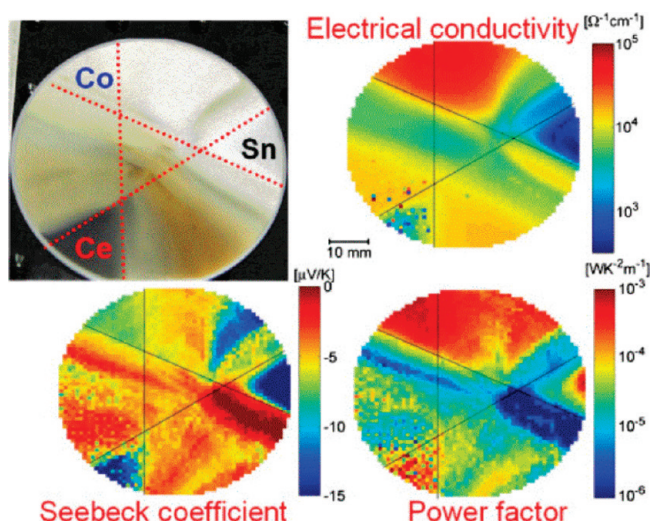
Figure 21. Composition spread exploration of thermoelectric materials. Picture of the Co−Ce−Sn composition spread wafer (upper left); Electrical conductivity map (upper right); Seeback coefficient map (lower left); Power factor map (lower right). Reproduced with permission from JJAP 48, 05EB02 (2009).

Figure 22. Exploration of novel gate electrode material. Leakage current density of sputtered Ni−Ti−Pt library is mapped. The dielectric was 6 nm HfO_2 on Si. From ref 230. Applied physics letters by AMERICAN INSTITUTE OF PHYSICS. Reproduced with permission of AMERICAN INSTITUTE OF PHYSICS. in the format Journal via Copyright Clearance Center.

composition spreads were fabricated using natural cosputtering. 50 nm thick library thin films were deposited on Si wafers coated with 6-nm-thick HfO_2 through a shadow mask so as to generate arrays of 250 μm × 250 μm capacitors with top metal electrode having continuously varying composition. Capacitance−voltage and current−voltage characteristics were measured for the hundreds of capacitors to attain mapping of the equivalent oxide thickness (EOT), flatband voltage, and the leakage current. EOT is an important figure of merit, and the International Technology Roadmap for Semiconductors dictates that EOT as thin as 0.8 nm is necessary for the next generation technology.[232] The library showed that because of the formation of interface oxide between HfO_2 and Si, the average value of EOT was 1.9 nm. Figure 22 shows the leakage current map measured at 1 V. High leakage is observed near Ti-rich composition, consistent with the fact that the extracted values of the work function are the lowest within the ternary in this region. This experiment demonstrated that one can use the combinatorial approach to effectively decipher the complex and convoluted issues of the work function, flatband voltage shift, oxide charge, and thermal stability for metal gate stack integration. There is large compositional phase space of metallic alloys to be explored for identification of the ideal metal electrode, and this is an important step in implementing the high-throughput strategy to materials topics which are established with advanced semiconductor manufacturing and processing technologies.

3.2.3. Combinatorial Mapping of Structural Phases Across Ternary Metallic Alloy Systems. There have been many other examples of combinatorial studies of metallic alloy systems. Among the notable developments are methodology for mapping the metallic glass and amorphous metal systems[233] and the use of molecular beam epitaxy for fabrication of epitaxial composition spreads in search of magnetic semiconductors.[234] These examples underscore the significance of tracking subtle structural changes across composition spread samples in pseudobinary and pseudomultinary solid solution systems. In other instances, it is of interest to map distribution of structural phases across, for instance, entire ternary phase diagrams containing compositions
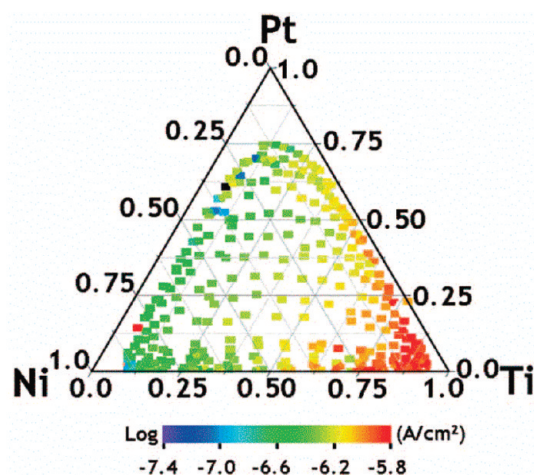
regions with vastly different structures. For such studies, full range XRD spectra need to be analyzed for the entire spread. This becomes a daunting task since one needs to analyze the details of a large number of diffraction spectra which are very different from each other. To reduce the difficulty of this task, tools and techniques, which can be used to analyze many diffraction spectra at once, instead of the traditional one at a time approach are being developed. In an earlier work, techniques for visualization of diffraction data from ternary composition libraries,[235] as well as clustering analysis to sort spectra into discrete groups in an effort to rapidly map the distribution of structural phases across ternary phase diagrams had been reported.[236] More recently, a technique called non-negative matrix factorization (NMF) has been applied to the problem of identifying the unique patterns which are present in a set of XRD spectra as well as quantifying the contribution of those patterns to each experimental spectrum.[237] As an example system, a composition region of the Fe−Ga−Pd ternary system was examined. The interest in the Fe−Ga−Pd ternary system stems from the fact that the Fe−Ga and Fe−Pd binary phase diagrams contain compositions with unusual magnetic actuator properties. Fe−Ga is a well-known material system exhibiting large magnetostriction for Ga content between 20 and 30 atomic percent. The origin of this property is attributed to the complexity of the Fe−Ga binary phase diagram in this region.[238] $Fe_{0.7}Pd_{0.3}$ is a ferromagnetic shape memory alloy[239] whose martensitic transition is associated with a magnetic field induced strain of about 10 000 ppm.[240] Given the significance of these compositions, it is of interest to see how structures and functional properties evolve across the Fe−Ga−Pd ternary phase diagram. Natural thin film composition spreads of the Fe−Ga−Pd system were deposited at room temperature using an ultra high-vacuum three gun magnetron cosputtering system on 3-in. (76.2 mm) diameter (100) oriented Si wafer. The samples were then post annealed. XRD of the fabricated films was performed using the ω-scan mode of the D8 DISCOVER using the two-dimensional detector. The composition spread wafer contained a grid of 1.75 mm × 1.75 mm squares with continuously changing

602

dx.doi.org/10.1021/co200007w |*ACS Comb. Sci.* 2011, 13, 579–633

composition, and XRD was performed on 273 patterned squares. The X-ray beam spot size was 1 mm diameter. Once the data acquisition was complete, the raw detector images were integrated to obtain 2θ angles and peak intensities.

NMF is a relatively new technique which has been applied to problems in several fields. NMF has been used to perform image segmentation,[241] document clustering,[242] and spectral unmixing of satellite reflectance data,[243] among other applications. To the best of our knowledge, this is the first time that it has been applied to XRD data. The basic idea of NMF is to deconvolve a large number of non-negative spectral patterns into a smaller number of non-negative basis patterns. The experimental patterns can then be described as a weighted superposition of the deconvolved basis patterns. We have two main reasons why we have chosen to use NMF over other multivariate techniques. First, since NMF describes experimental spectra as a superposition of basis patterns, it can easily handle diffraction patterns which result from mixtures of different crystal structures. This makes NMF a good choice when compared to techniques, which sort patterns into discrete groups. NMF therefore represents a significant improvement over our prior work using hierarchical clustering analysis.[236] Second, NMF produces basis patterns, which can be directly interpreted as diffraction patterns. This makes NMF a more suitable technique when dealing with XRD data in comparison to PCA since PCA produces basis patterns, which contain negative values. The inner workings of the NMF technique as applied to XRD analysis is detailed in ref 35. In the example of the Fe−Ga−Pd composition spread, nine basis patterns are found using NMF. There are several patterns, which are only present as mixtures in the experimental data, but which show up as separate patterns in the extracted basis patterns. This indicates that NMF can identify the correct basis patterns even when there are no end-members present in the data set. Figure 23 shows how one experimental XRD spectrum is separated into different weights of basis patterns.

To identify the structural phases corresponding to the basis patterns found using NMF, the basis patterns were compared to a set of reference spectra from the crystallographic databases available at NIST. In particular, we used the Inorganic Crystal Structure Database[244] and the NIST Structural Database.[245] Figure 24 presents a ternary diagram in which the weights of the basis patterns found using NMF have been represented as pie charts for each composition. Since the basis patterns found using NMF correspond to structural phases, this diagram gives us a quantitative distribution of structural phases as a function of composition, including the existence of multiphase regions. Although the full ternary phase diagram of this system is not available for comparison, the projection of the identified distributions to the two binary (Fe−Ga and Fe−Pd) systems matches the known phase diagrams reasonably well. The ultimate goal of this effort is to reach a point where the analysis of hundreds of XRD spectra automatically identifies all of the pure phases present in a system and quantifies the percent of each phase present for each composition. The work described here represents significant progress toward this goal.

3.3. Polymer-Based Industrial Coatings. Surface coatings are ubiquitous in our society. They are used largely to protect the underlying substrate, provide aesthetics to objects, and impart desirable surface characteristics such as lubricity, hydrophobicity, and antimicrobial activity. Polymer-based surface coatings or paints, commonly used in applications including building interiors and exteriors, industrial infrastructure, automobiles, ships, industrial equipment, and civil infrastructure include a large
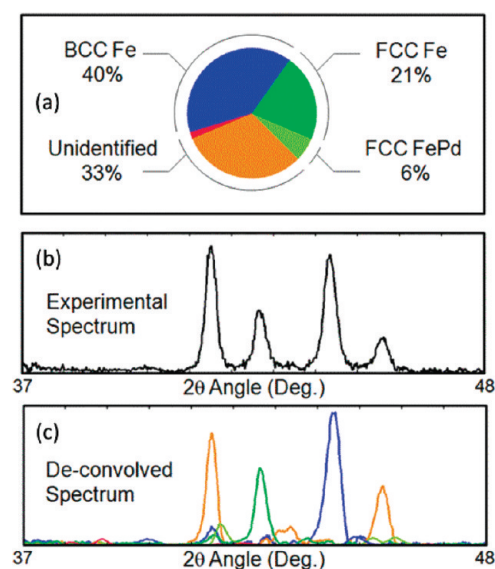
Figure 23. Non-negative matrix factorization of X-ray diffraction spectra from a combinatorial library. The weights of the basis patterns for the spectrum taken for $Fe_{0.46}Pd_{0.26}Ga_{0.28}$ (a). Experimental diffraction spectrum for this composition (b). The weighted basis patterns displaying the deconvolution of the experimental spectrum (c). From ref 237. Applied physics letters by AMERICAN INSTITUTE OF PHYSICS. Reproduced with permission of AMERICAN INSTITUTE OF PHYSICS. in the format Journal via Copyright Clearance Center.

number of ingredients to obtain the balance of properties required for the application. As a result of the compositional complexity of most coatings, extensive experimentation is required to develop an optimum coating composition. Considering the compositional complexity of polymer-based coatings, it was recognized that the application of CHT methods to coating research and development could have a major impact on the coatings industry.[246] Unlike more mature application areas for CHT technologies, such as drug discovery and catalyst discovery, the application of CHT methods to coating development was viewed as being particularly challenging because of the need to screen for multiple properties of interest. In essentially every case, a coating must exhibit multiple performance attributes to be of interest for further investigation. For example, a coating designed to protect a transparent plastic substrate, such as polycarbonate, in an application, such as an automobile headlamp, cover must exhibit excellent scratch/abrasion resistance, adhesion to the substrate, optical clarity, chemical resistance, weatherability, and resistance to environmental stress microcracking. Developing a CHT workflow that only screens one of these properties provides little value. An additional challenge associated with the application of CHT methods to coating development is that the performance attributes of interest can vary greatly depending on the end-use application. For example, the performance attributes of a coating designed to combat marine fouling of ship hulls will have a very different set of critical performance attributes than the aforementioned coating designed for automotive headlamps.

Because of the diversity of end-use applications associated with polymer-based coatings, much of the literature associated with the application of CHT methods to coating discovery/development has involved the development of high-throughput methods for various performance attributes. Properties that have been the focus of high-throughput method development include optical clarity,[247]
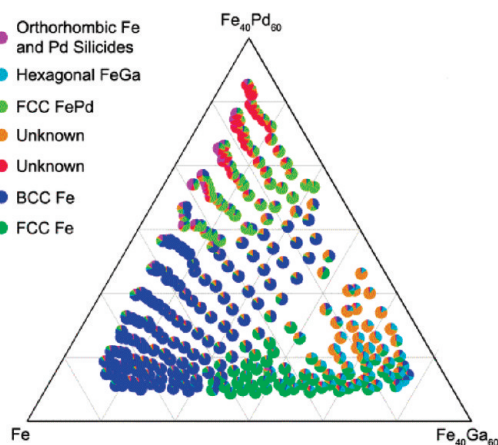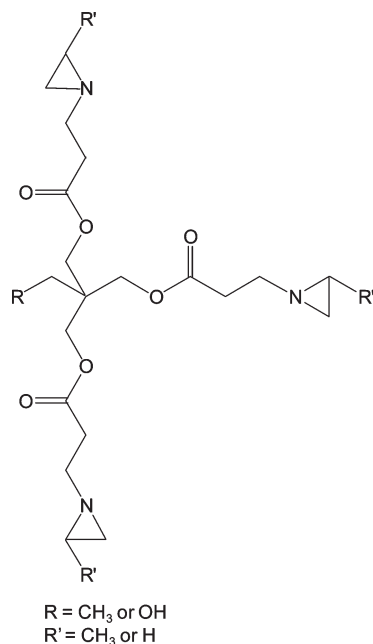
Figure 24. Structural phase diagram produced using the weights of the basis diffraction patterns found using non-negative matrix factorization (NMF). Each pie chart corresponds to a composition for which XRD was measured and each piece of the pie chart corresponds to the weight of one of the basis patterns found using NMF. Possible matches to a database of known patterns are presented at the top left. From 237. Applied physics letters by AMERICAN INSTITUTE OF PHYSICS. Reproduced with permission of AMERICAN INSTITUTE OF PHYSICS. in the format Journal via Copyright Clearance Center.

R = CH$_3$ or OH
R' = CH$_3$ or H

Figure 25. Chemical structure of the polyazirdine cross-linkers utilized by Bach and co-workers.[270]

adhesion,[35,247,248] abrasion/scratch resistance,[34,247] viscosity,[249] surface energy,[249−251] weatherability,[252] pot-life,[253] corrosion inhibition,[254] viscoelastic properties,[255] fouling-release,[256−262] antimicrobial properties,[263,264] scrub resistance,[265,266] hardness,[267] cross-link density,[268] and barrier properties.[269]

3.3.1. Cross-Linkers for Polyurethane Dispersions. The application of CHT methods to coating development is relatively new with the first description of a full CHT workflow being reported in 2002.[247] One of the first reports focused on the CHT production and characterization of coating libraries using a CHT workflow was that of Bach and co-workers.[270] This report pertained to the use of a CHT workflow to assess the relative degree of cross-linking for binders derived from polyurethane dispersions. The cross-linkers studied were polyaziridine compounds with the general structure shown in Figure 25. Polyazirdine cross-linkers react with carboxylic acid groups of water-dispersible polyurethanes to form an ester cross-link. The study involved variations in polyurethane composition, cross-linker composition, cosolvent composition, urethane dispersion pH, and the time period between cross-linker addition and film formation. The cross-linked networks were screened using a fluorescence assay that involved: (1) dissolution of a chemically inert fluorescent dye in the coating solution; (2) production of a cured film in a container using film casting; (3) extraction of a portion of the dye from the coating by the addition of a solvent to the container holding the cured film; and (4) quantification of the amount of dye extracted using a fluorescence intensity measurement. With this assay, it is assumed that lower fluorescence intensity is indicative of higher cross-link density. Several thousand coating films were screened in the study, and it was found that polyurethane composition and cross-linker concentration dominated the response. Polyaziridine cross-linker composition resulted in relatively small differences in cross-link density. A major observed second-order interaction was between cross-linker concentration and pH of urethane dispersion.

3.3.2. Polyurethane-Siloxane Fouling-Release Coatings. A large majority of the polymer-based coating libraries described

in the literature pertain to coatings designed to combat biofouling, primarily, marine biofouling. The Webster Research Group at North Dakota State University has been investigating the concept of producing tough, fouling-release coatings from cross-linked polyurethanes modified with polysiloxane segments.[271−273] With this concept, the lower surface energy polysiloxane was expected to self-segregate to the coating/air interface while the majority of the coating bulk was expected to be the tough polyurethane. With this morphology, good-fouling release properties were anticipated based on the low surface energy, PDMS-rich surface. Initial screening studies involved the production of coatings based on either aminopropyl-terminated polydimethylsiloxane (NH$_2$−PDMS−NH$_2$) or hydroxyethyloxypropyl-terminated polydimethylsiloxane (HOCH$_2$CH$_2$−PDMS−CH$_2$CH$_2$OH) as the PDMS component and isocyanurate trimers of isophorone diisocyanate or hexamethylene diisocyanate as the isocyanate component.[273] Numerous compositional variables were explored using CHT methods including siloxane content, solvent composition, and siloxane chemical composition. A total of 82 unique coating compositions were screened. High-throughput measurements of surface energy and pseudobarnacle adhesion were used to characterize coating surface compositional stability after water immersion and fouling-release properties, respectively. A key observation was that solvent composition played an important role in coating surface stability and fouling-release performance.

Follow-up efforts were focused on coatings derived from a hydroxy-functional PDMS, a trifunctional polycarprolactone polyol, and a polyfunctional isocyanate based on isophorone diisocyanate.[271] With this coating system, segregation of PDMS chain segments to the coating/air interface was demonstrated. Interestingly, coating compositions derived from the lowest concentration of hydroxy-functional PDMS, which was 10 wt %, showed a microstructured surface comprised of dispersed domains rich in PDMS with an average domain diameter of 1.4 μm and height of 50 nm. Surface microstructure was found to be dependent on solvent composition and mixing time after the addition of
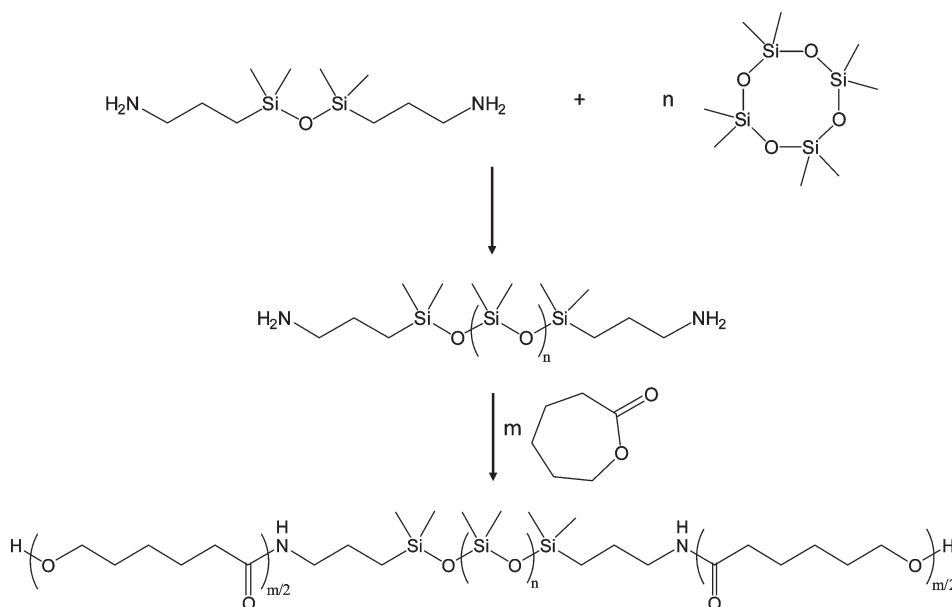
Figure 26. Synthetic scheme used by Ekin et al.[279] to produce amino-terminated PDMSs and hydroxy-terminated poly(ε-caprolactone)-b-PDMS-b-poly(ε-caprolactone) copolymers.

the isocyanate cross-linker.[274] After having demonstrated self-stratification of this coating system, a study was conducted that utilized high-throughput measurements of surface energy, contact angle hysteresis, pseudobarnacle adhesion,[275,276] and reattached barnacle adhesion[260] to investigate the effect of mixing time after the addition of the cross-linker on surface properties.[277] The results showed that coatings produced with longer mixing times were more homogeneous than those produced with shorter mixing times and provided better fouling-release properties as characterized using pseudobarnacle and reattached barnacle adhesion.

In addition to polyurethane-siloxane coatings based on hydroxy-functional PDMS, Ekin and Webster reported similar coatings based on NH_2–PDMS–NH_2, as well as hydroxy-terminated poly(ε-caprolactone)-b-PDMS-b-poly(ε-caprolactone) copolymers (PCL–PDMS–PCL).[272,278] The ability to synthesize and characterize arrays of NH_2–PDMS–NH_2 polymers and PCL–PDMS–PCL copolymers using the synthetic scheme shown in Figure 26 and high-throughput methods was demonstrated.[279] Polymers were prepared in 24-element arrays and characterized using high-throughput methods for measuring molecular weight, chemical composition, and thermal properties. Arrays of polymers were produced that possessed variations in PDMS and PCL block molecular weight. In addition to PCL–PDMS–PCL copolymers produced by reaction of NH_2–PDMS–NH_2 directly with ε-caprolactone (Figure 26), Ekin and Webster produced arrays of PCL–PDMS–PCL copolymers by first reacting NH_2–PDMS–NH_2 with ethylene carbonate to produce hydroxyalkyl carbamate-terminated PMDS polymers that were subsequently used to initiate ε-caprolactone polymerization, as shown in Figure 27.[280] This general synthetic method was also used to produce arrays of "H-type" block copolymers (Figure 28) by substituting ethylene carbonate with glycerine carbonate.

NH_2–PDMS–NH_2 polymers and PCL–PDMS–PCL copolymers synthesized according to the scheme shown in Figure 26 were incorporated into polyurethane coatings using a multifunctional isocyanate, trihydroxy-functional poly(ε-caprolactone),

cure catalyst, pot-life extender, and solvent.[272] The CHT experiment designed to investigate this compositional space involved variations in PDMS molecular weight, PCL block molecular weight, and PDMS content. In total, 192 unique coating compositions were prepared using multiple 24-element arrays. The high-throughput characterization tools utilized for the study enabled measurements of surface energy and pseudobarnacle adhesion. Measurements were made on "as produced" coatings as well as coatings conditioned in water for 30 days. In general, it was found that surface properties were largely unaffected by water immersion indicating a stable surface composition and morphology. The primary variables that affected surface energy and pseudobarnacle adhesion were the introduction of PCL blocks into the PDMS, PDMS molecular weight, and PDMS content. Coatings based on NH_2–PDMS–NH_2 polymers were found to result in lower pseudobarnacle adhesion than analogous coatings based on PCL–PDMS–PCL copolymers. With regard to PDMS content, higher levels of PDMS resulted in higher pseudobarnacle adhesion. Increasing PDMS molecular weight reduced surface energy, but increased pseudobarnacle adhesion.

NH_2–PDMS–NH_2 polymers and PCL–PDMS–PCL copolymers synthesized according to the scheme shown in Figure 4 were also incorporated into polyurethane coatings.[278] In addition to coatings based on the triblock copolymers, coatings were produced for the H-type block copolymers shown in Figure 28. A total of 288 unique coating compositions were prepared and screened using high-throughput measurements for surface energy, pseudobarnacle adhesion, and glass transition temperature (Tg). The compositional variables investigated were PDMS molecular weight, PCL block molecular weight, copolymer architecture (i.e., linear vs H-type), and PDMS content. Similar to the previous study based on PDMS polymers produced using the synthetic scheme shown in Figure 26, surface energy decreased with increasing PDMS molecular weight and was independent of PDMS copolymer architecture. With regard to pseudobarnacle adhesion, adhesion was lowest for coatings based on hydroxyalkyl carbamate-terminated PDMS polymers
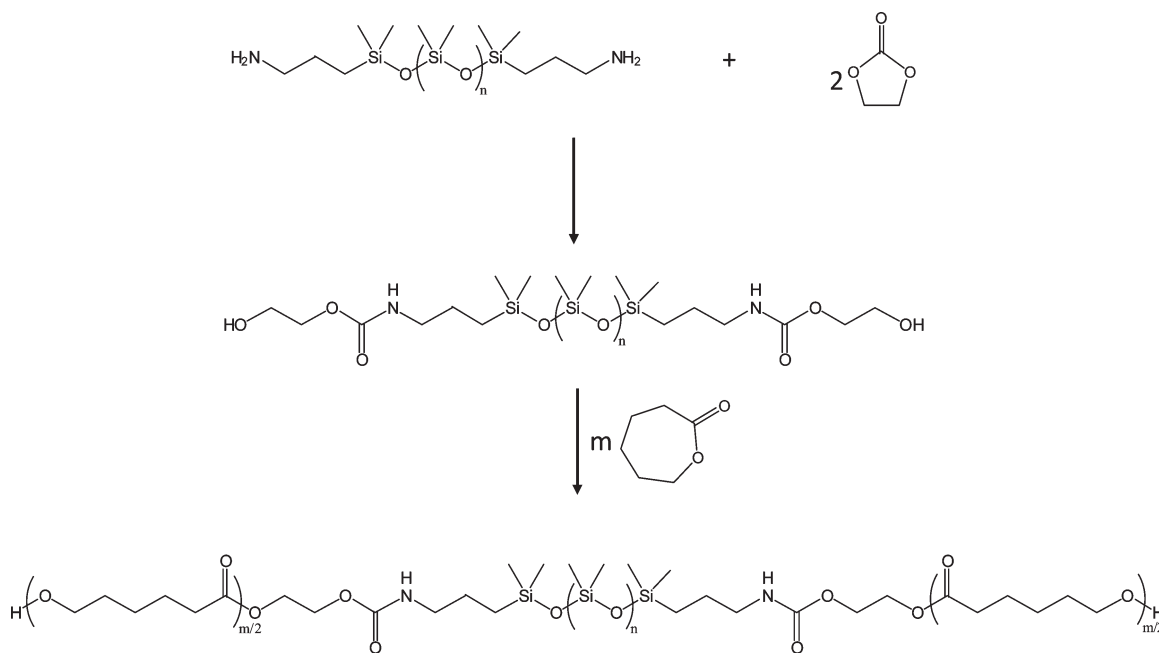
Figure 27. Schematic illustrating the synthetic method used by Ekin and Webster[280] to produce arrays of PCL—PDMS—PCL copolymers by first reacting NH$_2$—PDMS—NH$_2$ with ethylene carbonate to produce hydroxyalkyl carbamate-terminated PMDS polymers that were subsequently used to initiate ε-caprolactone polymerization.
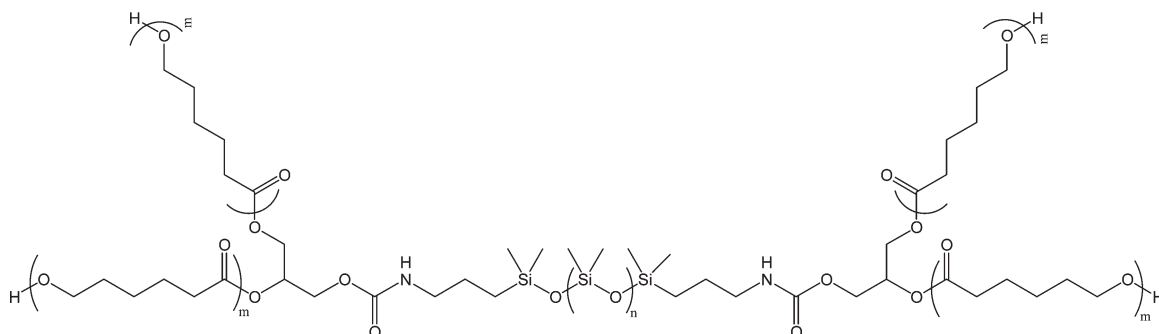

Figure 28. Chemical structure of "H-type" block copolymers produced by Ekin and Webster.[280]

(i.e., polymers free of PCL blocks) possessing a molecular weight greater than 15,000 g/mol. Coatings based on dihydroxyalkyl carbamate-terminated PDMS polymers showed higher pseudo-barnacle adhesion values compared to analogous coatings based on hydroxyalkyl carbamate-terminated PDMS polymers presumably due to the higher cross-link density associated with the tetrafunctional PDMS. Similar to the previous study, higher levels of PDMS resulted in higher pseudobarnacle adhesion strength. From the HT screening of the 288 unique coatings, eight coatings were selected for additional characterization. The coating subset possessed variations in PDMS molecular weight (10 000 g/mol and 35 000 g/mol), polymer functionality (di- vs tetrafunctional), and the presence of a PCL blocks (no PCL vs 3 PCL units per block). The concentration of PDMS in the coatings was kept constant at 20 wt %. With this coating subset, characterization included HT measurements of bacterial biofilm retention,[263] retraction,[258] and adhesion,[256] *Ulva* sporeling growth and removal,[281] and reattached barnacle adhesion.[260] In addition to the experimental coatings, two commercially available polysiloxane coatings were incorporated for comparison purposes. Overall, two

of the experimental coatings performed very well with regard to fouling-release properties and were targeted for scale-up and ocean testing.

More recent investigations by the Webster Research Group have involved the generation of siloxane-polyurethane coatings derived from acrylic polyols. Acrylic polyols have been tradition-ally used for polyurethanes because of the superior weatherability and hydrolytic stability, lower cost, and lower isocyanate require-ments compared to other polyols, such as polyether and polye-ster polyols.[282] A library of acrylic polyols was synthesized using a batch reactor system and conventional solution free-radical polymerization.[283] The acrylic monomers utilized were 2-hydro-xyethyl acrylate (HEA), butyl methacrylate (BMA), and *n*-butyl acrylate (BA). The library of acrylic polyols varied with respect to HEA content and BA/BMA ratio. A total of 24 different acrylic polyols were produced in a single run. The polyols were characterized using high-throughput methods for determining Tg, relative molecular weight, and molecular weight distribution. As expected, at a constant HEA repeat unit content, acrylic polyol Tg increased with decreasing BA/BMA ratio. At a constant
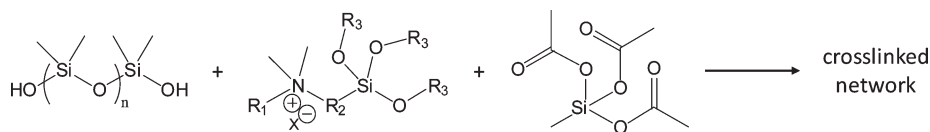
Figure 29. Description of the general compositional space investigated by researchers at the Center for Nanoscale Science and Engineering of the North Dakota State University for the production of antimicrobial coatings.

BA/BMA ratio, Tg increased with increasing HEA repeat unit content at high BA/BMA ratios, but converged to the same Tg (i.e., 10 °C) at a BA/BMA ratio of 0. Overall, the compositional space provided variations in acrylic polyol Tg ranging from −48 to 10 °C. These acrylic polyols were subsequently used to generate a 24-element array of siloxane-polyurethane coatings in which the siloxane component was derived from a 10 000 g/mol 3-aminopropyl-terminated PDMS. The library of siloxane-polyurethane coatings was produced by maintaining a constant molar ratio acrylic polyol hydroxy-functionality to isocyanate-functionality at 1.0/1.1 and a $NH_2-PDMS-NH_2$ content of 10 wt % based on coating solids. With this experimental design, a 24-element library was produced in which each acrylic polyol resulted in a single unique siloxane-polyurethane coating. The HT tools used for screening enabled measurements of coating Tg, water contact angle, pseudo-barnacle adhesion strength, algal biofilm removal,[261,262] and *Ulva* sporeling growth and removal. In general, results of the study showed that: (1) trends in coating Tg were similar to that of the acrylic polyols with Tgs ranging from approximately −22 to 50 °C; (2) all coatings were hydrophobic with water contact angles ranging between 95° and 100°; and (3) increasing BA and HEA repeat unit content in the acrylic polyol increased fouling-release properties toward both the algal species, *Navicula*, and *Ulva* zoospores.

3.3.3. Polysiloxane-Based Coatings Possessing Tethered Quaternary Ammonium Salt Groups. Researchers at the Center for Nanoscale Science and Engineering of the North Dakota State University have also been using CHT methods to investigate polysiloxane-based coatings possessing tethered quaternary ammonium salt (QAS) groups for combating marine biofouling.[284−288] The rationale for incorporating QAS groups into the polysiloxane matrix was based on the well-known inhibitory effect of QASs toward many microorganisms including Gram-positive and Gram-negative bacteria, yeasts, and molds.[289−293] The positively charged nitrogen atom of QASs can bind to the negatively charged cell wall of a microorganism resulting in disruption of the integrity of the cell wall and, as a result, cell death.[294,295] By tethering QASs groups to the polymer matrix, it was thought that an antimicrobial effect could be obtained without causing harm to the environment, which is stark contrast to current antifouling coatings that function by releasing copious amounts of biocide into the ocean.[296] The rationale for utilizing a polysiloxane-based coating was based on the good fouling-release properties previously observed for polysiloxanes.[297] Thus, in the event that adsorption of molecular species such as proteins or polysaccharides occurs and interferes with the antifouling effect, it may be possible to reactivate the antifouling effect by cleaning the coating surface. The general compositional space investigated is described in Figure 29. Initial C/HT experimentation to explore this compositional space involved variations in trimethoxysilane-functional QAS (TMS-QAS) composition, TMS-QAS concentration, and silanol-terminated PDMS (HO-PDMS−OH) molecular weight. A total of 75 unique coating compositions were prepared and screened using HT methods for measuring surface energy,

water contact angle hysteresis, leachate toxicity, bacterial biofilm retention, and algal biofilm growth. The results of the study showed that all three compositional variables influenced coating surface properties as well as antifouling and fouling-release characteristics. Interestingly, the incorporation of QAS moieties into a polysiloxane matrix generally resulted in an increase in coating surface hydrophobicity. Characterization of coating surface morphology revealed a heterogeneous, two-phase morphology for many of the coatings investigated. A correlation was found between water contact angle and coating surface roughness with the contact angle increasing with increasing surface roughness. Coatings derived from octadecyldimethyl(3-trimethoxysilylpropyl) ammonium chloride displayed the highest microroughness and, thus, the most hydrophobic surfaces. With regard to antifouling and fouling-release properties, coatings based on the 18 carbon QAS moieties (i.e., octadecyldimethyl(3-trimethoxysilylpropyl) ammonium chloride) were very effective at inhibiting *C. lytica* biofilm formation and enabling easy removal of *Ulva* sporelings (young plants); while coatings based on 14 carbon QAS moieties (i.e., tetradecyldimethyl(3-trimethoxysilylpropyl) ammonium chloride) were very effective at inhibiting biofilm growth of *N. incerta*.

Because of the antimicrobial activity exhibited by some of the QAS-functional PDMS coatings, the scope of the potential applications for these coatings was broadened to include biomedical applications, such as catheters, contact lenses, ophthalmic lenses, and medical implants.[298−300] In general, polysiloxanes have been shown to exhibit biocompatibility, and the ability to introduce antimicrobial properties via the incorporation of covalently bound QAS groups may enable the production of devices that reduce the occurrence of infection. In addition, unlike coatings that release an antibiotic to inhibit infection, these coatings should have a lower potential for producing resistant strains of microorganisms.[301,302] A study was conducted by Majumdar et al.[302] that involved the development of structure−antimicrobial relationships in which 20 different TMS-QASs were synthesized and incorporated into polysiloxane coatings to produce 60 unique coating compositions. Antimicrobial activity of the coatings was determined using three different, biomedically relevant microorganisms, namely, *Escherichia coli*, *Staphylococcus aureus*, and *Candida albicans*. This suite of microorganisms represents significant diversity considering that *E. coli* is a Gram-negative bacterium, *S. aureus* is a Gram-positive bacterium, and *C. albicans* is a yeast pathogen. The QAS-functional polysiloxanes were derived from solution blends of a HO−PDMS−OH, a TMS-QAS, and methylacetoxysilane. Since the QAS moieties provide antimicrobial activity through interaction with the microorganism cell wall, most of the compositional variables that were investigated were associated with the chemical structure of the TMS-QAS. The results of the study showed that essentially all of the compositional variables significantly influenced antimicrobial activity. Surface characterization indicated that the compositional variables also significantly affected coating surface morphology and surface chemistry.

Overall, compositional variables that produced heterogeneous surface morphologies provided the highest antimicrobial activity suggesting that the antimicrobial activity was primarily derived from the relationship between coating chemical composition and self-assembly of QAS moieties at the coating/air interface. Using data modeling software, a narrow region of the compositional space was identified that provided broad-spectrum antimicrobial activity. An optimized coating composition was further evaluated by coating sections of a urinary catheter and comparing the antimicrobial response of the coated catheter sections to uncoated catheter sections.[300] The coated catheter sections showed a 54%, 94%, 80%, and 89% reduction in biofilm formation for *E. coli*, *S. epidermidis*, *P. aeruginosa*, and *C. albicans*, respectively, compared to the uncoated catheter sections.
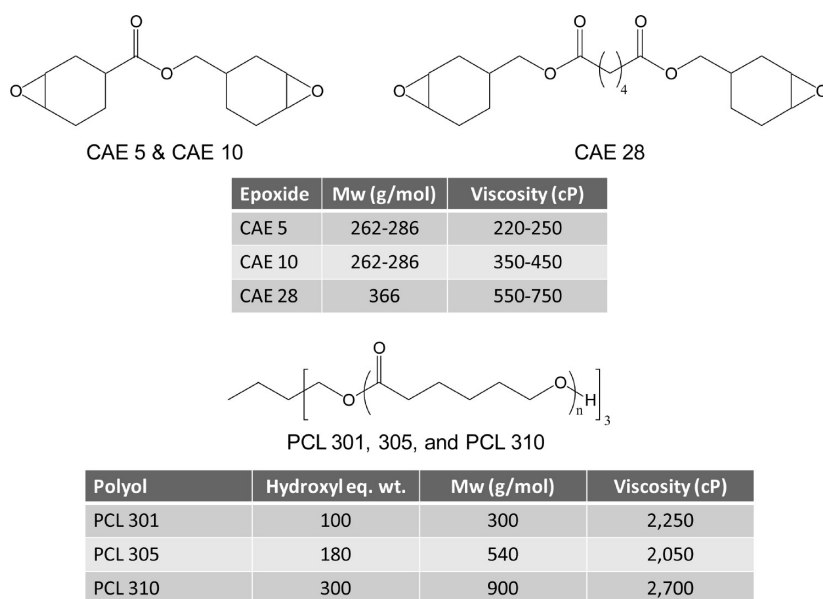
3.3.4. Polyurethane-Based Coatings Containing Tethered Triclosan Groups. In addition to antimicrobial coatings derived from tethered QAS moieties, researchers at the Center for Nanoscale Science and Engineering of the North Dakota State University have been investigating coatings derived from tethered triclosan moieties.[303−308] Triclosan (i.e., 5-chloro-2-(2,4-diclorophenoxy)phenol) is a broad-spectrum antimicrobial agent used extensively in personal-care products, healthcare, and household goods. It has been formulated into hand soaps, surgical scrubs, shower gels, underarm deodorants, toothpastes, hand lotions, and mouthwashes; incorporated into fabrics and plastics, such as children's toys, surgical drapes, cutting boards and toothbrush handles; and even infused into concrete for floors.[309] Kugel et al. investigated polyurethane-based coatings containing tethered triclosan groups using C/HT methods.[310] First, an array of acrylic polyols was produced using free-radical copolymerization of triclosan acrylate (i.e., 5-Chloro-2-(2,4-dichlorophenoxy)phenyl acrylate) (TA), HEA, and BA, as shown in Figure 30. The compositional parameters varied to produce the library included BA/TA ratio and HEA concentration. The array of acrylic polyols were characterized using nuclear magnetic resonance spectroscopy, DSC, and a HT GPC system. In addition, polymer yield was determined gravimetrically with the assistance of a parallel evaporator and a weighing robot. High yield (>90%) was obtained for each copolymerization and polymer composition was consistent with the monomer feed. With regard to thermal properties, Tg of the acrylic polyols increased with increasing TA content which was attributed to the relatively bulky triclosan-ester pendent group. From the array of acrylic polyols, a 24-element array of polyurethane coatings was produced using hexamethylene diisocyanate trimer and a 1.1/1.0 molar ratio of isocyanate functionality to hydroxy functionality. The coatings were characterized using a parallel DMTA measurements, automated surface energy measurements, and HT biological assays utilizing four different microorganisms, namely, *C. lytica*, *E. coli*, *Staphylococcus epidermidis*, and *Navicula incerta*. From parallel DMTA measurements, Tg was determined and two distinct trends were observed. First, at constant HEA content of the acrylic polyol, coating Tg increased with increasing TA content of the polyol. Second, at a given TA content, coating Tg increased with increasing polyol HEA content, which was attributed to obtainment of higher cross-link densities with higher HEA contents. With regard to antimicrobial properties, the coatings were found to be very effective at inhibiting *S. epidermidis* biofilm formation without leaching triclosan or other toxic components from the coating.
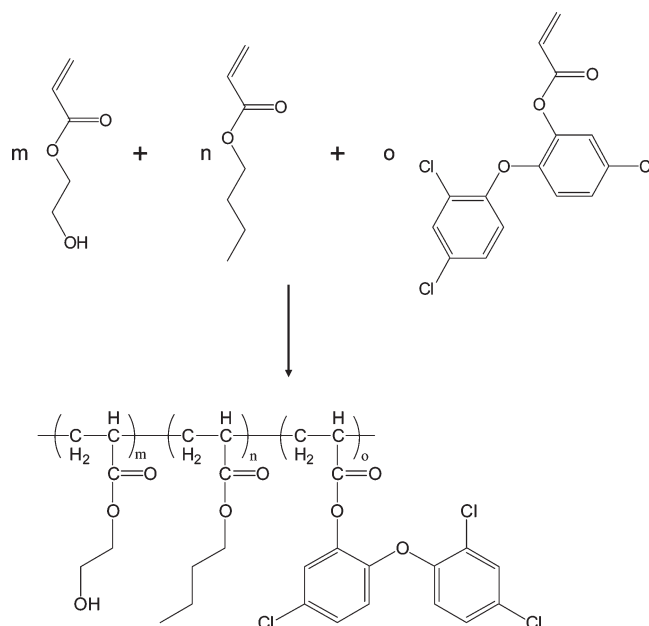
Figure 30. Synthetic scheme used to produce an array of polyols with triclosan pendent groups.[310]

3.3.5. Radiation-Curable Coatings. CHT methods have also been used to develop structure−property relationships for radiation-curable coatings. Uhl and co-workers[311] investigated a compositional space comprised of three different cycloaliphatic epoxides and three different polyester polyols, as shown in Figure 31. The experiment involved variations in epoxide composition, polyol composition, and the ratio of epoxy equivalents to hydroxy equivalents to produce three 24-element arrays of coatings in which each array was based on a single cycloaliphatic epoxide. The photoinitiator used for the study was a mixed arylsulfonium hexafluoroantimonate salt (UVI-6974 from Dow Chemical) that decomposes to produce a strong protic acid upon absorption of ultraviolet light. With this initiator, cross-linking occurs through a propagating oxonium ion.[312] The coatings produced were characterized using parallel DMTA measurements, automated surface energy measurements, and automated adhesion measurements. Some of the general trends observed were: (1) Tg varied as a function of cycloaliphatic epoxy composition with the higher molecular weight epoxide (CAE 28) resulting in lower Tgs; (2) coating Tg increased with an increase the ratio of epoxy equivalents to hydroxy equivalents; (3) although the nominal chemical structure of CAE5 and CAE10 were the same, differences in coating properties between analogous compositions were consistently observed; (4) storage modulus above and below the Tg was dependent on polyol composition; and (5) water contact angles did not vary significantly over the compositional space. Potyrailo and co-workers[313] also described the results of a C/HT experiment involving radiation-curable coatings. This work was focused on the HT screening of optical clarity and abrasion resistance of coatings produced in array format on a transparent, plastic substrate (i.e., polycarbonate). The report basically involved validation of the HT methods developed for screening optical clarity and abrasion resistance.

3.3.6. Hybrid Organic−Inorganic Coatings. Recently, a C/HT workflow was reported that was focused on the development

608

dx.doi.org/10.1021/co200007w |*ACS Comb. Sci.* 2011, 13, 579–633

Epoxide	Mw (g/mol)	Viscosity (cP)
CAE 5	262-286	220-250
CAE 10	262-286	350-450
CAE 28	366	550-750

PCL 301, 305, and PCL 310

| Polyol	Hydroxyl eq. wt.	Mw (g/mol)	Viscosity (cP)
PCL 301	100	300	2,250
PCL 305	180	540	2,050
PCL 310	300	900	2,700

Figure 31. Description of the coating components used by Uhl and co-workers[311] to investigate a compositional space based on ultraviolet light-curable coatings.

of hybrid organic—inorganic (HOI) coatings derived from sol—gel-type synthesis. The workflow,[314] shown schematically in Figure 32, was based on a tiered screening process in which "primary" screening was focused on identifying compositions that provide adequate solution stability and coating film forming characteristics. "Secondary" screening, which was designed to only be conducted on compositions that met solution stability and film forming requirements, involved measurements of corrosion protection. Initial experiments with this workflow involved screening of both "homogeneous" and "heterogeneous" HOI coatings. Homogeneous HOI materials are one-phase materials in which the organic and inorganic components are linked to each other through covalent bonds; while heterogeneous HOI materials are two-phase materials in which the domains sizes are in the nanometer scale.[315] With this definition, polymer composites based on micrometer-size inorganic fillers or fibers are not considered to be HOI materials. The library of homogeneous HOI coatings produced were derived from sols based on a trimethoxy or triethoxy silane, tetraethoxysilane (TEOS), water, acetic acid as a catalyst, and isopropanol as a solvent. The variables involved in the experiment which produced 60 unique compositions were trimethoxy or triethoxysilane composition, ratio of TEOS to trialkoxysilane, and mole ratio of water to alkoxysilane silane groups. Of the 60 compositions produced, 10 met the criterion for secondary screening (i.e., stable solution and tack-free/crack-free film). The 10 compositions identified with primary screening were all based on either methyltrimethoxysilane (MeTMS) or diethylphosphatoethyltriethoxysilane (DTES) as the trialkoxysilane component. Because of this result, a follow-up experiment was conducted that involved blends of MeTMS and DTES as the trialkoxysilane component. A total of 110 unique compositions were produced in this follow-up experiment. As a result of both primary and secondary screening, 4 compositions were identified for further experimentation in the development of new primers for protection of aluminum alloys from corrosion. One of the 4 homogeneous HOI compositions produced a primer that enabled good performance after 2500 h of ASTM B117 salt spray exposure.

In addition to homogeneous HOI compositions, compositions based on an approach that resulted in heterogeneous HOI coatings were screened.[314] The approach involved the reaction of colloidal silica nanoparticles with a trimethoxysilane. Three different trimethoxysilanes were used for the study. The three different trimethoxysilanes were phenethyltrimethoxysilane (PhEtTMS), (3-glycidoxypropyl)trimethoxysilane, and 2-(3,4-epoxycyclohexyl)ethyltrimethoxysilane. The variables investigated were trimethoxysilane composition, moles of trimethoxysilane per gram of colloidal silica, presence of a condensation catalyst (tetrabutylammonium fluoride), and reaction time. The results of the study showed that only coatings based on PhEtTMS enabled the production of stable, homogeneous coating solutions. Select compositions identified with the C/HT workflow were incorporated into primers and evaluated for their ability to protect the aerospace aluminum alloy from corrosion. The results of ASTM B117 salt spray testing showed excellent corrosion protection using one of the primers. There was essentially no visible evidence of corrosion in the scribe after 3100 h of salt spray exposure.

3.4. Sensing Materials. The broad goals of CHT development of sensing materials are to discover and optimize performance parameters and to optimize fabrication parameters of sensing materials.[19] The key performance parameters of sensing materials include sensitivity, selectivity, dynamic range, accuracy, response speed, recovery speed, shelf life, long-term stability, sample compatibility, mechanical robustness, resistance to poisoning, temperature range of operation, sterilizability, and some others. Factors affecting performance of sensing material films can be categorized as those originating from the sample (temperature stability, contaminating particulates, levels of interferences), sample/film interface (initial morphology, long-term surface contamination, long-term surface aging), the bulk of the film (initial film composition, microstructure, long-term material stratification, long-term aging of components), and the film/substrate interface (initial contact, long-term delamination).

For CHT screening, sensing materials candidates are arranged as discrete and gradient materials arrays. A wide variety of array

609

dx.doi.org/10.1021/co200007w |ACS Comb. Sci. 2011, 13, 579–633
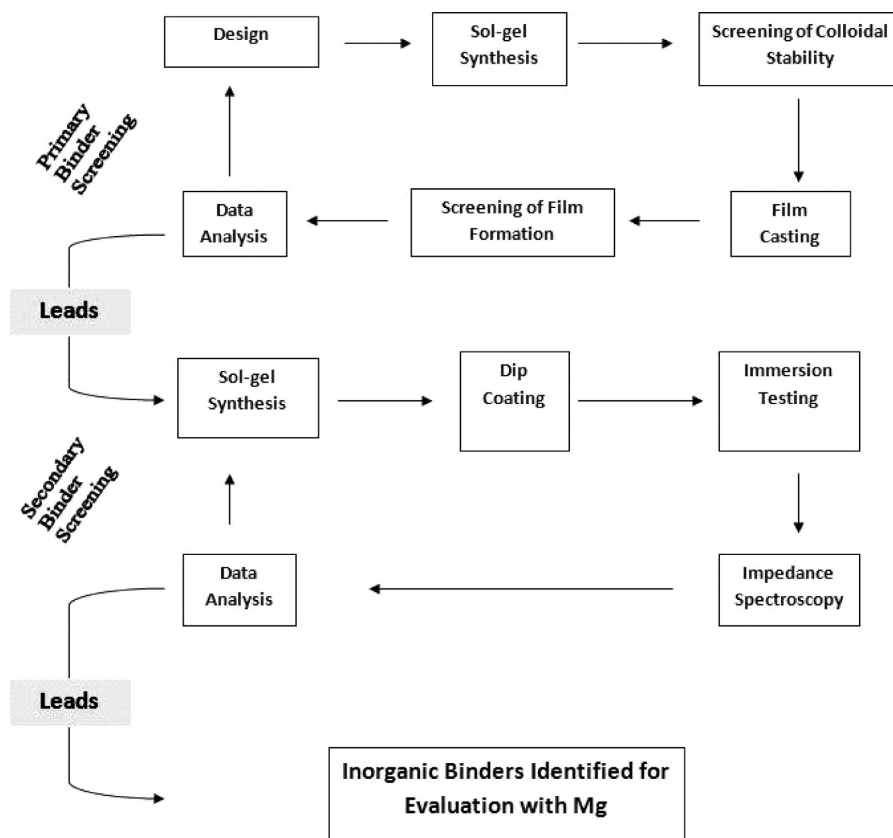
Figure 32. Schematic description of a C/HT workflow developed for the research and development of hybrid organic−inorganic coatings based on sol−gel processing.[314]

fabrication methods have been reported as summarized in Table 4.[316−344] A specific type of library layout depends on the required density of space to be explored, available library-fabrication capabilities, and capabilities of high-throughput characterization techniques. Upon array fabrication, the array is exposed to an environment of interest and steady-state or dynamic measurements are acquired to assess materials performance. Serial scanning mode of analysis (e.g., optical or impedance spectroscopies) is often performed to provide more detailed information about materials property over parallel analysis (e.g., imaging). When monitoring a dynamic process (e.g., response/recovery time, aging) of sensing materials arranged in an array with a scanning system, the maximum number of elements in sensor library that can be measured with the required temporal resolution can be limited by the data-acquisition ability of the scanning system.[338] In addition to measurements of materials performance parameters, it is important to characterize intrinsic materials properties.[40] Combinatorial development of sensing materials can be categorized based on sensors that utilize various energy-transduction principles for their operation that involve radiant, mechanical, and electrical types of energy.

3.4.1. Materials for Sensors Based on Radiant Energy Transduction. Sensors based on radiant energy transduction can be categorized on the basis of the five parameters that completely describe a lightwave, such as its amplitude, wavelength, phase, polarization state and time dependent waveform. The majority of the developed sensing materials for these types of sensors rely on the formulated colorimetric and fluorescent materials and intrinsically conducting polymers.

Optimizing formulated sensor materials is a cumbersome process because theoretical predictions are often limited by practical issues, such as poor solubility and compatibility of formulation components.[319,345−347] These practical issues represent significant knowledge gaps that prevent a more efficient rational design of formulated sensor materials. Thus, combinatorial methods have been employed for the development of multicomponent formulated sensor materials for gaseous[319,329,348,349] and ionic[320,337,338,350,351] species.

Applying polymers with an intrinsic conductivity also permits development of chemical and biological sensors based on radiant energy transduction.[352−356] A variety of conjugated organic monomers readily undergo polymerization and form linear polymers. For example, acetylene, *p*-phenylenevinylene, *p*-phenylene, pyrrole, thiophene, furane, and aniline form conducting polymers that are widely employed in sensors.[353,357−359] However, as prepared, conducting polymers lack selectivity and often are unstable. Thus, such polymers are chemically modified to reduce these undesirable effects. Modification methods include side-group substitution of heterocycles, doping of polymers, charge compensation upon polymer oxidation by incorporation of functionalized counterions, formation of organic−inorganic hybrids, incorporation of various biomaterials (e.g., enzymes, antibodies, nucleic acids, cells), and others.[357,360,361] Variations in polymerization conditions (e.g., oxidation potential, oxidant, temperature, solvent, electrolyte concentration, monomer concentration, etc.) can be also employed to produce diverse polymeric materials from the same monomer because polymerization conditions affect sensor-related polymers properties
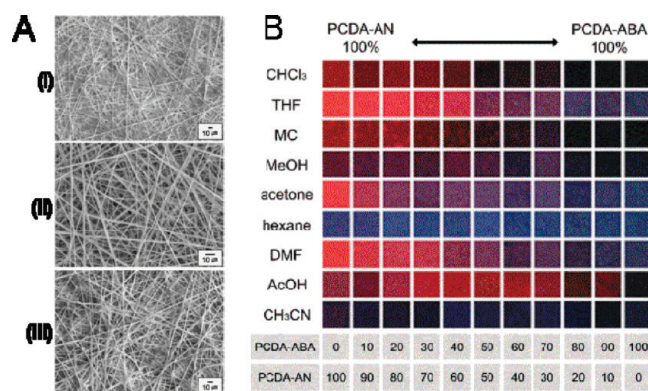
Table 4. Examples of Fabrication Methods of Discrete and Gradient Materials Arrays

| types of arrays of sensing materials	fabrication methods	ref
discrete arrays	ink jet printing	316–318
	robotic liquid dispensing	319, 320
	robotic slurry dispensing	321
	microarraying	322
	automated dip-coating	323
	electropolymerization	324, 325
	chemical vapor deposition	326
	pulsed-laser deposition	327
	spin coating	328, 329
	screen printing	330
	electrospinning	331
gradient arrays	in situ photopolymerization	332
	microextrusion	333–335
	solvent casting	336–338
	colloidal self-assembly	339
	surface-grafted orthogonal polymerization	340
	ink jet printing	341
	temperature-gradient chemical vapor deposition	326
	thickness-gradient chemical vapor deposition	342
	2-D thickness gradient evaporation of two metals	343
	gradient surface coverage and gradient particle size	344

Figure 33. Combinatorial approach for colorimetric differentiation of organic solvents based on conjugated polymer-embedded electrospun fibers. (A) SEM images of electrospun fiber mats embedded with (I) PCDA-ABA, (II) PCDA-AN, and (III) 1:1 molar ratio of PCDA-ABA and PCDA-AN after UV irradiation. (B) Photographs of the polymerized PDA-embedded electrospun fiber mats after exposure to organic solvents at 25 °C for 30 s.[331]

(e.g., morphology, molecular weight, connectivity of monomers, conductivity, band gap, etc.).[353,362]

Recently, a combinatorial approach for the colorimetric differentiation of organic solvents was developed utilizing intrinsically conducting polymers.[331] A polydiacetylene (PDA)-embedded electrospun fiber mat, prepared with aminobutyric acid-derived diacetylene monomer (PCDA-ABA), displayed colorimetric stability when exposed to common organic solvents. In contrast, a fiber mat prepared with the aniline-derived diacetylene (PCDA-AN) exhibited a solvent-sensitive color transition. Arrays of PDA-embedded microfibers were constructed by electrospinning poly-(ethylene oxide) solutions containing various ratios of two diacetylene monomers. Unique color patterns were developed when the conjugated polymer-embedded electrospun fiber arrays were exposed to common organic solvents in a manner which enabled direct colorimetric differentiation of the tested solvents. Results of these experiments are presented in Figure 33. The scanning electron microscopy (SEM) images of electrospun fiber mats encapsulated with DA monomers prepared from pure PCDA-ABA, pure PCDA-AN, and 1:1 molar mixture of PCDA-ABA and PCDA-AN are presented in Figure 33A. No significant morphological differences were observed among these electrospun fiber mats and polymer fibers with an average diameter of ∼1 μm. The color patterns of the combinatorial arrays of fiber mats derived from different combinations of DA monomers (see Figure 33B), demonstrated the significance of the combinatorial approach for sensor development. This methodology enables the generation of a

compositionally diverse array of sensors starting with only two DA monomers for the visual differentiation of organic solvents.

Optimization of concentrations of formulation components can require significant effort because of the nonlinear relationship between additive concentration and sensor response.[332,363–369] For detailed optimization of formulated sensor materials, concentration-gradient sensor material libraries were employed.[370] The one, two-, and three-component composition gradients were made by flow-coating individual liquid formulations onto a flat substrate and allowing them to merge under diffusion control when still containing solvents.[371] This method combines the fabrication of gradients of materials composition with recording the materials response before and after analyte exposure and taking the ratio or difference of responses. These gradient films were applied for optimization of sensor material formulations for analysis of ionic and gaseous species.[338,371] A very low reagent concentration in the film is expected to produce only a small signal change. The small signal change is also expected when the reagent concentration is too high. Thus, the optimal reagent concentration will depend on the analyte concentration and activity of the immobilized reagent.

Concentration optimization of a colorimetric reagent was performed in a polymer film for detection of trace concentrations of chlorine in water. A concentration gradient of a near-infrared cyanine dye was formed in a poly(2-hydroxyethyl methacrylate) hydrogel sensing film. The optical absorption profile $A_0(x)$ was obtained before analyte exposure to map the reagent concentration gradient in the film. A subsequent scanning across the gradient after the analyte exposure (1 ppm of chlorine) resulted in the determination of the optical response profile $A_E(x)$. The difference in responses, $\Delta A(x) = A_0(x) - A_E(x)$, revealed the spatial location of the optimal concentration of the reagent that produced the largest signal change (see Figure 34A). Sensing films with the optimized concentration of the cyanine dye for chlorine determinations in industrial water were further screen-printed as a part of sensing arrays[372,373] onto conventional optical disks. The quantitative readout of changes in film absorbance was performed in a conventional optical disk drive in a recently developed lab-on-a-disk system.[330,372–374]

This concentration-optimization method was also applied to optimize sensor material formulations for analysis of gaseous

611

dx.doi.org/10.1021/co200007w |*ACS Comb. Sci.* 2011, 13, 579–633
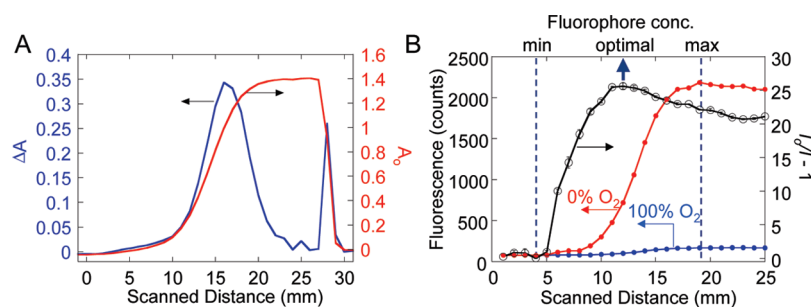
Figure 34. Optimization of formulated sensing materials using sensing films with gradient reagent concentration along the film length. (A) Concentration optimization of a colorimetric chlorine-responsive reagent in a formulated polymeric poly(2-hydroxyethyl methacrylate) hydrogel sensing film for detection of ions in water. Exposure, 1 ppm of chlorine. (B) Concentration optimization of an oxygen-responsive Pt octaethylporphyrin fluorophore in polystyrene sensing film for detection of oxygen in air.
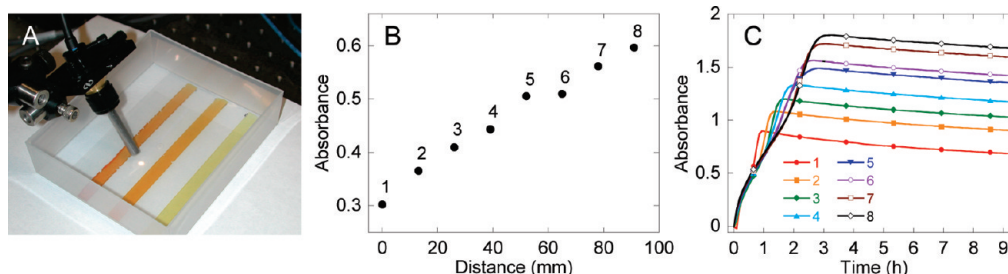
Figure 35. Application of gradient-thickness sensor film arrays for evaluation of reagent leaching kinetics. (A) Three gradient-thickness sensor film arrays with different loadings of an analyte-sensitive indicator. (B) Film thickness as a function of film length. (C) Reagent-leaching kinetics at pH10.[338]

species.[370] Figure 34B shows optimization of concentration of Pt octaethylporphyrin in a polystyrene film for detection of oxygen by fluorescence quenching. This data demonstrates the simplicity, yet tremendous value, of such determinations for the rapid assessment of sensor film formulations. It shows if the optimal concentration has been reached or exceeded depending on the nonlinearity and decrease of the sensor response at the highest tested additive concentration. Unlike traditional concentration optimization approaches,[366,369] the new method provides a more dense evaluation mesh and opens opportunities for time-affordable optimization of concentration of multiple formulations components with tertiary and higher gradients.[370]

The effect of thickness of sensing films on the stability of the response in water to ionic species has been also evaluated using gradient-thickness sensing films.[338] Sensor reagent stability in a polymer matrix upon water exposure is one of key requirements. For deposition of gradient sensor regions, several sensor coatings were flow-coated onto a 2.5-mm thick polycarbonate sheet. Typical coating dimensions were 1 − 1.5 cm wide and 10 − 15 cm long. To produce thickness gradients, the coatings were positioned vertically until the solvent evaporation in air at room temperature. The coating thickness was further evaluated using optical absorbance or profilometry. An example of a gradient sensor coating array is shown in Figure 35A. The gradient thickness of sensing films was determined from the absorbance of the film-incorporated bromothymol blue reagent (Figure 35B). When these arrays were further exposed to a pH10 buffer (Figure 35C), an "activation" period was observed before leaching of the reagent from the polymer matrix as detected from the absorbance decrease. This activation period was roughly proportional to the film thickness.

The leaching rate was independent of the film thickness as indicated by the same slopes of the response curves at 3−9.5 h exposure time.

3.4.2. Materials for Sensors Based on Mechanical Energy Transduction. Sensors based on mechanical energy transduction can be categorized on the basis of the transducer functionality that include acoustic-wave and cantilever devices. The mass loading and/or changes in the viscoelastic properties of the sensing materials lead to the transducer response.

Polymeric materials are widely used for sensors based on mechanical energy transduction because they provide the ability for room temperature sensor operation, rapid response and recovery times, and long-term stability over several years.[375−377] In gas sensing with polymeric materials, polymer − analyte interaction mechanisms include dispersion, dipole induction, dipole orientation, and hydrogen bonding.[378,379] These mechanisms facilitate a partial selectivity of response of different polymers to diverse vapors. An additional molecular selectivity in response is added by applying molecular imprinting of target vapor molecules into polymers and formulating polymers with molecular receptors. While there have been several models developed to calculate polymer responses,[380−384] the most widely employed model is based on the linear solvation energy relationships (LSER).[380,381] This LSER method has been applied as a guide to select a combination of available polymers to construct an acoustic wave sensor array based on thickness shear mode (TSM) resonators for determination of organic solvent vapors in the headspace above groundwater.[385] Field testing of the sensor system[386] demonstrated that its detection limit with available polymers was too high (several ppm) to meet the requirements for detection of groundwater contaminants. However, a new polymer has been found for sensing such as silicone block polyimide,
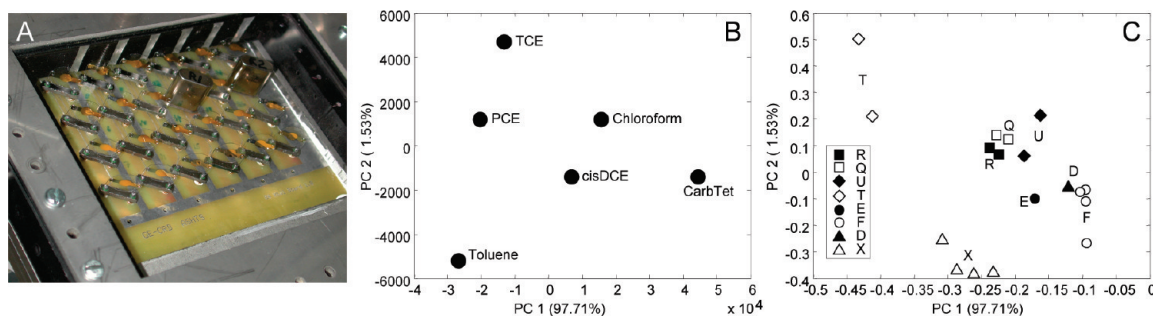
Figure 36. Approach for high-throughput evaluation of sensing materials for field applications: (A) Setup of a 24-channel TSM sensor array for gas-sorption evaluation of sorbing polymeric films (including two reference sealed crystals) in a gas flow cell; (B) scores;[389] (C) loadings plots of the first two principal components of developed PCA model for determination of differences in the response pattern of the sensor materials toward analytes (PCE, TCE, and *cis*-DCE) and interferences (carbon tetrachloride, toluene, and chloroform).[389]

that had the partition coefficient >200 000 to part-per-billion concentrations of trichloroethylene (TCE) and provided at least 100 times more sensitive response for detection of chlorinated organic solvent vapors than other known polymers.[376,387]

For development of materials for more selective part-per-billion detection of chlorinated solvent vapors in presence of interferences, six families of polymeric materials were fabricated based on silicone block polyimide. Performance of these polymeric materials was evaluated with respect to the differences in partition coefficients to analytes perchloroethylene (PCE), trichloroethylene (TCE), and *cis*-dichloroethylene (*cis*-DCE) and interferences (carbon tetrachloride, toluene, and chloroform). For quantitative screening of sensing materials candidates, a 24-channel TSM sensor system was built that matched a 6 × 4 microtiter wellplate format (see Figure 36A). The sensor array was further positioned in a gas flow-through cell and kept in an environmental chamber. A comprehensive materials screening was performed with three levels.[388,389] In the primary (discovery) screen, materials were exposed to a single analyte concentration. In the secondary (focused) screen, the best materials subset was exposed to analytes and interferences. Finally, in the tertiary screen, remaining materials were tested under conditions mimicking the long-term application. While all the screens were valuable, the tertiary screen provided the most intriguing data because aging of base polymers and copolymers is difficult or impossible to model.[390] From the tertiary screening, the decrease in materials response to the nonpolar analyte vapors and the increase in response to a polar interference vapor were quantified.

For the detailed evaluation of diversity of the fabricated materials, the PCA tools[95] were applied as shown in Figure 36B and C. The capability for discriminating of six vapors using eight types of polymers was evaluated using a scores plot (see Figure 36B). It demonstrated that these six vapors are well separated in the PCA space when these eight types of polymers are used for determinations. To understand what materials induce the most diversity in the response, a loadings plot was constructed (see Figure 36C). The bigger the distance between the films of the different types, the better the differences between these films. The loadings plot also demonstrates the reproducibility of the response of replicate films of the same materials. Such information served as an additional input into the materials selection for the tertiary screen. However, material selection on the basis of PCA alone does not guarantee optimal discrimination of particular vapors in the test set, because PCA measures variance, not discrimination.[379]

This 24-channel TSM sensor array system was further applied for the high-throughput screening of solvent-resistance of a family of polycarbonate copolymers prepared from the reaction of bisphenol A, hydroquinone, and resorcinol with the goal to use these copolymers as solvent-resistant supports for deposition of solvent-containing sensing formulations.[391] During the periodic exposure of the TSM crystals to polymer/solvent combinations,[323] the mass increase of the crystal was determined which was proportional to the amount of polymer dissolved and deposited onto the sensor from a polymer solution. The high mass sensitivity of the resonant TSM sensors (10 ng), use of only minute volume of a solvent (2 mL), and parallel operation (matching a layout of available 24 microtiter wellplates) made this system a good fit with available polymer combinatorial synthesis equipment. These parallel determinations of polymer–solvent interactions also eliminated errors associated with serial determinations. The data was further mined to construct detailed solvent-resistance maps of polycarbonate copolymers and to determine quantitative structure–property relationships.[90] The application of this sensor-based polymer-screening system provided a lot of stimulating data, difficult to obtain using conventional one-sample-at-a-time approach.

To eliminate the direct wiring of individual TSM sensors and to permit materials evaluation in environments where wiring is not desirable or adds a prohibitively complex design, a wireless TSM sensor array system[392] was developed where each sensor resonator was coupled to a receiver antenna coil and an array of these coils was scanned with a transmitter coil (Figure 37A). Using this sensor wireless system, sensing materials can be screened for their gas-sorption properties, analyte-binding in liquids, and for the changes in chemical and physical properties upon weathering and aging tests. The applicability of the wireless sensor materials screening approach has been demonstrated for the rapid evaluation of the effects of conditioning of polymeric sensing films at different temperatures on the vapor-response patterns. In one set of high-throughput screening experiments, Nafion film-aging effects on the selectivity pattern were studied. Evaluation of this and many other polymeric sensing materials lacks the detailed studies on the change of the chemical selectivity patterns as a function of temperature conditioning and aging. Conditioning of Nafion-coated resonators was performed at 22, 90, and 125 °C for 12 h. Temperature-conditioned sensing films were exposed to water (H_2O), ethanol (EtOH), and acetonitrile (ACN) vapors, all at concentrations (partial pressures) ranging
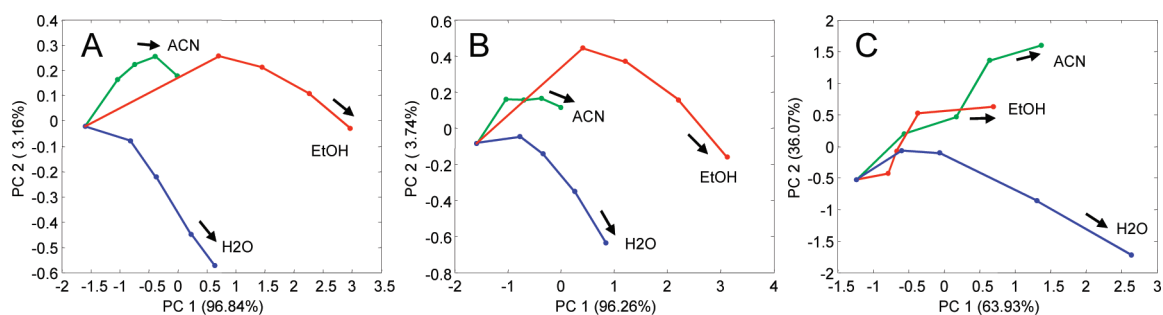
Figure 37. Wireless high-throughput screening of materials properties using thickness shear mode resonators. Evaluation of selectivity of Nafion sensing films to several vapors after conditioning at different temperatures: (A) 22, (B) 90, and (C) 125 °C. Vapors: H_2O (water), EtOH (ethanol), and ACN (acetonitrile). Concentrations of vapors are 0, 0.02, 0.04, 0.07, and 0.10 P/P_o. Arrows indicate the increase of concentrations of each vapor.[392]

from 0 to 0.1 of the saturated vapor pressure P_o as shown in Figure 37 B–D. It was found that conditioning of sensing films at 125 °C compared to room temperature conditioning provided (1) an improvement in the linearity in response to EtOH and ACN vapors, (2) an increase in relative response to ACN, and (3) a 10-fold increase of the contribution to principal component 2. The latter point signifies an improvement in the discrimination ability between different vapors upon conditioning of the sensing material at 125 °C. This new knowledge will be critical in designing sensors for practical applications where the need exists to preserve sensor response selectivity over the long exploitation time or when there is a temperature cycling for an accelerated sensor-film recovery after vapor exposure.

Other materials for sensors based on mechanical energy transduction that were explored using CHT techniques are alkane thiol materials. A 2-D multiplexed cantilever array platform was developed for an elegant combinatorial screening of vapor responses of alkane thiols with different functional end groups.[393,394] The cantilever sensor array chip (size 2.5 × 2.5 cm) had ~720 cantilevers and was fabricated using surface and bulk micromachining techniques. The optical readout has been developed for parallel analysis of deflections from individual cantilevers. To evaluate the performance of this 2-D sensor array for screening of sensing materials, nonpolar and polar vapors such as toluene and water vapor were selected as analytes. The screening system was tested with three candidate alkane thiol materials as sensing films with different functional end groups such as mercaptoundecanoic acid SH–$(CH_2)_{10}$–COOH (MUA), mercaptoundecanol SH–$(CH_2)_{11}$–OH (MUO), and dodecanethiol SH–$(CH_2)_{11}$–CH_3 (DOT). Each type of sensing films had a different chemical and physical property because –COOH group is acidic in nature and can dissociate to give –COO– group, –OH group does not dissociate easily but can form hydrogen bonds with polar molecules, and –CH3 group would be inert to polar molecules and the only interactions that it can have are from van der Waals and hydrophobic effects.

3.4.3. Materials for Sensors Based on Electrical Energy Transduction. Sensors based on electrical energy transduction utilize sensing materials that undergo electrically detectable changes, for example changes in resistance, capacitance as related to different mechanisms of material-analyte interactions. Typical devices for these applications include electrochemical and electronic transducers.[395–399]

The simplicity of microfabrication of electrode arrays and their subsequent application as transducer surfaces makes sensors based on electrical energy transduction a very attractive platform

for construction of discrete arrays for screening of sensor materials. The possibility to regulate polymerization on solid conductive surfaces by application of corresponding electrochemical potentials suggested a realization of this process in the form of multiple polymerization regions on multiple electrodes of an electronic sensor system.[324,400] Arranging such polymerization electrodes in an array eliminated the need for dispensing systems and allowed an electrically addressable immobilization. This approach has been demonstrated on electropolymerization of aniline that was independently performed on different electrodes of the array.[324,400] Thin layer polymerization of defined mixtures of monomers was performed directly on the 96 interdigital addressed electrodes of an electrode array on an area of less than 20 mm ×20 mm (see Figure 38A). The electrodes had an interdigital configuration designed for four-point measurements and fabricated by lithography on an oxidized silicon wafer. Using this electropolymerization system, numerous copolymers have been screened.[19] An introduction of nonconductive monomers into polymer decreased the polymer conductance and therefore decreased the difference between conductive and insulating polymer states. This has caused the decrease of the absolute sensitivity (Figure 38B). Normalization to the polymer conductance without analyte exposure compensated this effect and demonstrated that the polymer synthesized from the mixture of aminobenzoic acid and aniline possessed the highest relative sensitivity (Figure 38C). This effect may be explained by the strong dependence of polymer conductance on the defect number in polymer chains. In comparison with pure polyaniline, this copolymer had better recovery efficiency but a slower response time (Figure 38D, E). The developed high-throughput screening system was capable of reliable ranking of sensing materials and required only ~20 min of manual interactions with the system and ~14 h of computer controlled combinatorial screening compared to ~2 weeks of laboratory work using traditional electrochemical polymer synthesis and materials evaluation.[324]

Semiconducting metal oxides is another type of sensing materials that benefits from the combinatorial screening technologies. Semiconducting metal oxides are typically used as gas-sensing materials that change their electrical resistance upon exposure to oxidizing or reducing gases. While over the years, significant technological advances have been made that resulted in practical and commercially available sensors, new materials are being developed that improve further sensing performance of these sensors. To enhance the response selectivity and stability, an accepted approach is to formulate multicomponent materials

614

dx.doi.org/10.1021/co200007w |*ACS Comb. Sci.* 2011, 13, 579–633
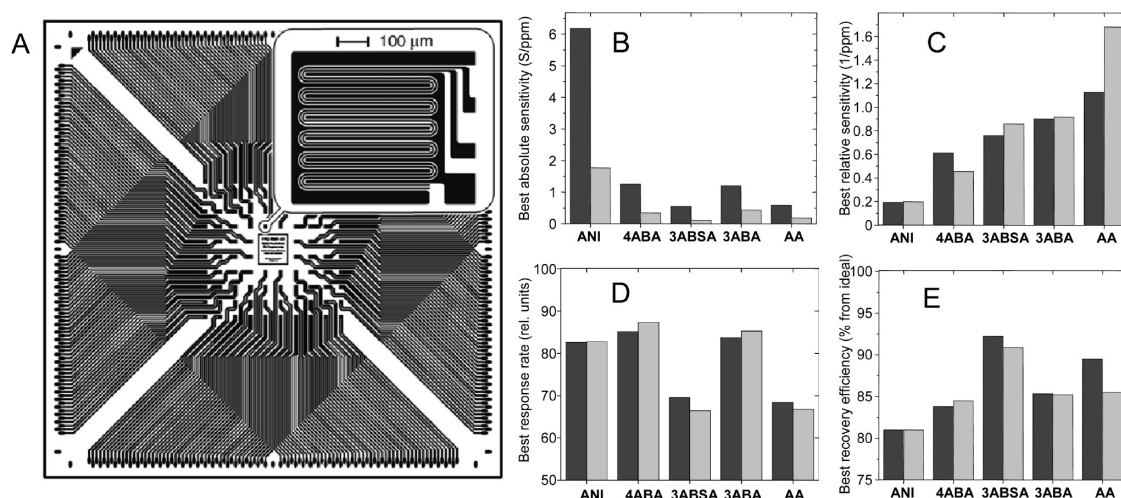
Figure 38. Application of a microfabricated electrode sensor array for multiple electropolymerizations and characterization of resulting conducting polymers as sensor materials. (A) Layout of the interdigital addressed electrode array. Inset: Detailed structure of the single electrode for four-point measurements. (B–E) Selected results of screening of sensing materials for their response to HCl gas: (B) best absolute sensitivity, (C) best relative sensitivity, (D) best response rate, and (E) best recovery efficiency, performed by heating. Sensor materials: ANI indicates polyaniline; 4ABA, 3ABSA, 3ABA, and AA indicate polymers synthesized from aniline and 4-aminobenzoic acid, 3-aminobenzenesulfonic acid, 3-aminobenzoic acid, and anthranilic acid, respectively. Gray and black bars are the results obtained by 2- and 4-point techniques, respectively.[19,400]
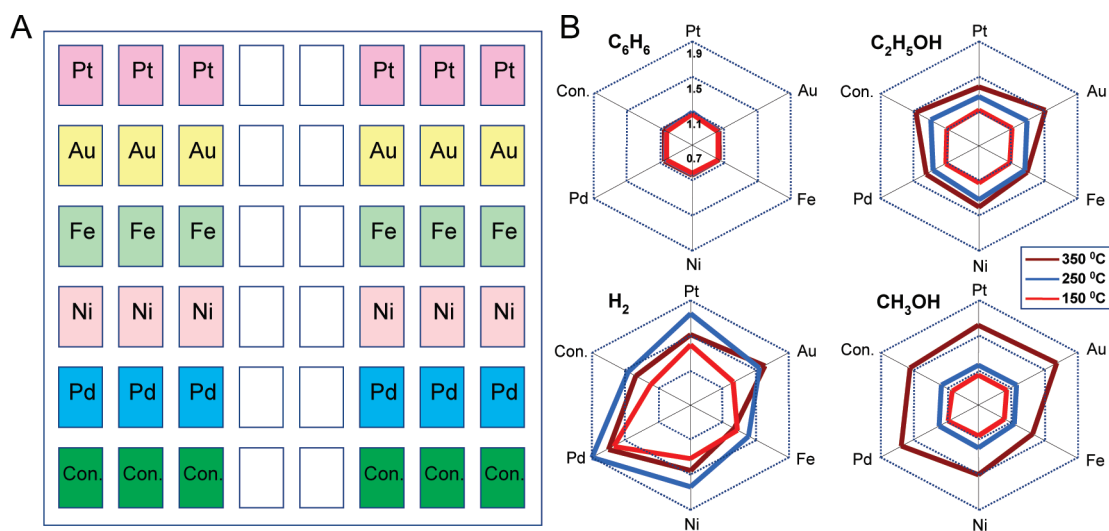

Figure 39. Combinatorial study of effects of surface dispersion of metals into CVD-deposited SnO_2 films. (A) Layout of a 36-element library for study of the sensing characteristics of SnO_2 films with 3 nm of surface-dispersed Pt, Au, Fe, Ni, or Pd (Con. = control). Each sample was made with six replicates. (B) Radar plots of sensitivity results to benzene, hydrogen, methanol, and ethanol for operation at 150, 250, and 350 °C.[404]

that contain additives in metal oxides. Introduction of additives into base metal oxides can change a variety of materials properties including concentration of charge carriers, energetic spectra of surface states, energy of adsorption and desorption, surface potential and intercrystallite barriers, phase composition, sizes of crystallites, catalytic activity of the base oxide, stabilization of a particular valence state, formation of active phases, stabilization of the catalyst against reduction, the electron exchange rate, etc. Dopants can be added at the preparation stage (bulk dopants) that will affect the morphology, electronic properties of the base material, and its catalytic activity. However, the fundamental effects of volume dopants on base materials are not yet predictable.[101] Addition of dopants to the preformed base material (surface dopants) can lead to different dispersion and segregation effects depending on the mutual solubility[401]

and influence the overall oxidation state of the metal oxide surface.[101,401−403]

To improve the productivity of materials evaluation by using combinatorial screening, a 36-element sensor array was employed to evaluate various surface-dispersed catalytic additives on SnO_2 films.[404,405] Catalysts were deposited by evaporation to nominal thicknesses of 3 nm, and then the microhot plates were heated to affect the formation of a discontinuous layer of catalyst particles on the SnO_2 surfaces. The layout of the fabricated 36-element library is shown in Figure 39A. The response characteristics of SnO_2 with different surface-dispersed catalytic additives are presented in Figure 39B. These radar plots show sensitivity results to benzene, hydrogen, methanol, and ethanol for operation at three temperatures.

To expand the capabilities of screening systems, it is attractive to characterize not only the conductance of the sensing materials
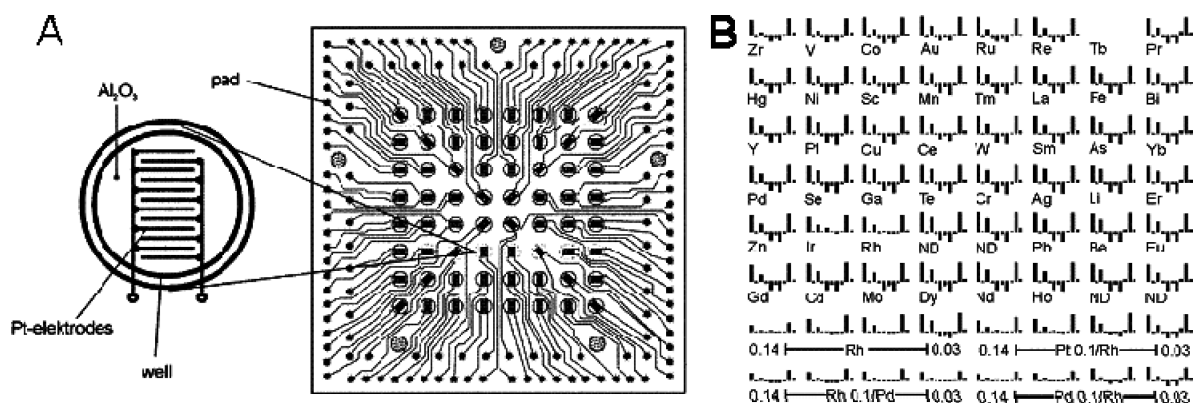
Figure 40. Screening of sensor metal oxide materials using complex impedance spectroscopy and a multielectrode 64-sensor array. (A) Layout of 64-sensor array. (B) Relative gas sensitivities at 350 °C of the In_2O_3 base oxide materials library surface-doped with multiple salt solutions, concentration 0.1 atom % if not denoted otherwise, ND = undoped. Sequence of test gases and their concentrations (with air in between) was H_2 (25 ppm), CO (50 ppm), NO (5 ppm), NO_2 (5 ppm), propene (25 ppm). (A) Reprinted from ref 407. Copyright 2002 American Chemical Society. (B) Reprinted from ref 409. Copyright 2007 American Chemical Society.

with DC measurements but also their complex impedance spectra.[406] The use of complex impedance spectroscopy provides the capability to test both, ion- and electron-conducting materials and to study electrical properties of sensing materials that are determined by the material microstructure, such as grain boundary conductance, interfacial polarization, and polarization of the electrodes.[407,408] A 64 multielectrode array has been designed and built for high-throughput impedance spectroscopy $(10-10^7$ Hz) of sensing materials (see Figure 40A).[407] In this system, an array of interdigital capacitors was screen-printed onto a high-temperature-resistant Al_2O_3 substrate. To ensure the high quality of determinations, parasitic effects caused by the leads and contacts have been compensated by a software-aided calibration.[407] After the system validation with doped In_2O_3 and automation of the data evaluation,[408] the system was implemented for screening of a variety of additives and matrices with the long-term goal to develop materials with improved selectivity and long-term stability. Sensing films were applied using robotic liquid-phase deposition based on optimized sol–gel synthesis procedures. Surface doping was achieved by the addition of appropriate salt solutions followed by library calcination. Screening results at 350 °C of thick films of In_2O_3 base oxide surface doped with various metals are presented as bar diagrams in Figure 40B.[409] It was found that some doping elements lead to changes in both the conductivity in air as well as in the gas sensing properties toward oxidizing (NO_2, NO) and reducing (H_2, CO, propene) gases. Correlations between the sensing and the electrical properties in reference atmosphere indicated that the effect of the doping elements was due to an influence on the oxidation state of the metal oxide surface rather that to an interaction with the respective testing gases. This accelerated approach for generating reliable systematic data was further coupled to the data mining statistical techniques that resulted in the development of (1) a model associating the sensing properties and the oxidation state of the surface layer of the metal oxide based on oxygen spillover from doping element particles to the metal oxide surface and (2) an analytical relation for the temperature-dependent conductivity in air and nitrogen that described the oxidation state of the metal oxide surface taking into account sorption of oxygen.[409]

This high-throughput complex impedance screening system was further employed for the reliable screening of a wide variety
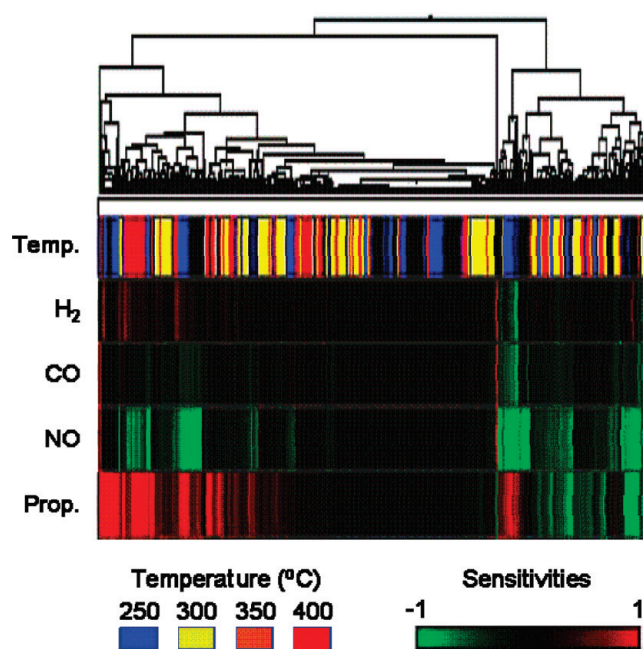
Figure 41. Hierarchical clustering map of 2112 responses of diverse sensing materials to H_2, CO, NO, and propene (Prop.) at four temperatures established from the high-throughput constant current measurements and processed with Spotfire data-mining software (clustering algorithm was "complete linkage" of the Euclidean distances).[100]

of less explored material formulations. Polyol-mediated synthesis has been known as an attractive method for preparation of nanoscaled metal oxide nanoparticles.[410] It requires only low annealing temperatures and provides the opportunity to tune the composition of the materials by mixing the initial components on the molecular level.[411,412] To explore previously unknown combinations of p-type semiconducting nanocrystalline $CoTiO_3$ with different volume dopants as sensing materials, the polyol-mediated synthesis method was used to synthesize nanometer-sized $CoTiO_3$, followed by the volume-doping with Gd, Ho, K, La, Li, Na, Pb, Sb, and Sm (all at 2 at. %). The significant amount of data collected during experiments with numerous sensing materials candidates facilitated the successful
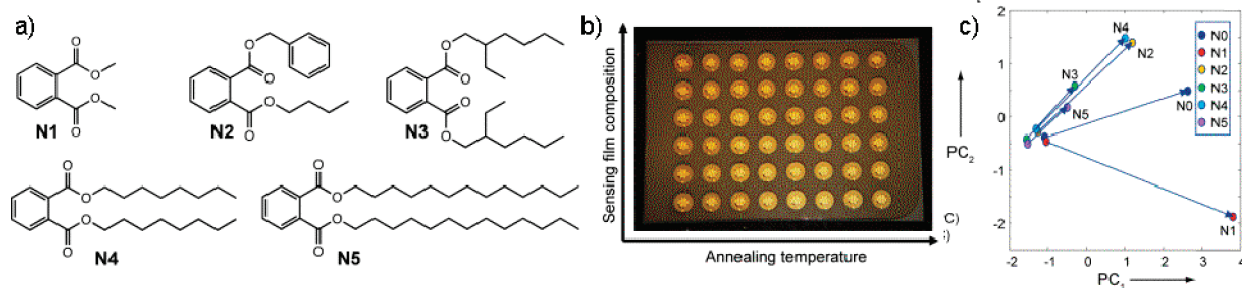
Figure 42. Combinatorial screening of sensing film compositions using passive RFID sensors. (a) Phthalate plasticizers dimethyl phthalate **N1**, butyl benzyl phthalate **N2**, di-(2-ethylhexyl) phthalate **N3**, dicapryl phthalate **N4**, and diisotridecyl phthalate **N5**. (b) Photo of an array of 48 RFID sensors prepared for temperature-gradient evaluations of response of Nafion/phthalate compositions. (c) Results of principal components analysis of ΔF_1, ΔF_2, ΔF_p, and ΔZ_p responses of RFID sensors with six types of sensing films to H_2O and ACN vapors upon annealing at 110 °C. Arrows illustrate the H_2O−ACN Euclidean distances and the response direction of sensing films N0−N5 starting with ACN and ending with H_2O response.[414]

efforts to develop data mining techniques[97,98] and a database system.[413] The developed data mining tools based on hierarchical clustering maps (see Figure 41) have been applied to identify several promising materials candidates such as $In_{99.5}Co_{0.5}O_x$, $W_{99}Co_{0.5}Y_{0.5}O_x$, $W_{98.3}Ta_{0.2}Y_1Mg_{0.5}O_x$, $W_{99.5}Ta_{0.5}O_x$, and $W_{99.5}Rh_{0.5}O_x$ with different gas-selectivity patterns.[100]

Sensing materials have been also arranged into discrete arrays and evaluated for their temperature stability using resonance impedance measurements[414] based on passive radio frequency identification (RFID) sensors with multivariable response.[415−417] These sensing materials were Nafion polymeric materials formulated with five phthalate plasticizers as shown in Figure 42A. Sensing film formulations and control sensing films without plasticizers were deposited onto RFID sensors to form a 6 × 8 sensor array (Figure 42B), which was exposed to eight temperatures ranging from 40 to 140 oC using a gradient temperature heater, and their response stability and gas-selectivity response patterns were evaluated upon exposure to water and acetonitrile vapors. The multivariable responses of these sensors were further examined using PCA (see Figure 42C). Nafion sensing films formulated with dimethyl phthalate showed the largest improvement in response diversity to these two vapors as indicated by the largest Euclidean distance. This RFID-based sensing approach demonstrated rapid, cost-effective, combinatorial screening of sensing materials and preparation conditions.

The effects of variable 2-D composition of materials arrays were investigated in sensors based on the change in the work function of the catalytic metal gate (Pd, Pt, Rh, Ir) because of chemical reactions on the metal surface.[418,419] These sensors are attractive for detection of different gases (e.g., hydrogen sulphide, ethylene, ethanol, different amines, and others). The chemical reaction mechanisms in these sensors depend on the specific gas molecules. Optimization approaches of materials for these sensors involve several degrees of freedom.[420] To simplify screening of the desired material compositions and to reduce a common problem of batch-to-batch differences of hundreds of individually made sensors for materials development, the scanning light pulse technique (SLPT) has been developed.[421−423] In SLPT, a focused light beam is scanned over a large area semitransparent catalytic metal−insulator−semiconductor structure and the photocurrent generated in the semiconductor depletion region is measured to create a 2-D response pattern of the sensing film (aka "a chemical image").

These chemical images were used to optimize properties such as chemical sensitivity, selectivity, and stability.[343] When combined with surface-characterization methods, this information also has led to the increased knowledge of gas response phenomena. It was suggested that a 2-D gradient made from two types of metal films as a double layer structure should provide new capabilities for sensor materials optimization, unavailable from thickness gradients of single metal films.[424] To make a 2-D gradient, the first metal film was evaporated on the insulator with the linear thickness variation in one dimension by moving a shutter with a constant speed in front of the substrate during evaporation. On top of the first gradient thickness film, a second metal film was evaporated with a linear thickness variation perpendicular to the first film. As the validation of the 2-D array deposition, the response of devices with 1-D thickness gradients of Pd, Pt, and Ir films to several gases has been studied with SLPT demonstrating results similar to those of corresponding discrete components.[343]

The 2-D gradients have been used for studies and optimization of the two-metal structures[343,424] and for determination of the effects of the insulator surface properties on the magnitude of sensing response.[425] 2-D gradients of Pd/Rh film compositions were also studied to identify materials compositions for the most stable performance.[343] The Pd/Rh film compositions were tested for their response stability to 1000 ppm of hydrogen upon aging for 24 h at 400 °C while exposed to 250 ppm of hydrogen (see Figure 43A, B). This accelerated aging experiment of the 2-D gradient film surface demonstrated the existence of two most stable local regions. One region was a "valley" of a stable response shown as a dark color in Figure 43C. Another region was a thicker part of the two-component film with a ∼20-nm thick Rh film and a ∼23-nm thick Pd film. This new knowledge inspired new questions of position stability of the "valley" and the possibility to improve sensor stability by an initial annealing process.

3.5. Biomaterials. Biomaterials are defined as any substance (other than a drug) or combination of substances, synthetic or natural in origin, which can be used for any period of time, as a whole or as a part of a system which treats, augments, or replaces any tissue, organ, or function of the body.[426] Biomaterials can be biopolymers, ceramics, and composites of organic/organometallic/inorganic materials that can be used for in vivo/in vitro applications.[426−428] Examples of biomaterials uses are implants, organs or parts of them, materials designed and used for drug delivery, heart valves, bone cement, artificial ligaments/tendons, blood vessel prosthesis, contact lenses, skin repair devices, and dental implants.[428] Most of recent research on biomaterials is in the areas of reparative medicine and delivery of biologically active substances (e.g., drugs or gene) for therapeutic applications.[429]

617

dx.doi.org/10.1021/co200007w | *ACS Comb. Sci.* 2011, 13, 579–633
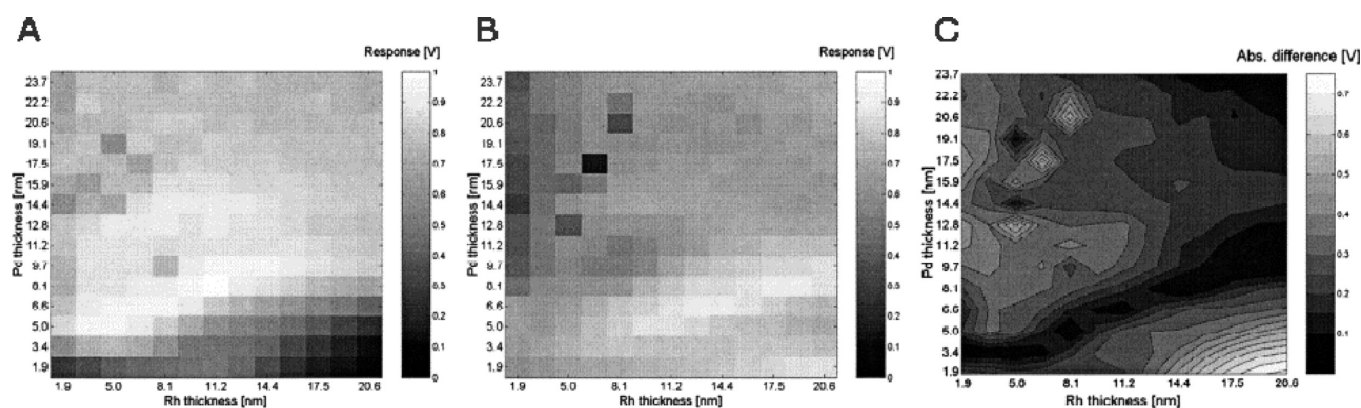
Figure 43. Results of the accelerated aging of 2-D combinatorial library of Rh/Pd film. Chemical response images to 1000 ppm of hydrogen (A) before and (B) after the accelerated aging. (C) Differential response after and before the accelerated aging, the most stable regions have the darkest color.[343]

Also, due to the advances in analytical techniques and nanosciences, biomaterials research has seen the emergence of nanoscaled biomaterials in the areas of drug or gene delivery, tissue regeneration, and in materials for body implants.[426−430]

Biomaterials should meet biocompatibility and other application-specific requirements summarized by the International Organization for Standardization (ISO).[431] Biomaterials used for in vivo applications should be also biocompatible. The lack of consensus on the standardization of biocompatibility tests has hampered this field for years. However, recently, toxicity tests for biocompatibility and safety assessments and becoming more standardized[432] due to intensive efforts from various research groups and governments to identify routine testing cascades for biocompatibility of materials.[433,434] The interactions between the material and the body or more particularly to the different subsystems are usually complex. Thus, exploration of these multiple dimensions can be daunting. Advances in CHT techniques in surface chemistry, analytical chemistry, and materials chemistry have enabled the rapid and effective evaluation of these complex spaces.[12,435,436]

One of significant areas of biomaterials research is to develop artificial materials for use in the human body to restore, repair and replace diseased tissue to enhance survival and quality of life. There has been an explosion of research activity on the work on biomaterials made from polymers as well as peptides that has been used in biological systems and more particularly in the delivery of drugs or genes for therapeutic applications. In light of these recent trends, polymeric biomaterials that are degradable in nature are the preferred candidates, especially for tissue engineering applications, drug delivery, and temporary therapeutic devices. These materials are ultimately made into a system and injected post formulation into the body, typically for therapeutic applications. In most cases, the biomaterials have been made and tested combinatorially as discrete arrays or gradient 2D films for further biological testing.[435,437]

Surfaces of biomaterials can be also used to trigger biological responses and their interaction with biological systems. These surfaces are being used in evaluating the viability of materials in regenerative medicine and more particularly in triggering the growth of stem cells for tissue regeneration as well as repair.[438] Being able to rapidly make, characterize and test these materials enables the accelerated discovery of new materials in regenerative medicine.[439,440]

In the last few decades, small molecules have played a central role in many areas of research, especially in drug discovery but

also in materials research and development. With the explosion of laboratory automation and high throughput synthesis and characterization techniques, interest in libraries of small molecules to support drug discovery and materials research have grown significantly.[441−443] In a recent review, Wu and Schultz have reviewed selected examples of synthesis of unnatural aminoacids by genetically modified organisms.[441] These materials are typically difficult to access in a synthetic point of view and may find unique applications in the realm of biomaterials/biopolymers but also been used in medicine for gene delivery.

Biomaterials can also be synthesized and fabricated by using bioorganisms to access building blocks that are traditionally difficult to make.[444,445] This technology allows chemists to probe, and change, the properties of proteins, in vitro or in vivo, by directing novel, lab-synthesized chemical moieties specifically into any chosen site of any protein of interest. Biomaterials that have been generated by combinatorial phage display have been reviewed elsewhere.[444,445]

3.5.1. Biomaterials Used for Drug/Gene Delivery. Polymeric biomaterials are among the most important materials in drug and gene delivery for in vivo applications. When new classes of pharmaceuticals and biologics (peptides, proteins and DNA-based therapeutics) are being introduced, these new drugs typically require efficient delivery to the therapeutic targets. Additionally, for many conventional pharmaceutical therapies, the efficacy may be improved and the side effects reduced if the therapy is administered continuously, in a controlled fashion, rather than through conventional burst release techniques (oral ingestion, injection, etc). Development of materials that can enable the encapsulation of these pharmaceuticals and biologics has attracted significant interest.[435]

The main advantages of these polymeric materials are ease of synthesis, reproducibility but also the access to materials platforms that can be tuned easily to achieve the desired physicochemical properties, such as water solubility and biodegradability/release. A wide range of highly diverse but also focused materials has been used and considered in this field and especially polymeric backbones such as PLGA (poly lactic and glycolic acid) or polycaprolactam and polyhydroxyethylmethacrylate moieties, which typically break down in in vivo into innocuous byproducts. In recent years, due to more stringent regulations from a materials requirement standpoint, synthetic approaches have shown an increasing level of sophistication employing nanotechnology, microfluidics, and micropatterning. The CHT
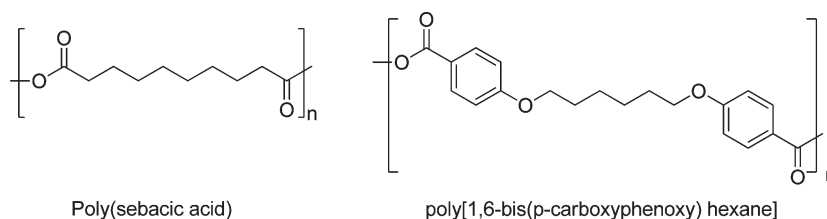
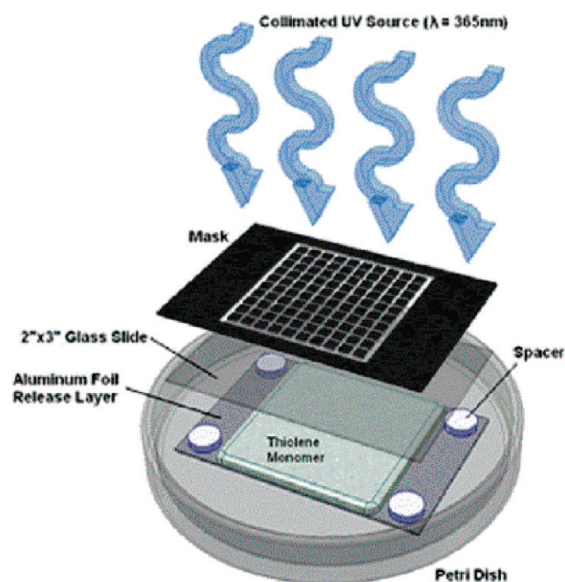**Figure 44.** Polysebacic acid and poly[1,6-bis(p-carboxyphenoxy) hexane] based monomers used in biocopolymers.

Figure 45. Schematic of photolithographic design of discrete thiolene well substrates.[449]

Figure 46. Discrete and continuous experimental phase diagrams used in poly(CPH)/poly(SA) blends.[449]

technologies have been extensively used by various research groups to accelerate discovery of these important materials.

Biodegradable polymers for drug delivery have been the focus of engineered materials used for the delivery of drug molecules or genes but also used as encapsulant for gene therapy. In 2008, Meredith has reviewed recent advances in the past 10 years.[446−448]

Recently, Thortensen et al. developed biodegradable polymers bearing a poly[1,6-bis(p-carboxyphenoxy) hexane] (CPH) and poly-[sebacic anhydride] (SA) backbone and evaluated them as vehicles for drug delivery (see Figure 44).[449] Libraries of those polymers were made by using a combination of solution-based gradient deposition and rapid prototyping.[450−452] These materials have been the focus of studies looking at the effect of blend miscibility on the biodegradability of the material using CHT techniques. The discrete libraries were made on a Si wafer via the thiolene chemistry. The fabrication of discrete well plates was accomplished by photolithography. The basic idea is to form wall-like structures by selectively polymerizing areas of a thiolene-based resin by means of a collimated UV source and discriminating mask as shown in Figure 45.

On the other hand, the continuous libraries were prepared by using a modified procedure to the one published by Meredith et al. in a 3 step standard workflow (gradient mixing, gradient deposition, and film spreading (see Figure 45 and 46) using custom-made automation platforms.[453]

Blend compositions were characterized by high throughput transmission Fourier transform infrared (FTIR). The phase diagrams of CPH/SA polymers, the effect of blend composition
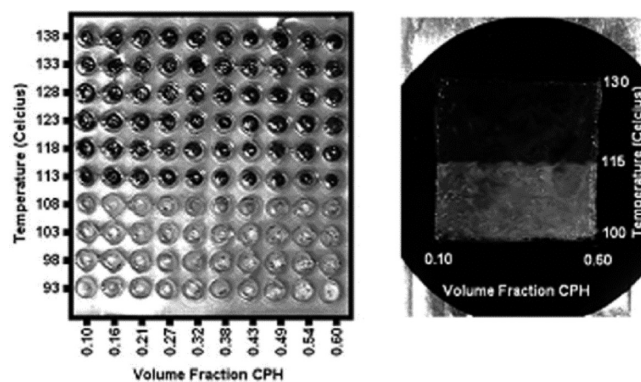
and annealing temperature on the miscibility of the blend were studied to determine blend miscibility, which is a great indication for polymer viability and stability. The gradient library was further examined with optical microscopy and Atomic Force Microscopy for surface morphology and roughness but also to locate the miscibility phase boundary marked by differential microstructure-induced opacity fluctuations (cloud points). A good correlation was found between results obtained by theoretical phase diagrams determination and with surface analysis obtained with these blends.[454] Evaluation of those materials of similar chemical composition made by CHT was carried out by the same research group and the effect of polymer chemistry and device geometry on the in vitro activation of murine dendritic cells was determined.[105]

Petersen et al. described the development of polyanhydrides and the subsequent use for materials enabling controlled drug release, drug stability, or immune regulation (adjuvant effect). Understanding the induction of immunomodulatory mechanisms of this polymer system is important for the design and development of efficacious vaccines and tissue compatible multicomponent implantable devices. In light of this, combinatorial libraries of polyanhydride materials of various sebacic acid (SA) and 1,6 bis(p-carboxyphenoxy)hexane (CPH) were made as films and/or nanospheres and tested rapidly in in vitro tests. Discrete, combinatorial film libraries, linearly varying in copolymer composition of the CPH:SA system, were automatically characterized with FTIR.[105]

The polyanhydride array of biomaterials was tested in cell surface marker expression and cytokine production. Figure 47 showed the interleukine IL-6 and IL12p40 by C57BL/6 DCs results with the multiplexed CPH:SA libraries. The CPH:SA polymer film system provided a gentle, biocompatible environment necessary for multicomponent implants. In contrast, the CPH:SA nanosphere system provided an adjuvant effect by
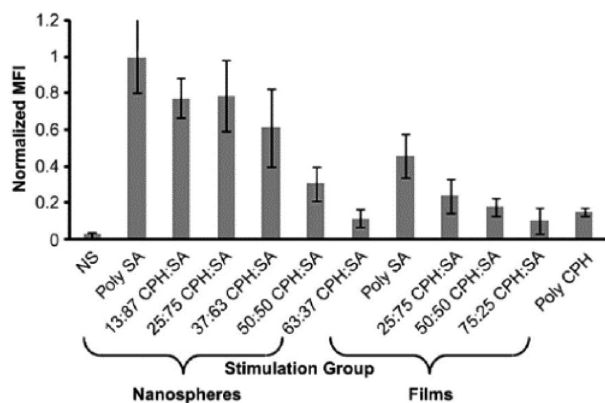
Figure 47. Effect of poly CPH/SA blends on dendritic cells stimulation.[105]
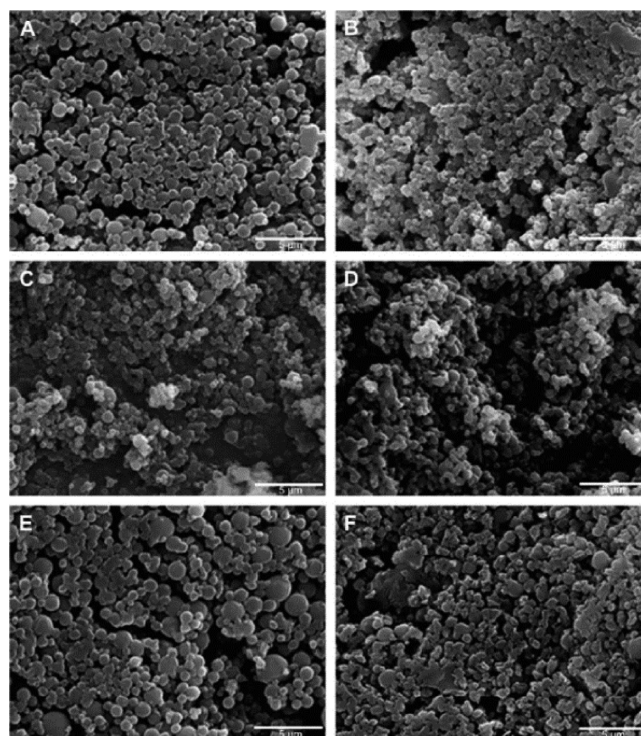

Figure 48. SEM images of the discrete library of combinatorially fabricated nanospheres starting with (A) Poly(SA), (B) 13:87 CPH:SA, (C) 25:75 CPH:SA, (D) 37:63 CPH:SA, (E) 50:50 CPH:SA, and (F) 63:37 CPH:SA.[105]

enhancing DC activation. Further, PCA modeling of the results of the in vitro tests employed in this study delineated the clear differences between these chemistry and device geometry. It has been showed that the CPH:SA system has immunomodulatory capabilities to regulate both cellular expression of surface markers and production of cytokines. The generality of the technique promises to facilitate a more rational development of biomaterials for specific applications in drug/vaccine delivery and tissue engineering.

In a similar approach, a parallel screening method has been developed to rapidly evaluate discrete library substrates of biomaterials based on sebacic acid (SA), 1,6-bis(p-carboxyphenoxy)hexane (CPH), and 1,8-bis(p-carboxyphenoxy)-3,6-dioxaoctane (CPTEG). Linearly varying compositional libraries of 25 different polyanhydride random copolymers (based on CPH:SA and CPTEG:CPH) were designed, fabricated, and synthesized, characterized at high throughput using infrared microscopy and validated using ^{1}H NMR and size exclusion chromatography. The discrete libraries were rapidly screened for biocompatibility using myeloma, fibroblasts, and macrophage cell lines. No cytotoxic effect on any of the four cell lines evaluated by any of the CPH:SA or CPTEG:CPH compositions was observed. Furthermore, the activation of J774 macrophages was evaluated by incubating the cells with the polyanhydride libraries and quantifying the secreted cytokines (IL-6, IL-10, IL-12, and TNFalpha), which are typically indicators of potential acute inflammation response. The results indicated that copolymer compositions containing at least 50% CPH induced elevated amounts of TNFalpha, which is indicative of the immune response triggering factor. This work provided crucial information toward rapid and rational design of materials for use in biomedical applications.[449]

Lin and Gibson reported the development of dimethacrylate polymers for usage in orthopedic applications.[455] Dimethacrylate polymers and composites that are found commonly in dental restorative materials have gained interest in regenerative medicine. However, it was highly emphasized that because these resin based dimethacrylate materials can show some cytotoxicity even at small concentrations, a battery of toxicity tests needed to be carried out to demonstrate the viability of these new materials for use as body implant parts. In light of these requirements, effective exploration of the multivariable space must be carried in order to get to evaluate critical biological response rapidly. The authors[449] developed a combinatorial approach that allows the accelerated

preparation and testing of dimethacrylate polymers and composites and subjected them to numerous cell based assays for toxicity evaluation. Various surfaces were prepared on small glass slides with varying composition of monomers, increasing irradiation time, filler mass ratio, but also small variations in silica based filler material.

Arrays of the discrete and continuos experimental phase diagrams used in poly(CPH)/poly(SA) blends were described by Petersen and co-workers.[456,105] The objective of this study was to quantify the osteoblast response to dimethacrylate-based composites using a combinatorial approach around the degree of conversion, surface roughness, composition in the filler material, and hydrophobicity. A thorough characterization of combinatorial samples allowed for an improved interpretation of the resulting cell response. As an example, SEM images shown in Figure 48, highlight the effects of blend chemistries on the surface morphology/topology of the materials. Low degree of conversion samples displayed light cytotoxicity, but no obvious effect of filler content on MC3T3-E1 viability was evident. While compositions with less than 50 wt % filler showed decreasing cell density with decreasing DC/increasing roughness/increasing hydrophobicity, an increased filler content of 65 wt % successfully overcame these effects and enabled the recovery of normal cell density at low DC for some compositions. This study reveals the importance of some of these developed battery of cell based assay test that might be appropriate for future evaluation of photopolymerized composites for use in orthopedic applications.

3.5.2. Hydrogels for Drug/Gene Delivery. Among the polymeric structures used in drug delivery, hydrogels have remained the cornerstone of materials used in drug delivery.[457,458] The

620

dx.doi.org/10.1021/co200007w |*ACS Comb. Sci.* 2011, 13, 579–633
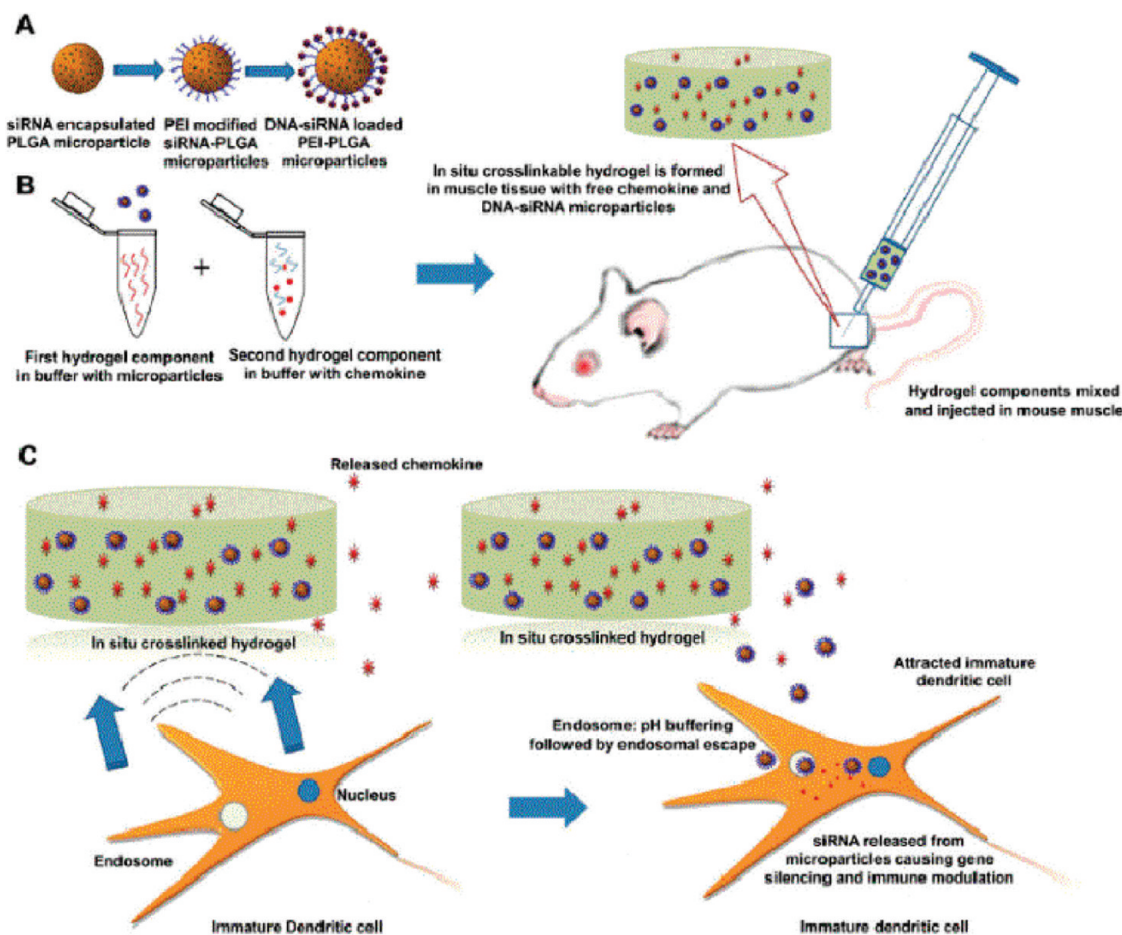
Figure 49. siRNA-DNA materials encapsulated by hydrogels (A) Encapsulation of DNA-siRNA loaded with PEI-PLGA microparticles approach. (B) Incorporation of hydrogel compents in buffer with microparticles and chemokine. (C) In situ cross-linking of hydrogel.[459]

main advantages of hydrogels include unusual high water solubility and physicochemical properties that can easily be tuned. Hydrogels are typically porous, making them perfect hosts to accommodate drug molecules in the gel matrix. On the other hand, due to this unique property, small molecule drugs can be delivered by controlled diffusion of the latter to the target site. Equally, hydrogels can be formulated in a wide range of forms such as microparticles, nanoparticles and coatings to injectable materials for drug delivery.

Roy et al. recently reported a microparticle-based system capable of simultaneously delivering siRNA and DNA to APCs.[459] The biomaterial is made from PLGA (poly lactic acid and glycolic acid) and polyvinylalcohol and functionalized polyethylene imine with encapsulated siRNA-DNA microparticles (Figure 49A). This system is then further encapsulated with an in situ dextran or PEG cross-linkable, injectable formulation containing dendritic cell (DC)-chemo-attractants. The system is designed as such to attract immature DCs and simultaneously deliver, to the migrated cells, immunomodulatory siRNA and plasmid DNA antigens. These low cross-link density hydrogels were designed to degrade within 2−7 days in vitro and released chemokines in a sustained manner.

Figure 49B shows the approach in which the si-RNA-DNA materials from plasmids are integrated into a microparticle which is then functionalized to a polyethyleneimine microparticle. The hydrogel is now incorporated alongside with the microparticles.

Cross-linking and formulation of this system will yield the formation of injectable solutions. A small library of hydrogels (2 backbones (dextran vinylsulfone vs PEG diacrylate)), various degree of substitution and gelation times and compositions was synthesized and characterized using standard characterization techniques.[436,458]

An array of dextran VS and PEGDA hydrogels was made with and without encapsulated microparticles, (Figure 49C) with various % of the original monomer and different gelation times to ensure a high degree of cross-linking. Those materials that displayed complete gelation were carried forward and further examined with ELISA, SEM as well as in vitro tests for viability of these biomaterials in gene delivery. This parallel approach allowed the rapid identification of promising biomaterials for gene delivery by just varying the chemical composition, the degree of cross-linking and the porosity, which all affected the stability of the hydrogel as well as the release kinetics significantly. Overall, the studies showed that these novel biomaterials can deliver genes effectively to the desired sites during the immunotherapy.

3.5.3. Organic Biomaterials with Cell and Stem Cell Systems. Understanding interactions between organic or polymeric biomaterials remains one of the main research directions. Typically biomaterials that have been designed and made to be used in regenerative medicine and especially as components used in body implants have to be tested for biocompatibility and have to

show absence of a significant cytotoxicity. In a mechanistic point of view, biomaterials enter in a three-way interaction with tissue or blood proteins present in vivo as well as with some cellular systems. Hence understanding the chemistry of these surfaces and their subsequent surface-cell interactions is becoming critical for the design of the perfect organic biomaterials. Such complex surface interactions have been examined rapidly and effectively by powerful combinatorial and high throughput methodologies. Recent advances in cell interactions with biomaterials in an array form (discrete libraries) or in a gradient form have been recently reviewed.[436]

The most commonly used biodegradable polylactic/glycolic acid and polycaprolactam materials have been used in the development of a high throughput cell-material screening strategy, based upon local cell-feature analysis (LCFA) This methodology was applied to screen osteoblast proliferation behavior on combinatorial libraries of phase separated poly lactic/glycolic acid and polycaprolactam materials.[437] The LCFA method, based on histograms of distances between cells and microstructures, was able to identify nonlinear, discrete relationships between proliferation, PCL diameter, and cell-PCL distance. Using these results, the authors proposed a model for classifying the material—microstructure interactions, in which small PCL islands far from the cell nucleus act as holders for attachment and large islands close to cells act to shape the cell.

Similarly, tyrosine derived biomaterials have been examined using a high throughput characterization of the cell adhesive responses to biomaterials. The substrates were made from poly DTE carbonate and poly DTO carbonate substrates which corresponding surfaces are made by gradient annealing.[460] Saos-2 cells engineered with a green fluorescent protein (GFP) reporter for farnesylation (GFP-f) were cultured on the gradient substrates to assess the effects of nanoscale surface topology and roughness that arise during the phase separation process on cell attachment and adhesion strength. The high throughput imaging approach allowed the rapid establishment of a structure—property relationships between cell adhesion and biomaterial properties. This study found that cell attachment and spreading increased monotonically with DTE content and was significantly elevated at the position with intermediate regions corresponding to the highest "gradient" of surface roughness, while GFP-f farnesylation intensity descriptors were sensitively altered by surface roughness, even in cells with comparable levels of spreading. Simon et al. highlighted the recent advances on the use of gradients and arrays for combinatorial screening and development of biomaterials toward tissue engineering.[436]

Langer and co-workers reviewed the use of combinatorial chemistry and high throughput screening tools to investigate the optimization of stem cell microenvironments, which are critical component to cell growth and proliferation.[461] Key studies of stem cell/biomaterial interactions using combinatorial libraries of polymers (array of discrete materials or gradient) were reviewed comprehensively.

An interesting work on the investigation of protein—cell interactions was also highlighted and specifically the high importance of such interactions in helping the optimization of stem cell microenvironments.[462] As an example, a diverse set of 496 arrayed materials have been designed and prepared with 16 major monomers and 6 minor monomers. Combining high throughput polymer synthesis and rapid quantification of material/protein/cell interactions, it was possible to quickly map out the interactions among human embryonic body (hEB) cell attachment,
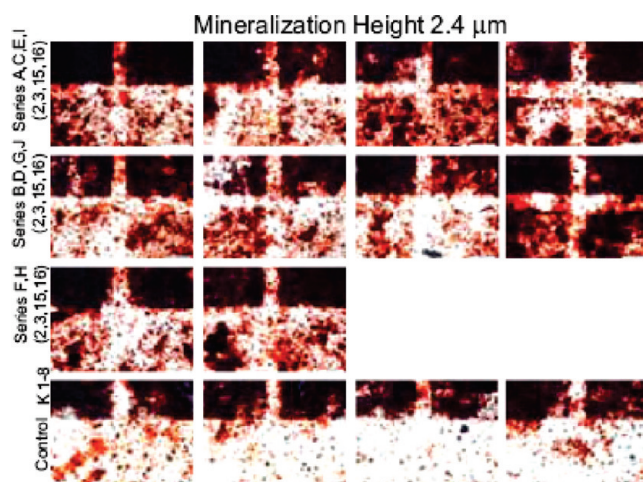
Figure 50. Mineralization height as a function of various surface topographies.[463]

fibronectin (Fn) adsorption, and the chemical structures structures of the substrates. Both the major and minor monomers have been shown to affect Fn adsorption and hEB cell attachment. Further analysis revealed that the chemistry diversity created here can generate a diverse collection of materials with varying amounts of adsorbed Fn and cell adhesion. Controllable hEB cell attachment was shown to be reproducible on four polymer films with three distinct cell-attachment capacities, and the biological properties of the scaled up films were found to be similar to their microscale counterparts. It was believed the integrated high-throughput synthesis and rapid quantification of materials/protein/cell interactions may accelerate the development of biomaterials for various applications, such as materials-directed stem cell differentiations.[462]

3.5.4. Inorganic Surfaces with Cell Systems. Biomaterials, including those used as part of body implants, often contain inorganic components. Work in elucidating and studying surface interaction between these components attracted increasing interest. A significant amount of work in the area has already been reviewed recently by Simon et al.[436] Lovmand et al. explored the use of combinatorial topographical libraries for the screening of enhanced osteogenic expression and mineralization.[463] In this study, micro and nanofunctionalized surfaces have been screened in a combinatorial approach for cell response. This strategy has the merit to be able to provide crucial information toward the optimization of the design of the biomaterials that will be able to regulate cellular differentiation. A library of 504 unique distinct surfaces (created using the Biosurface structure array platform) has been screened for the osteoblastic cell line interaction and subsequent mineralization. Each BSSA is a wafer which is composed by a 13×13 array with 169 unique area testers. These platforms have been constructed rapidly using boron-doped p-type Si-wafers. The "combinatorial patterns" were created using standard lithography and subsequent etching processes using Cl_2, NF_3, and HBr. The micro and nanostructured surfaces of various sizes, shapes and heights which were obtained were then screened for cellular response and more particularly osteoblast cell expression and subsequent mineralization. An example of the effect of mineralization height as a function of surface topography is shown in Figure 50. Once exposed to the optimal micro/nano surfaces, the surfaces were
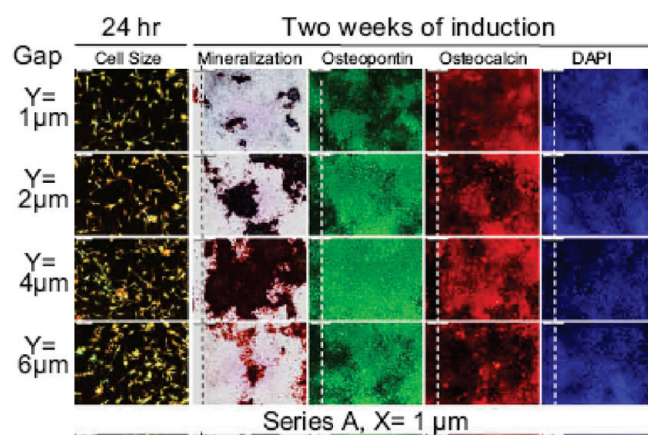
Figure 51. Example of cell expression assay using the immuno-fluorescence assay.[463]

subjected to an immunofluorescence assay using an Antiosteopontin, an antiosteocalcin and a monoclonal antivinculin as the primary antibodies and an Anti IGg mouse (labeled) as the secondary antibodies. Each area tester contains up to 3600 cells that are being scrutinized by a state of the art custom designed fluorescence microscope and an automated picture taking software (Figure 51). This approach promises to facilitate identification of optimal surface heights, shapes and sizes that would yield the highest cell proliferation profile as well as the best mineralization capacity for silicon containing nano- and microsurfaces.

4. SUMMARY AND OUTLOOK

Combinatorial technologies in materials science have been successfully accepted by the research groups in the academia and governmental laboratories that have overcome the entry barrier of dealing with new emerging aspects in materials research such as automation and robotics, computer programming, informatics and materials data mining. The main driving forces for combinatorial materials science in industry include broader and more detailed explored materials and process parameters space and faster time to market. Industrial research laboratories working on new catalysts were among the first adopters of combinatorial methodologies in industry. The classical example of an effort by Mittasch who has spent 10 years (over 1900−1909) to conduct 6500 screening experiments with 2500 catalyst candidates to find a catalyst for industrial ammonia synthesis[464] will never happen again because of the availability and affordability of modern tools for high-throughput synthesis and characterization.

CHT screening technologies are increasingly impacting the development of materials in several distinct ways. The availability of the parallel synthesis and high-throughput characterization tools has already provided previously unavailable capabilities to perform multiple experiments on a much shorter time scale. In these experiments, the quality of data can be even better than in conventional one-at-a-time experiments because of the elimination of possible experimental artifacts because of an uncontrolled variation of experimental conditions. Time savings and data quality inspire scientists in academia and industry to explore more risky ideas, which were previously too time-consuming to experiment with. The application of only small amounts of reagents needed for combinatorial experiments makes this approach very cost-effective per experiment basis. New combinatorial schemes should be developed where various reaction variables can be altered simultaneously and where important cooperative effects can be carefully probed to provide better understanding of variation sources. This information should lead to the development of new desired materials performance models that will relate intrinsic and performance material properties.

Advances in computational chemistry, data mining, and informatics will provide more capabilities for virtual screening and more guided selection of space for experimental screening of materials as diverse as detailed in this review: catalysts, electronic and functional materials, polymer-based industrial coatings, sensing materials, and biomaterials. Overall, gathered and analyzed data will provide new opportunities for reduction of gaps in materials-development knowledge, and for the more cost- and time-effective materials design. There is a strong need to link combinatorial library synthesis to the significant advances in computational modeling related to a variety of phenomena including interdiffusion, microstructural evolution, and thermomechanical processing. Achieving these links to theory and the related assessment of accuracy of measurements in high throughput screening is also critical if for instance combinatorial libraries actually are to become a source of generating reference data. The value of materials informatics lies in its ability to establish quantitative and mathematically robust interpretation of data, uncertainty analysis, and model driven fabrication. This will ensure that combinatorial experimentation is not simply a platform for high throughput empirical observations but truly an accelerated knowledge discovery tool.

Production of combinatorial leads on a larger scale reveals how reliable and realistic is the data obtained on the combinatorial scale. Materials developed at the combinatorial scale and validated on scale-up versions or in practical applications include catalysts,[465−469] phosphors,[470] formulated organic coatings,[35] sensing polymers,[471] and some others. Unfortunately, applications of CHT methods are not always revealed, making it difficult to reliably judge the impact of CHE on science and industry.

The true multidisciplinary aspects of combinatorial techniques will continue to impact the researchers as well. An effective combinatorial chemist and materials scientist will acquire skills as diverse as experimental planning, automated synthesis, basics of high-throughput materials characterization, chemometrics, and data mining. Perhaps, everyone who will deal with massive amounts of data will be able to perform standard multivariate statistical and cluster analysis using available tools for rapid assessment of materials trends that are not visually noticeable due to several components involved in the experimental design. These skills will provide a powerful vision for the design of new materials, including those within the Materials Genome Initiative, impossible to imagine in the 20th century.

■ AUTHOR INFORMATION

Corresponding Author
*E-mail: potyrailo@crd.ge.com.

■ ACKNOWLEDGMENT

■ EXTENDED GLOSSARY

abrasion resistance: ability of a material to withstand mechanical action, such as rubbing, scraping, or erosion, that tends progressively to remove material from its surface

accuracy: in characterization, closeness of the agreement between the result of a measurement and a true value of the measurand

biocompatibility: refers to specific properties of a material that is compatible with biological systems without triggering adverse cellular, immunological, biological response in vitro or in vivo

biodegradable material: a material designed in a way that it can serve its function for a determined amount of time and can degrade in the environment to yield perfectly safe components that are cleared by the environment system

biofilm: a complex aggregation of microorganisms growing on a solid substrate

biofouling: the undesirable accumulation of microorganisms, plants, algae, etc. on wetted structures

biomaterial: any substance (other than a drug) or combination of substances, synthetic or natural in origin, which can be used for any period of time, as a whole or as a part of a system which treats, augments, or replaces any tissue, organ, or function of the body

cross-link: chemical bonds that link one polymer chain to another

database: a systematic compilation of data whether it be from combinatorial experiments or those producing reference data

data mining: an interdisciplinary field merging ideas from statistics, machine learning, databases, and parallel and distributed computing providing a unique tool to integrate scientific information and theory for materials discovery

descriptor: a piece of stored information that represents an atom, a molecule or a material by capturing its physicochemical characteristics and properties; it is often the final result of a logical and mathematical procedure that transforms chemical information encoded within a symbolic representation of a molecule into an useful number

drug delivery: a field that focuses on the delivery of active drugs in the body via formulation or via entities that can transport the active agent to the sites of therapeutic interest

dynamic range: in characterization, the range between the maximum usable measurement result and the minimum usable measurement result; a distinction may be made between the linear dynamic range, where the response is directly proportional to concentration, and the dynamic range where the response may be nonlinear, especially at higher concentrations

effective oxide thickness (EOT): equivalent thickness of SiO_2 layer that would give the same capacitance compared to the capacitance of a given dielectric material

ferromagnetic shape memory alloy: metallic alloy that displays large magnetic field induced strain due to motion of martensitic variants which are coincident with magnetic domains

fingerprint: in characterization and sensing, a unique pattern indicating the presence of a particular molecule, based on specialized analytic techniques such as mass- or X-ray-spectroscopy, used to identify a pollutant, drug, contaminant, or other chemical in a test sample

flat-band voltage: voltage that induces zero net charge in the underlying semiconductor; bias conditions of a metal-oxide-semiconductor capacitor for which the energy band diagram of the silicon is flat

fouling-release: the ease of removal of biofouling from a surface

glass transition temperature: the temperature at which a polymeric material undergoes a transition from the glassy state to the rubbery state

Hotelling's T^2 statistic: the sum of normalized squared scores and is a measure of the variation in each sample within the Principal Components Analysis (PCA) model; the T^2 contributions describe how individual variables contribute to the Hotelling's T^2 value for a given sample

informatics: academic field focused on human-computer interactions, processing, management, and retrieval of information

linear solvation energy relationships (LSER): equations involving the application of solvent parameters in linear or multiple (linear) regression expressing the solvent effect on the rate or equilibrium constant of a reaction

loadings plot: shows the relations between analyzed variables based on a developed Principal Components Analysis (PCA) model

loss tangent: the ratio of the imaginary part of the dielectric constant over the real part of the dielectric constant. A measure of loss in dielectric constant

multiferroic material: material that possesses or displays more than one of the three ferroic properties, namely, ferroelectricity, magnetism, and ferroelasticity

nanobiomaterial: a nanomaterial that can be used in the area of nanobiotechnology toward applications in regenerative medicine, tissue engineering, drug delivery, and surfaces for cell growth

one-bead-one-compound (OBOC): first recognized by Lam et al.[472] is based on the fact that combinatorial bead libraries, prepared via an S&P approach, contain single beads displaying only one type of compound although there may be up to 10^{13} copies of the same compound on a single 100μm diameter bead

optical clarity: a materials ability to allow visible light to pass through without scattering

pattern: a set of elements repeating in a predictable manner

pattern recognition: is the identification of patterns in large data sets, using appropriate mathematical methodology

piezoelectric material: materials which displays piezoelectricity, where electrical charges are accumulated because of mechanical strain; piezoelectric materials are used for sensors and actuators utilizing this effect, as well as the converse effect, where applied voltage in the material leads to mechanical strain

624

dx.doi.org/10.1021/co200007w |*ACS Comb. Sci.* 2011, 13, 579–633

polysiloxane: polymers possessing a backbone comprised of alternating silicon and oxygen atoms

precision: in characterization, the closeness of agreement between independent test results obtained by applying the experimental procedure under stipulated conditions; the smaller the random part of the experimental errors that affect the results, the more precise the procedure

principal component (PC): the weighted sum of the original variables in a developed Principal Components Analysis (PCA) model

Principal Component Analysis or Principal Components Analysis (PCA): a mathematical technique useful for an unsupervised reduction of the dimensionality of data

Q residual: the squared prediction error and describes how well the Principal Components Analysis (PCA) model fits each sample; it is a measure of the amount of variation in each sample not captured by principal components retained in the model

quantitative structure—activity relationship (QSAR) (sometimes **QSPR, quantitative structure—property relationship**): the dependency by which a chemical molecular or crystal structure is quantitatively correlated with a chemical activity or a physical property

regenerative medicine: a field that encompasses medical sciences aiming at facilitating tissue healing, bones repair and more broadly enabling accelerated patient's recovery from surgical intervention, wounds or diseases, fully exploiting technology in biomaterials

scores plot: shows the relations between analyzed samples based on a developed Principal Components Analysis (PCA) model

Seebeck coefficient: a measure of the magnitude of an induced thermoelectric voltage in response to a temperature difference across that material

selectivity: in characterization, the extent to which other substances interfere with the determination of a substance according to a given procedure

sensing material: a material that demonstrates a predictable response (property change) to a change in the environment

sensitivity: in characterization, sensitivity is the slope of the calibration curve; if the curve is in fact a "curve", rather than a straight line, then of course sensitivity will be a function of analyte concentration or amount

sensor: a miniature system that recognizes a change in a single or multiple environmental parameters and converts this information into an analytically useful signal

Split and Pool (S&P) or "Mix and Split", "Split and Combine", **"Selectide-Process"**: a concept proposed by Furka et al.[122] that is originating from multiple peptide synthesis and describing the division of spherical beads, porous, and homogeneous in size and loading capacity, into equal aliquots, addition of different molecular fragments or ions to each aliquot and recombination of the aliquots after washing into one pool; after a number of cycles S the total number of library elements N is calculated as $N = M^S$, if the number of precursors is denoted as M. As a large number of compounds can be evaluated with very little effort the method is suited for very high-throughput (vHT) screening

tissue engineering: the use of cells as building blocks to regenerate tissues to enable bone or organ reconstruction or replacement, wound healing, facilitating recovery or replacing biological functions

transduction: in characterization and sensing, is converting one form of energy into another

transducer: an analytical instrument which provides an output quantity having a given relationship to the input quantity

weatherability: the ability of a material to withstand changes in appearance and structure resulting from outdoor exposure

■ REFERENCES

(1) Schultz, P. G. *Appl. Catal., A* **2003**, *254*, 3–4.

(2) Eberhart, M. E.; Clougherty, D. P. *Nat. Mater.* **2004**, *3*, 659–661.

(3) Jansen, M.; Schön, J. C. *Angew. Chem., Int. Ed.* **2006**, *45*, 3406–3412.

(4) Jandeleit, B.; Schaefer, D. J.; Powers, T. S.; Turner, H. W.; Weinberg, W. H. *Angew. Chem., Int. Ed.* **1999**, *38*, 2494–2532.

(5) Amis, E. J.; Xiang, X.-D.; Zhao, J.-C. *MRS Bull.* **2002**, *27*, 295–297.

(6) Meredith, J. C.; Smith, A. P.; Crosby, A. J.; Amis, E. J.; Karim, A. In *Encyclopedia of Polymer Science and Technology*; Wiley: New York, NY, 2002.

(7) Malhotra, R., Ed. *Combinatorial Approaches to Materials Development*; American Chemical Society: Washington, DC, 2002; Vol. 814.

(8) Potyrailo, R. A. *Trends Anal. Chem.* **2003**, *22*, 374–384.

(9) Hoogenboom, R.; Meier, M. A. R.; Schubert, U. S. *Macromol. Rapid Commun.* **2003**, *24*, 15–32.

(10) Meier, M. A. R.; Hoogenboom, R.; Schubert, U. S. *Macromol. Rapid Commun.* **2004**, *25*, 77–94.

(11) Koinuma, H.; Takeuchi, I. *Nat. Mater.* **2004**, *3*, 429–438.

(12) Kohn, J. *Nat. Mater.* **2004**, *3*, 745–747.

(13) Rajan, K. *Mater. Today* **2005**, 38–45.

(14) Potyrailo, R. A. *Angew. Chem., Int. Ed.* **2006**, *45*, 702–723.

(15) Potyrailo, R. A., Maier, W. F., Eds. *Combinatorial and High-Throughput Discovery and Optimization of Catalysts and Materials*; CRC Press: Boca Raton, FL, 2006.

(16) Wang, Q., Potyrailo, R. A., Fasolka, M., Chikyow, T., Schubert, U. S., Korkin, A., Eds. *Combinatorial Methods and Informatics in Materials Science*; Materials Research Society: Warrendale, PA, 2006; Vol. 894.

(17) Maier, W. F.; Stöwe, K.; Sieg, S. *Angew. Chem., Int. Ed.* **2007**, *46*, 6016–6067.

(18) Narasimhan, B., Mallapragada, S. K., Porter, M. D., Eds. *Combinatorial Materials Science*; Wiley: Hoboken, NJ, 2007.

(19) Potyrailo, R. A.; Mirsky, V. M. *Chem. Rev.* **2008**, *108*, 770–813.

(20) Potyrailo, R. A., Mirsky, V. M., Eds. *Combinatorial Methods for Chemical and Biological Sensors*; Springer: New York, NY, 2009.

(21) Maier, W.; Kirsten, G.; Orschel, M.; Weiss, P.-A.; Holzwarth, A.; Klein, J. In *Combinatorial Approaches to Materials Development*; Malhotra, R., Ed.; American Chemical Society: Washington, DC, 2002; Vol. 814, pp 1−21.

(22) Takeuchi, I., Newsam, J. M., Wille, L. T., Koinuma, H., Amis, E. J., Eds. *Combinatorial and Artificial Intelligence Methods in Materials Science*; Materials Research Society: Warrendale, PA, 2002; Vol. 700.

(23) Xiang, X.-D., Takeuchi, I., Eds. *Combinatorial Materials Synthesis*; Marcel Dekker: New York, NY, 2003.

(24) Potyrailo, R. A., Amis, E. J., Eds. *High Throughput Analysis: A Tool for Combinatorial Materials Science*; Kluwer Academic/Plenum Publishers: New York, NY, 2003.

(25) Potyrailo, R. A., Karim, A., Wang, Q., Chikyow, T., Eds. *Combinatorial and Artificial Intelligence Methods in Materials Science II*; Materials Research Society: Warrendale, PA, 2004; Vol. 804.

(26) Potyrailo, R. A.; Takeuchi, I, Eds. Special Feature on Combinatorial and High-Throughput Materials Research; *Meas. Sci. Technol.*, **2005**; Vol. *16*.

(27) Birina, G. A.; Boitsov, K. A. *Zavod. Lab. (in Russ.)* **1974**, *40*, 855–857.

(28) Kennedy, K.; Stefansky, T.; Davy, G.; Zackay, V. F.; Parker, E. R. *J. Appl. Phys.* **1965**, *36*, 3808–3810.

(29) Hoffmann, R. *Angew. Chem., Int. Ed.* **2001**, *40*, 3337–3340.

(30) Anderson, F. W.; Moser, J. H. *Anal. Chem.* **1958**, *30*, 879–881.

(31) Eash, M. A.; Gohlke, R. S. *Anal. Chem.* **1962**, *34*, 713–713.

(32) Hanak, J. J. *J. Mater. Sci.* **1970**, *5*, 964–971.

(33) Xiang, X.-D.; Sun, X.; Briceño, G.; Lou, Y.; Wang, K.-A.; Chang, H.; Wallace-Freedman, W. G.; Chen, S.-W.; Schultz, P. G. *Science* **1995**, *268*, 1738–1740.

(34) Potyrailo, R. A.; Chisholm, B. J.; Olson, D. R.; Brennan, M. J.; Molaison, C. A. *Anal. Chem.* **2002**, *74*, 5105–5111.

(35) Potyrailo, R. A.; Chisholm, B. J.; Morris, W. G.; Cawse, J. N.; Flanagan, W. P.; Hassib, L.; Molaison, C. A.; Ezbiansky, K.; Medford, G.; Reitz, H. *J. Comb. Chem.* **2003**, *5*, 472–478.

(36) Potyrailo, R. A.; Olson, D. R.; Chisholm, B. J.; Brennan, M. J.; Lemmon, J. P.; Cawse, J. N.; Flanagan, W. P.; Shaffer, R. E.; Leib, T. K. High Throughput Analysis of Polymer Materials and Coatings. In *Analytical Tools For High Throughput Chemical Analysis and Combinatorial Materials Science*, Invited Symposium, The Pittsburgh Conference on Analytical Chemistry and Applied Spectroscopy, Inc.: Pittsburgh, PA, March 4−9, 2001.

(37) Potyrailo, R. A. "High-Throughput Experimentation In Early 21st Century: Searching For Materials Descriptors, Not For A Needle In The Haystack. Presented at the 6th DPI Workshop on Combinatorial and High-Throughput Approaches in Polymer Science, September 10−11, 2007.

(38) Jansen, M. *Angew. Chem., Int. Ed.* **2002**, *41*, 3746–3766.

(39) Cawse, J. *Acc. Chem. Res.* **2001**, *34*, 213–221.

(40) Göpel, W. *Sens. Actuators B* **1998**, *52*, 125–142.

(41) Harmon, L. *J. Mater. Sci.* **2003**, *38*, 4479–4485.

(42) Cawse, J. N., Ed. *Experimental Design for Combinatorial and High Throughput Materials Development*; Wiley-Interscience: Hoboken, NJ, 2003.

(43) Hendershot, R. J.; Benjamin Rogers, W.; Snively, C. M.; Ogunnaike, B. A.; Lauterbach, J. *Catal. Today* **2004**, *98*, 375–385.

(44) Castillo, F. A.; Sweeney, J.; Margl, P.; Zirk, W. *QSAR Comb. Sci.* **2005**, *24*, 38–44.

(45) Farrusseng, D.; Klanner, C.; Baumes, L.; Lengliz, M.; Mirodatos, C.; Schüth, F. *QSAR Comb. Sci.* **2005**, *24*, 78–93.

(46) MacLean, D.; Baldwin, J. J.; Ivanov, V. T.; Kato, Y.; Shaw, A.; Schneider, P.; Gordon, E. M. *J. Comb. Chem.* **2000**, *2*, 562–578.

(47) Potyrailo, R. A.; Takeuchi, I. *Meas. Sci. Technol.* **2005**, *16*, 1–4.

(48) Bever, M. B.; Duwez, P. E. *Mater. Sci. Eng.* **1972**, *10*, 1–8.

(49) Shen, M.; Bever, M. B. *J. Mater. Sci.* **1972**, *7*, 741–746.

(50) Ilschner, B. *J. Phys. IV* **1993**, *3*, 763–772.

(51) Pompe, W.; Worch, H.; Epple, M.; Friess, W.; Gelinsky, M.; Greil, P.; Hempel, U.; Scharnweber, D.; Schulte, K. *Mater. Sci. Eng., A* **2003**, *362*, 40–60.

(52) Kieback, B.; Neubrand, A.; Riedel, H. *Mater. Sci. Eng., A* **2003**, *362*, 81–105.

(53) 2001.

(54) Lombard, F. *Chemom. Intell. Lab. Syst.* **1997**, *37*, 281–289.

(55) Calvin, J. A. *Chemom. Intell. Lab. Syst.* **1997**, *37*, 291–294.

(56) Lyman, G. J. *Chemom. Intell. Lab. Syst.* **1997**, *37*, 295–297.

(57) Gremlich, H.-U. *Biotechnol. Bioeng. (Comb. Chem.)* **1998/1999**, *61*, 179–187.

(58) Swartz, M. E., Ed. *Analytical Techniques in Combinatorial Chemistry*; Marcel Dekker: New York, NY, 2000.

(59) Zhang, Y.; Gong, X.; Zhang, H.; Larock, R. C.; Yeung, E. S. *J. Comb. Chem.* **2000**, *2*, 450–452.

(60) Potyrailo, R. A. In *Fiber Optic Sensor Technology and Applications 2001*; Marcus, M. A., Culshaw, B., Eds.; Proceedings of SPIE-Int. Soc. Opt. Eng., SPIE − The International Society for Optical Engineering: Bellingham, WA, 2002; Vol. 4578, pp 366−377.

(61) Schmatloch, S.; Meier, M. A. R.; Schubert, U. S. *Macromol. Rapid Commun.* **2003**, *24*, 33–46.

(62) Booksh, K. S.; Kowalski, B. R. *Anal. Chem.* **1994**, *66*, 782A–791A.

(63) Potyrailo, R. A.; Wroczynski, R. J.; Lemmon, J. P.; Flanagan, W. P.; Siclovan, O. P. In *Analysis and Purification Methods in Combinatorial Chemistry*; Yan, B., Ed.; Wiley-Interscience: Hoboken, NJ, 2004; pp 87−123.

(64) Potyrailo, R. A.; Lemmon, J. P. Method for direct measurement of polycarbonate compositions by fluorescence. U.S. Patent 6,193,850, 2001.

(65) Potyrailo, R. A.; Lemmon, J. P.; Leib, T. K. *Anal. Chem.* **2003**, *75*, 4676–4681.

(66) Potyrailo, R. A.; Wroczynski, R. J.; Lemmon, J. P.; Flanagan, W. P.; Siclovan, O. P. *J. Comb. Chem.* **2003**, *5*, 8–17.

(67) Klein, J.; Stichert, W.; Strehlau, W.; Brenner, A.; Demuth, D.; Schunk, S. A.; Hibst, H.; Storck, S. *Catal. Today* **2003**, *81*, 329–335.

(68) Hahndorf, I.; Buyevskaya, O.; Langpape, M.; Grubert, G.; Kolf, S.; Guillon, E.; Baerns, M. *Chem. Eng. J.* **2002**, *89*, 119–125.

(69) Sanchez, E.; Kowalski, B. R. *J. Chemom.* **1988**, *2*, 265.

(70) Cohan, P. E. In *2002 COMBI—The 4th Annual International Symposium on Combinatorial Approaches for New Materials Discovery*; Knowledge Foundation: Arlington, VA, 2002.

(71) Meguro, S.; Lippmaa, M.; Ohnishi, T.; Chikyow, T.; Koinuma, H. *Appl. Surf. Sci.* **2006**, *252*, 2634–2639.

(72) Meguro, S.; Ohnishi, T.; Lippmaa, M.; Koinuma, H. *Meas. Sci. Technol.* **2005**, *16*, 309–316.

(73) Yen, C. H.; Shan, D.; Wong, H.; Jang, S. S. *Comput.-Aided Chem. Eng.* **2003**, *15*, 364–369.

(74) Corma, A.; Serra, J. M.; Serna, P.; Moliner, M. *J. Catal.* **2005**, *232*, 335–341.

(75) Watanabe, Y.; Umegaki, T.; Hashimoto, M.; Omata, K.; Yamada, M. *Catal. Today* **2004**, *89*, 455–464.

(76) Rodemerck, U.; Baerns, M.; Holena, M.; Wolf, D. *Appl. Surf. Sci.* **2004**, *223*, 168–174.

(77) Baumes, L.; Farrusseng, D.; Lengliz, M.; Mirodatos, C. *QSAR Comb. Sci.* **2004**, *23*, 767–778.

(78) Schüth, F.; Baumes, L.; Clerc, F.; Demuth, D.; Farrusseng, D.; Llamas-Galilea, J.; Klanner, C.; Klein, J.; Martinez-Joaristi, A.; Procelewska, J.; Saupe, M.; Schunk, S.; Schwickardi, M.; Strehlau, W.; Zech, T. *Catal. Today* **2006**, *117*, 284–290.

(79) Tan, P.-N.; Steinbach, M.; Kumar, V. *Introduction to Data Mining*; Addison-Wesley: Boston, MA, 2006.

(80) Bajorath, J. *Nat. Rev. Drug Discovery* **2002**, *11*, 882–894.

(81) Quakenbush, J. *Nat. Rev. Genet.* **2001**, *2*, 418.

(82) Lavine, B. K. *Anal. Chem.* **2000**, *72*, 91R–97R.

(83) Lavine, B. K.; Workman, J., Jr. *Anal. Chem.* **2002**, *74*, 2763–2770.

(84) Potyrailo, R. A. In *Encyclopedia of Materials: Science and Technology*; Buschow, K. H. J., Cahn, R. W., Flemings, M. C., Ilschner, B., Kramer, E. J., Mahajan, S., Eds.; Elsevier: Amsterdam, The Netherlands, 2001; Vol. 2, pp 1329−1343.

(85) Rajan, K.; Suh, C.; Rajagopalan, A.; Li, X. In *MRS Symposium Proceedings. Combinatorial and Artificial Intelligence Methods in Materials Science*; Takeuchi, I., Newsam, J. M., Wille, L. T., Koinuma, H., Amis, E. J., Eds.; Materials Research Society: Warrendale, PA, 2002; Vol. 700, pp 223−232.

(86) Singh, J.; Ator, M. A.; Jaeger, E. P.; Allen, M. P.; Whipple, D. A.; Soloweij, J. E.; Chowdhary, S.; Treasurywala, A. M. *J. Am. Chem. Soc.* **1996**, *118*, 1169–1679.

(87) Stanton, D. T.; Morris, T. W.; Roychoudhury, S.; Parker, C. N. *J. Chem. Inf. Comput. Sci.* **1999**, *39*, 21–27.

(88) Guessasma, S.; Montavon, G.; Coddet, C. In *MRS Symposium Proceedings. Combinatorial and Artificial Intelligence Methods in Materials Science*; Takeuchi, I., Newsam, J. M., Wille, L. T., Koinuma, H., Amis, E. J., Eds.; Materials Research Society: Warrendale, PA, 2002; Vol. 700, pp 253−258.

(89) Reynolds, C. H. *J. Comb. Chem.* **1999**, *1*, 297–306.

(90) Potyrailo, R. A.; McCloskey, P. J.; Wroczynski, R. J.; Morris, W. G. *Anal. Chem.* **2006**, *78*, 3090–3096.

(91) Potyrailo, R. A.; May, R. J.; Shaffer, R. E.; Lemmon, J. P.; Wroczynski, R. J. Method for high-throughput fluorescence screening of polymerization reactions. PCT Int. Appl. WO 02/33384 A1, 2002.

(92) Potyrailo, R. A.; May, R. J. *Rev. Sci. Instrum.* **2002**, *73*, 1277–1283.

(93) Yan, B.; Yan, H. *J. Comb. Chem.* **2001**, *3*, 78–84.

(94) Li, G.; Rosenthal, C.; Rabitz, H. *J. Phys. Chem. A* **2001**, *105*, 7765–7777.

(95) Beebe, K. R.; Pell, R. J.; Seasholtz, M. B. *Chemometrics: A Practical Guide*; Wiley: New York, NY, 1998.

(96) Otto, M. *Chemometrics: Statistics and Computer Application in Analytical Chemistry*; Wiley-VCH: Weinheim, Germany, 1999.

(97) Sieg, S. C.; Suh, C.; Schmidt, T.; Stukowski, M.; Rajan, K.; Maier, W. F. *QSAR Comb. Sci.* **2007**, *26*, 528–535.

(98) Sieg, S.; Stutz, B.; Schmidt, T.; Hamprecht, F.; Maier, W. F. *J. Mol. Model.* **2006**, *12*, 611–619.

(99) Frenzer, G.; Maier, W. F. *Annu. Rev. Mater. Res.* **2006**, *36*, 281–331.

(100) Frenzer, G.; Frantzen, A.; Sanders, D.; Simon, U.; Maier, W. F. *Sensors* **2006**, *6*, 1568–1586.

(101) Siemons, M.; Koplin, T. J.; Simon, U. *Appl. Surf. Sci.* **2007**, *254*, 669–676.

(102) Suh, C.; Sieg, S. C.; Heying, M. J.; Oliver, J.; Maier, W. F.; Rajan, K. *J. Comb. Chem.* **2009**, *11*, 385–392.

(103) Suh, C.; Rajan, K.; Vogel, B. M.; Eidelman, N.; Cabral, J. T.; Mallapragada, S.; Narasimhan, B. In *Combinatorial Materials Science*; Narasimhan, B., Mallapragada, S. K., Porter, M. D., Eds.; Wiley: Hoboken, NJ, 2007.

(104) Li, X.; Petersen, L.; Broderick, S.; Narasimhan, B.; Rajan, K. *ACS Combi. Sci.* **2011**10.1021/co100019d.

(105) Petersen, L. K.; Xue, L.; Wannemuehler, M. J.; Rajan, K.; Narasimhan, B. *Biomaterials* **2009**, *30*, 5131–5142.

(106) Schüth, F. *Chemie in unserer Zeit* **2006**, *40*, 92–103.

(107) Weitkamp, J.; Glaeser, R. In *Winnacker–Kuechler: Chemische Technik*; Dittmeyer, R., Keim, W., Kreysa, G., Oberholz, A., Eds.; Wiley-VCH: Weinheim, Germany, 2004; pp 645–718.

(108) Weitkamp, J. *Chem. Ing. Technol.* **2003**, *75*, 1529–1533.

(109) Röper, M. *Chem. Unserer Zeit* **2006**, *40*, 126–135.

(110) http://www.processnet.org/processnet_media/Sporleder/PosPap_AK_Hochdurchsatzforschung+_Druck_2010.pdf, 2009.

(111) Gasparini, G.; Dal Molin, M.; Prins, L. *Eur. J. Org. Chem.* **2010**, 2429–2440.

(112) Bercaw, J. E.; Day, M. W.; Golisz, S. R.; Hazari, N.; Henling, L. M.; Labinger, J. A.; Schofer, S. J.; Virgil, S. *Organometallics* **2009**, *28*, 5017–5024.

(113) Vriamont, N.; Govaerts, B.; Grenouillet, P.; de Bellefon, C.; Riant, O. *Chem.—Eur.J.* **2009**, *15*, 6267–6278.

(114) Lefort, L.; Boogers, J. A. F.; Kuilman, T.; Vijn, R. J.; Janssen, J.; Straatman, H.; de Vries, J. G.; de Vries, A. H. M. *Org. Process Res. Dev.* **2010**, *14*, 568–573.

(115) Goudriaan, P. E.; van Leeuwen, P. W. N. M.; Birkholz, M. N.; Reek, J. N. H. *Eur. J. Inorg. Chem.* **2008**, 2939–2958.

(116) Kolb, H. C.; Finn, M. G.; Sharpless, K. B. *Angew. Chem., Int. Ed.* **2001**, *40*, 2004–2021.

(117) Tornoe, C. W.; Meldal, M. *Pept., Proc. Second Int. Seventeenth Am. Pept. Symp.* **2001**, 263–264.

(118) Srinivasan, R.; Tan, L. P.; Wu, H.; Yang, P. Y.; Kalesh, K. A.; Yao, S. Q. *Org. Biomol. Chem.* **2009**, *7*, 1821–1828.

(119) Uttamchandani, M.; Lu, C. H. S.; Yao, S. Q. *Acc. Chem. Res.* **2009**, *42*, 1183–1192.

(120) Houghten, R. A. *Proc. Natl. Acad. Sci. U.S.A.* **1985**, *82*, 5131–5135.

(121) Geysen, H. M.; Meloen, R. H.; Barteling, S. J. *Proc. Natl. Acad. Sci. U.S.A.* **1984**, *81*, 3998–4002.

(122) Furka, A.; Sebestyen, F.; Asgedom, M.; Dibo, G. *Int. J. Pept. Protein Res.* **1991**, *37*, 487–493.

(123) Arai, T.; Yokoyama, N.; Yanagisawa, A. *Chem.—Eur. J.* **2008**, *14*, 2052–2059.

(124) Broussy, S.; Waldmann, H. *J. Comb. Chem.* **2007**, *9*, 1138–1143.

(125) Thomas, J. M.; Raja, R. *Acc. Chem. Res.* **2008**, *41*, 708–720.

(126) Maschmeyer, T.; Rey, F.; Sankar, G.; Thomas, J. M. *Nature* **1995**, *378*, 159–162.

(127) Malek, K.; Li, C.; van Santen, R. A. *J. Mol. Catal. A: Chem.* **2007**, *271*, 98–104.

(128) Malek, K.; Jansen, A. P. J.; Li, C.; van Santen, R. A. *J. Catal.* **2007**, *246*, 127–135.

(129) Fraile, J. M.; Garcia, J. I.; Herrerias, C. I.; Mayoral, J. A.; Pires, E. *Chem. Soc. Rev.* **2009**, *38*, 695–706.

(130) Niall, H. D. In *Methods in Enzymology, Part D: Enzyme Structure*; Hirs, H. W., Ed.; Academic Press: New York, NY, 1973; pp 942–1010.

(131) Youngquist, R. S.; Fuentes, G. R.; Lacey, M. P.; Keough, T. *J. Am. Chem. Soc.* **1995**, *117*, 3900–3906.

(132) Kuramochi, K.; Haruyama, T.; Takeuchi, R.; Sunoki, T.; Watanabe, M.; Oshige, M.; Kobayashi, S.; Sakaguchi, K.; Sugawara, F. *Bioconjugate Chem.* **2004**, *16*, 97–104.

(133) Shin, D. S.; Kim, Y. G.; Kim, E. M.; Kim, M.; Park, H. Y.; Kim, J. H.; Lee, B. S.; Kim, B. G.; Lee, Y. S. *J. Comb. Chem.* **2008**, *10*, 20–23.

(134) Maillard, N.; Darbre, T.; Reymond, J. L. *J. Comb. Chem.* **2009**, *11*, 667–675.

(135) Stanton, M. L.; Holcombe, J. A. *J. Comb. Chem.* **2007**, *9*, 359–365.

(136) Sakai, T.; Tsutsumi, Y.; Ema, T. *Green Chem.* **2008**, *10*, 337–341.

(137) Ramnarayanan, R.; Chan, B. C.; Salvitti, M. A.; Mallouk, T. E.; Falih, F. M.; Davis, J.; Galloway, D. B.; Bare, S. R.; Willis, R. R. *J. Comb. Chem.* **2006**, *8*, 199–212.

(138) Sun, Y.; Chan, B. C.; Ramnarayanan, R.; Leventry, W. M.; Mallouk, T. E.; Bare, S. R.; Willis, R. R. *J. Comb. Chem.* **2002**, *4*, 569–575.

(139) Farrusseng, D.; Clerc, F.; Mirodatos, C.; Azam, N.; Gilardoni, F.; Thybaut, J. W.; Balasubramaniam, P.; Marin, G. B. *Comb. Chem. High Throughput Screen.* **2007**, *10*, 85–97.

(140) Procelewska, J.; Galilea, J. L.; Clerc, F.; Farrusseng, D.; Schueth, F. *Comb. Chem. High Throughput Screen.* **2007**, *10*, 37–50.

(141) Serra, J. M.; Baumes, L. A.; Moliner, M.; Serna, P.; Corma, A. *Comb. Chem. High Throughput Screen.* **2007**, *10*, 13–24.

(142) Pereira Silva, R. M.; Clerc, F.; Farrusseng, D.; Cornelis, v. d. W. J.; Maschmeyer, T. *Comb. Chem. High Throughput Screen.* **2007**, *10*, 149–159.

(143) Schunk, S. A.; Sundermann, A.; Hibst, H. *Catal. Today* **2008**, *137*, 36–43.

(144) Schunk, S. A.; Sundermann, A.; Hibst, H. *Comb. Chem. High Throughput Screen.* **2007**, *10*, 51–57.

(145) Gobin, O. C.; Martinez Joaristi, A.; Schueth, F. *J. Catal.* **2007**, *252*, 205–214.

(146) Llamas-Galilea, J.; Gobin, O. C.; Schuth, F. *J. Comb. Chem.* **2009**, *11*, 907–913.

(147) Breuer, C.; Lucas, M.; Schutze, F.; Claus, P. *Comb. Chem. High Throughput Screen.* **2007**, *10*, 59–70.

(148) 2020 vision: The IEA puts a date on peak oil production. *The Economist* December, 10, **2009**. "Fatih Birol, the chief economist of the International Energy Agency (IEA), believes that if no big new discoveries are made, 'the output of conventional oil will peak in 2020 if oil demand grows on a business-as-usual basis.'"

(149) He, T.; Kreidler, E. *Phys. Chem. Chem. Phys.* **2008**, *10*, 3731–3738.

(150) He, T.; Kreidler, E.; Xiong, L.; Ding, E. *J. Power Sources* **2007**, *165*, 87–91.

(151) He, T.; Kreidler, E.; Xiong, L.; Ding, E. *ECS Trans.* **2007**, *2*, 13–20.

(152) Kreidler, E.; He, T. In *Catalytic Oxygen Electroreduction—Recent Developments and New Directions*; He, T., Ed.; Transworld Research Network: Trivandrum, Kerala, India, 2009; pp 63–90.

(153) Jeon, M. K.; Liu, J. H.; Lee, K. R.; Lee, J. W.; McGinn, P. J.; Woo, S. I. *Fuel Cells* **2010**, *10*, 93–98.

(154) Jeon, M. K.; Zhang, Y.; McGinn, P. J. *Electrochim. Acta* **2010**, *55*, 5318–5325.

(155) Cooper, J. S.; Zhang, Y.; McGinn, P. J. In *Catalytic Oxygen Electroreduction —Recent Developments and New Directions*; He, T., Ed.; Transworld Research Network: Trivandrum, Kerala, India, 2009; pp 47–62.

(156) Neyerlin, K. C.; Bugosh, G.; Forgie, R.; Liu, Z.; Strasser, P. *J. Electrochem. Soc.* **2009**, *156*, B363–B369.

(157) Greeley, J.; Norskov, J. K. *J. Phys. Chem. C* **2009**, *113*, 4932–4939.

(158) Jeon, M. K.; Cooper, J. S.; McGinn, P. J. *J. Power Sources* **2009**, *192*, 391–395.

(159) Jeon, M. K.; Cooper, J. S.; McGinn, P. J. *J. Power Sources* **2008**, *185*, 913–916.

(160) Gregoire, J. M.; Kostylev, M.; Tague, M. E.; Mutolo, P. F.; van Dover, R. B.; DiSalvo, F. J.; Abruna, H. D. *J. Electrochem. Soc.* **2009**, *156*, B160–B166.

(161) Strasser, P. *J. Comb. Chem.* **2008**, *10*, 216–224.

(162) Lee, K. R.; Jeon, M. K.; Woo, S. I. *Appl. Catal., B* **2009**, *91*, 428–433.

(163) Jeon, M. K.; McGinn, P. J. *J. Power Sources* **2009**, *194*, 737–745.

(164) Reddington, E.; Sapienza, A.; Gurau, B.; Viswanathan, R.; Sarangapani, S.; Smotkin, E. S.; Mallouk, T. E. *Science* **1998**, *280*, 1735–1737.

(165) Prochaska, M.; Jin, J.; Rochefort, D.; Zhuang, L.; DiSalvo, F. J.; Abruña, H. D.; van Dover, R. B. *Rev. Sci. Instrum.* **2006**, *77*, 054104.

(166) Welsch, F. G.; Stöwe, K.; Maier, W. F. *Catal. Today* **2011**, *159*, 108–119.

(167) Jiang, R. *Rev. Sci. Instrum.* **2007**, *78*, 072209.

(168) Debe, M. K.; Drube, A. R. *J. Vac. Sci. Technol. B.* **1995**, *13*, 1236–1241.

(169) Gancs, L.; Kobayashi, T.; Debe, M. K.; Atanasoski, R.; Wieckowsk, A. *Chem. Mater.* **2008**, *20*, 2444–2454.

(170) Garsuch, A.; Stevens, D. A.; Sanderson, R. J.; Wang, S.; Atanasoski, R. T.; Hendricks, S.; Debe, M. K.; Dahn, J. R. *J. Electrochem. Soc.* **2010**, *157*, B187–B194.

(171) Kafizas, A.; Parkin, I. P. *J. Mater. Chem.* **2010**, *20*, 2157–2169.

(172) Mills, A.; Wang, J.; McGrady, M. *J. Phys. Chem. B* **2006**, *110*, 18324–18331.

(173) Koinuma, H.; Itaka, K.; Matsumoto, Y.; Yoshida, Y.; Aikawa, S.; Takeuchi, K. *Top.Catal.* **2010**, *53*, 35–39.

(174) Seyler, M.; Stoewe, K.; Maier, W. F. *Appl. Catal., B* **2007**, *76*, 146–157.

(175) http://www.suschem.org/upl/3/default/doc/SusChem_brochure.pdf.

(176) Lee, W. S.; Kim, T. Y.; Woo, S. I. *Top.Catal.* **2010**, *53*, 123–128.

(177) Yaccato, K.; Carhart, R.; Hagemeyer, A.; Herrmann, M.; Lesik, A.; Strasser, P.; Volpe, A.; Turner, H.; Weinberg, H.; Grasselli, R. K.; Brooks, C. J.; Pigos, J. M. *Comb. Chem. High Throughput Screen.* **2010**, *13*, 318–330.

(178) Hagemeyer, A.; Lesik, A.; Streukens, G.; Volpe, A. F., Jr.; Turner, H. W.; Weinberg, W. H.; Yaccato, K.; Brooks, C. *Comb. Chem. High Throughput Screen.* **2007**, *10*, 135–147.

(179) Na, N.; Zhang, S.; Wang, X.; Zhang, X. *Anal. Chem.* **2009**, *81*, 2092–2097.

(180) Breysse, M.; Claudel, B.; Faure, L.; Guenin, M.; Williams, R. J. J.; Wolkenstein, T. *J. Catal.* **1976**, *45*, 137–144.

(181) Nakagawa, M.; Yamashita, N. *Springer Ser. Chem. Sens. Biosens.* **2005**, *3*, 93–132.

(182) Almasian, M. R.; Na, N.; Wen, F.; Zhang, S.; Zhang, X. *Anal. Chem.* **2010**, *82*, 3457–3459.

(183) Oh, K. S.; Woo, S. I. *Appl. Surf. Sci.* **2007**, *254*, 677–681.

(184) Ozturk, S.; Senkan, S. *Appl. Catal., B* **2002**, *38*, 243–248.

(185) Kern, P.; Klimczak, M.; Lucas, M.; Doering, A.; Claus, P. *Chem. Ing. Technol.* **2009**, *81*, 289–296.

(186) http://www.dieselnet.com/tech/dpf_regen.html (accessed August 14, 2011).

(187) Bachmann, M. Volkswagen AG; private communication, 2009.

(188) Olong, N. E.; Stoewe, K.; Maier, W. F. *Appl. Catal., B* **2007**, *74*, 19–25.

(189) Hensgen, L.; Stöwe, K. *Catal. Today* **2011**, *159*, 100–107.

(190) Oh, K. S.; Kim, D. K.; Maier, W. F.; Woo, S. I. *Comb. Chem. High Throughput Screen.* **2007**, *10*, 5–12.

(191) Onal, I.; Duezenli, D.; Seubsai, A.; Kahn, M.; Seker, E.; Senkan, S. *Top. Catal.* **2010**, *53*, 92–99.

(192) Hernandez-Pichardo, M. L.; Montoya, J. A.; del Angel, P.; Vargas, A.; Navarrete, J. *Appl. Catal., A* **2008**, *345*, 233–240.

(193) Barton, D. G.; Shtein, M.; Wilson, R. D.; Soled, S. L.; Iglesia, E. *J. Phys. Chem. B* **1999**, *103*, 630–640.

(194) Stoyanova, M.; Rodemerck, U.; Bentrup, U.; Dingerdissen, U.; Linke, D.; Mayer, R. W.; Lansink Rot-gerink, H. G. J.; Tacke, T. *Appl. Catal., A* **2008**, *340*, 242–249.

(195) Morra, G.; Farrusseng, D.; Guillon, E.; Morin, S.; Bouchy, C.; Duchene, P.; Mirodatos, C. *Catal. Today* **2008**, *137*, 71–79.

(196) Trapp, O.; Weber, S. K.; Bauch, S.; Baecker, T.; Hofstadt, W.; Spliethoff, B. *Chem.—Eur. J.* **2008**, *14*, 4657–4666.

(197) Trapp, O.; Weber, S. K.; Bauch, S.; Hofstadt, W. *Angew. Chem., Int. Ed.* **2007**, *46*, 7307–7310.

(198) Weber, S. K.; Bremer, S.; Trapp, O. *Chem. Eng. Sci.* **2010**, *65*, 2410–2416.

(199) Trapp, O. *J. Chromatogr. A* **2010**, *1217*, 1010–1016.

(200) Farrusseng, D. *Surf. Sci. Rep* **2008**, *63*, 487–513.

(201) Su, G.; Yan, B. *J. Comb. Chem.* **2010**, *12*, 215–221.

(202) Koyama, M.; Tsuboi, H.; Endou, A.; Takaba, H.; Kubo, M.; Del Carpio, C. A.; Miyamoto, A. *Comb. Chem. High Throughput Screen.* **2007**, *10*, 99–110.

(203) Zhao, J.-C., Ed. *Methods for Phase Diagram Determination*; Elsevier: The Boulevard, Langford Lane, Kidlington, Oxford OX5 1GB, UK, 2007.

(204) Ikeda, T. *Fundamentals of Piezoelectricity*; Oxford University Press: New York, NY, 1996.

(205) Saito, Y.; Takao, H.; Tani, T.; Nonomiya, T.; Takatori, K.; Homma, T.; Nagaya, T.; Nakamura, M. *Nature* **2004**, *432*, 84.

(206) Fujino, S.; Murakami, M.; Anbusathaiah, V.; Lim, S.-H.; Nagarajan, V.; Fennie, C.-J.; Wuttig, M.; Salamanca-Riba, L.; Takeuchi, I. *Appl. Phys. Lett.* **2008**, *92*, 202904.

(207) Catalan, G.; Scott, J. F. *Adv. Mater.* **2009**, *21*, 2463–2485.

(208) Murakami, M.; Fujino, S.; Lim, S.-H.; Salamanca-Riba, L.-S.; Wuttig, M.; Takeuchi, I.; Varughese, B.; Sugaya, H.; Hasegawa, T. *Appl. Phys. Lett.* **2006**, *88*, 112505.

(209) Cox, D. E.; Noheda, B.; Shirane, G.; Uesu, Y.; Fujishiro, K.; Yamada, Y. *Appl. Phys. Lett.* **2001**, *79*, 400.

(210) Suchomel, M. R.; Davies, P. K. *J. Appl. Phys.* **2004**, *96*, 4405.

(211) Grinberg, I.; Suchomel, M. R.; Davies, P. K.; Rappe, A. R. *J. Appl. Phys.* **2005**, *98*, 094111.

(212) Fukumura, T.; Ohtani, M.; Kawasaki, M.; Okimoto, Y.; Kageyama, T.; Koida, T.; Hasegawa, T.; Tokura, Y.; Koinuma, H. *Appl. Phys. Lett.* **2000**, *77*, 3426.

(213) Chang, K. S.; Aronova, M.; Famodu, O.; Takeuchi, I.; Lofland, S. E.; Hattrick-Simpers, J.; Chang, H. *Appl. Phys. Lett.* **2001**, *79*, 4411.

(214) Takeuchi, I.; Yang, W.; Chang, K.-S.; Aronova, M.; Vispute, R. D.; Venkatesan, T.; Bendersky, L. A. *J. Appl. Phys.* **2003**, *94*, 7336–7340.

(215) Takeuchi, I.; Yang, W.; Chang, K.-S.; Aronova, M.; Vispute, R. D.; Venkatesan, T.; Bendersky, L. A. *J. Appl. Phys.* **2004**, *95*, 3840.

(216) Chang, K.-S.; Aronova, M. A.; Lin, C.-L.; Murakami, M.; Yu, M.-H.; Hattrick-Simpers, J.; Famodu, O. O.; Lee, S. Y.; Ramesh, R.; Wuttig, M.; Takeuchi, I.; Gao, C.; Bendersky, L. *Appl. Phys. Lett.* **2004**, *84*, 3091.

(217) Nagarajan, V.; Stanishevsky, A.; Chen, L.; Zhao, T.; Liu, B.-T.; Melngailis, J.; Royburd, A. L.; Ramesh, R.; Finder, J.; Yu, Z.; Droopad, R.; Eisenbeiser, K. *Appl. Phys. Lett.* **2002**, *81*, 4215.

(218) Jin, Y. M.; Wang, Y. U.; Khachaturyan, A. G.; Li, J. F.; Viehland, D. *Phys. Rev. Lett.* **2003**, *91*, 197601.

(219) Kan, D.; Suchoski, R.; Fujino, S.; Takeuchi, I. *Integr. Ferroelectr.* **2009**, *111*, 116–124.

(220) Takahashi, R.; Kubota, H.; Murakami, M.; Yamamoto, Y.; Matsumoto, Y.; Koinuma, H. *J. Comb. Chem.* **2004**, *6*, 50–53.

(221) Kan, D.; Pálová, L.; Anbusathaiah, V.; Cheng, C. J.; Fujino, S.; Nagarajan, V.; Rabe, K. M.; Takeuchi, I. *Adv. Funct. Mater.* **2010**, *20*, 1108–1115.

(222) Cheng, C.-J.; Kan, D.; Lim, S.-H.; McKenzie, W. R.; Munroe, P. R.; Salamanca-Riba, L. G.; Withers, R. L.; Takeuchi, I.; Nagarajan, V. *Phys. Rev. B* **2009**, *80*, 014109.

(223) Levin, I.; Karimi, S.; Provenzano, V.; Dennis, C. L.; Wu, H.; Comyn, T. P.; Stevenson, T. J.; Smith, R. I.; Reaney, I. M. *Phys. Rev. B* **2010**, *81*, 020103.

(224) Jones, J. L.; Pramanick, A.; Daniels, J. E. *Appl. Phys. Lett.* **2008**, *93*, 152904.

(225) Otani, M.; Lowhorn, N. D.; Schenck, P. K.; Wong-Ng, W.; Green, M. L. *Appl. Phys. Lett.* **2007**, *91*, 132102.

(226) Otani, M.; Itaka, K.; Wong-Ng, W.; Schenck, P. K.; Koinuma, H. *Appl. Surf. Sci.* **2007**, *254*, 765.

(227) Otani, M.; Thomas, E. L.; Wong-Ng, W.; Schenck, P. K.; Chang, K.-S.; Lowhorn, N. D.; Green, M. L.; Ohguchi, H. *Jpn. J. Appl. Phys.* **2009**, *48*, No. 05EB02.

(228) Choo, J. O.; Adomaitis, R. A.; Henn-Lecordier, L.; Cai, Y.; Rubloff, G. W. *Rev. Sci. Instrum.* **2005**, *76*, 062217.

(229) Kukuruznyak, D.; Reichert, H.; Ohmori, K.; Ahmet, P.; Chikyow, T. *Adv. Mater.* **2008**, *20*, 3827–3831.

(230) Chang, K.-S.; Green, M. L.; Suele, J.; Vogel, E. M.; Xiong, H.; Hattrick-Simpers, J.; Takeuchi, I.; Famodu, O.; Ohmori, K.; Ahmet, P.; Chikyow, T.; Majhi, P.; Lee, B.-H.; Gardner, M. *Appl. Phys. Lett.* **2006**, *89*, 142108.

(231) Chang, K.-S.; Green, M. L.; Levin, I.; Hattrick-Simpers, J. R.; Jaye, C.; Fischer, D. A.; Takeuchi, I.; De Gendt, S. *Appl. Phys. Lett.* **2010**, *96*, 192114.

(232) International Technology Roadmap for Semiconductors 2003, http://public.itrs.net (accessed August 14, 2011).

(233) Aono, Y.; Sakurai, J.; Ishida, T.; Shimokohbe, A.; Hata, S. *Appl. Phys. Express* **2010**, *3*, 125601.

(234) Tsui, F.; Collins, B. A.; He, L.; Mellnik, A.; Zhong, Y.; Vogt, S.; Chu, Y. S. *Appl. Surf. Sci.* **2007**, *254*, 709–713.

(235) Takeuchi, I.; Long, C. J.; Famodu, O. O.; Murakami, M.; Hattrick-Simpers, J.; Rubloff, G. W. *Rev. Sci. Instrum.* **2005**, *76*, 062223.

(236) Long, C. J.; Hattrick-Simpers, J.; Murakami, M.; Srivastava, R. C.; Takeuchi, I.; Karen, V. L.; Li, X. *Rev. Sci. Instrum.* **2007**, *78*, 072217.

(237) Long, C. J.; Bunker, D.; Li, X.; Karen, V. L.; Takeuchi, I. *Rev. Sci. Instrum.* **2009**, *80*, 103902.

(238) Petculescu, G.; Hathaway, K. B.; Lograsso, T. A.; Wun-Fogle, M.; Clark, A. E. *J. Appl. Phys.* **2005**, *97*, 10M315.

(239) Sugiyama, M.; Oshima, R.; Fujita, F. E. *Mater. Trans., JIM* **1984**, *25*, 585.

(240) Koeda, J.; Nakamura, Y.; Fukuda, T.; Kakeshita, T.; Takeuchi, T.; Kishio, T. *Trans. Mater. Res. Soc. Jpn.* **2001**, *26*, 215.

(241) Lee, D. D.; Seung, H. S. *Nature* **1999**, *401*, 788.

(242) Shahnaz, F.; Berry, M. W.; Pauca, V. P.; Plemmons, R. J. *Inf. Process. Manage.* **2006**, *42*, 373.

(243) Piper, J.; Pauca, V. P.; Plemmons, R. J.; Giffin, M. Proceedings AMOS Technical Conference 2004, Maui, HI.

(244) Belsky, A.; Hellenbrandt, M.; Karen, V. L.; Luksch, P. *Acta Crystallogr. B: Struct. Sci.* **2002**, *58*, 364.

(245) NIST Standard Reference Data Program, Gaithersburg, MD, 20899.

(246) Pilcher, G. R. *J. Coat. Technol.* **2001**, *73*, 135–143.

(247) Chisholm, B. J.; Potyrailo, R. A.; Cawse, J. N.; Shaffer, R. E.; Brennan, M. J.; Moison, C.; Whisenhunt, D. W.; Flanagan, W. P.; Olson, D. R.; Akhave, J. R.; Saunders, D. L.; Mehrabi, A.; Licon, M. *Prog. Org. Coat.* **2002**, *45*, 313–321.

(248) Chisholm, B.; Webster, D.; Bennett, J.; Berry, M.; Christianson, D.; Kim, J.; Mayo, B.; Gubbins, N. *Rev. Sci. Instrum.* **2007**, *78*, 072213-072213–072213-072219.

(249) Webster, D.; Bennett, J.; Kuebler, S.; Kossuth, M.; Jonasdottir, S. *JCT CoatingsTech* **2004**, *1*, 34–39.

(250) Thaburet, J.; Mizomoto, H.; Bradley, M. *Macromol. Rapid Commun.* **2004**, *25*, 366–370.

(251) Wijnans, S.; deGans, B.; Wiesbrock, F.; Hoogenboom, R.; Schubert, U. *Macromol. Rapid Commun.* **2004**, *25*, 1958–1962.

(252) Potyrailo, R. A.; Ezbiansky, K.; Chisholm, B. J.; Morris, W. G.; Cawse, J. N.; Hassib, L.; Medford, G.; Reitz, H. *J. Comb. Chem.* **2005**, *7*, 190–196.

(253) Majumdar, P.; Christianson, D.; Webster, D. *Prog. Org. Coat.* **2006**, *57*, 210–214.

(254) He, J.; Bahr, J.; Chisholm, B.; Li, J.; Chen, Z.; Balbyshev, S.; Bonitz, V.; Bierwagen, G. *J. Comb. Chem.* **2008**, *10*, 704–713.

(255) Kossuth, M. B.; Hajduk, D. A.; Freitag, C.; Varni, J. *Macromol. Rapid Commun.* **2004**, *25*, 243–248.

(256) Stafslien, S. J.; Bahr, J. A.; Daniels, J. W.; Wal, L. V.; Nevins, J.; Smith, J.; Schiele, K.; Chisholm, B. *Rev. Sci. Instrum.* **2007**, *78*, No. 072204.

(257) Ribeiro, E.; Stafslien, S.; Casse, F.; Callow, J.; Callow, M.; Pieper, R.; Daniels, J.; Bahr, J.; Webster, D. *J. Comb. Chem.* **2008**, *10*, 586–594.

(258) Stafslien, S. J.; Daniels, J.; Mayo, B.; Christianson, D.; Chisholm, B.; Ekin, A.; Webster, D.; Swain, G. *Biofouling* **2007**, *23*, 45–54.

(259) Webster, D. C.; Chisholm, B. J.; Stafslien, S. J. *Biofouling* **2007**, *23*, 79–192.

(260) Rittschof, D.; Orihuela, B.; Stafslien, S.; Daniels, J.; Christianson, D.; Chisholm, B.; Holm, E. *Biofouling* **2008**, *24*, 1–9.

(261) Casse, F.; Stafslien, S.; Bahr, J.; Daniels, J.; Finlay, J.; Callow, J.; Callow, M. *Biofouling* **2007**, *23*, 121–130.

(262) Casse, F.; Ribeiro, E.; Ekin, A.; Webster, D.; Callow, J.; Callow, M. *Biofouling* **2007**, *23*, 267–276.

(263) Stafslien, S. J.; Bahr, J. A.; Feser, J. M.; Weisz, J. C.; Chisholm, B. J.; Ready, T. E.; Boudjouk, P. *J. Comb. Chem.* **2006**, *8*, 156–162.

(264) Stafslien, S.; Daniels, J.; Chisholm, B.; Christianson, D. *Biofouling* **2007**, *23*, 37–44.

(265) Roper, J.; Johnson, M.; Keefe, M.; Mecca, J.; Cesaretti, R. *Mater. Res. Soc. Symp. Proc.* **2009**, *1159*, 13–18.

(266) Vratsanos, L.; Rusak, M.; Rosar, K.; Everatt, T.; Listemann, M. *Proc. Athens Conf. Coat.: Sci. Technol.* **2001**, *27*, 435–442.

(267) Warren, O.; Wyrobek, T. *Meas. Sci. Technol.* **2005**, *16*, 100–110.

(268) Bach, H.; Gambino, C.; Gindin, L.; Konitnsey, R.; Lunney, P.; Spitler, K. *Proc. Am. Chem. Soc.; Polym. Prep.* **2003**, *44*, 70–71.

(269) Grunlan, J. C.; Mehrabi, A. R.; Chavira, A. T.; Nugent, A. B.; Saunders, D. L. *J. Comb. Chem.* **2003**, *5*, 362–368.

(270) Bach, H.; Gambino, C. A.; Lunney, P. D.; Wicks, D. A. In *High Throughput Analysis: A Tool for Combinatorial Materials Science*; Potyrailo, R. A., Amis, E. J., Eds.; Kluwer Academic/Plenum Publishers: New York, NY, 2003; Ch. 24, pp 525–549.

(271) Majumdar, P.; Webster, D. *Macromolecules* **2005**, *38*, 5857–5859.

(272) Ekin, A.; Webster, D. *J. Comb. Chem.* **2007**, *9*, 178–188.

(273) Majumdar, P.; Ekin, A.; Webster, D. *ACS Symp. Ser.* **2007**, *957*, 61–75.

(274) Majumdar, P.; Webster, D. *Polymer* **2006**, *47*, 4172–4181.

(275) Berglin, M.; Loenn, N.; Gatenholm, P. *Biofouling* **2003**, *19*, 63–69.

(276) Kohl, J.; Singer, I. *Prog. Org. Coat.* **1999**, *36*, 15–20.

(277) Majumdar, P.; Stafslien, S.; Daniels, J.; Webster, D. *J. Coat. Technol. Res.* **2007**, *4*, 131–138.

(278) Ekin, A.; Webster, D.; Daniels, J.; Stafslien, S.; Casse, F.; Callow, J.; Callow, M. *J. Coat. Technol. Res.* **2007**, *4*, 435–451.

(279) Ekin, A.; Webster, D. *J. Polym. Sci., Part A: Polym. Chem.* **2006**, *44*, 4880–4894.

(280) Ekin, A.; Webster, D. *Macromolecules* **2006**, *39*, 8659–8668.

(281) Finlay, J.; Callow, M.; Schultz, M.; Swain, G.; Callow, J. *Biofouling* **2002**, *18*, 251–256.

(282) Wicks, Z. W., Jr.; Jones, F. N.; Pappas, S. P. *Organic Coatings: Science and Technology*; Wiley: New York, NY, 1999.

(283) Pieper, R.; Ekin, A.; Webster, D.; Casse, F.; Callow, J.; Callow, M. *J. Coat. Technol. Res.* **2007**, *4*, 453–461.

(284) Majumdar, P.; Lee, E.; Patel, N.; Ward, K.; Stafslien, S. J.; Daniels, J.; Chisholm, B. J.; Boudjouk, P.; Callow, M.; Callow, J.; Thompson, S. E. *Biofouling* **2008**, *24*, 185–200.

(285) Majumdar, P.; Mayo, B.; Kim, J.; Gallagher-Lein, C.; Lee, E.; Gubbins, N.; Chisholm, B. *J. Coat. Technol. Res.* **2010**, *7*, 239–252.

(286) Majumdar, P.; Stafslien, S.; Daniels, J.; Lee, E.; Patel, N.; Gubbins, N.; Thorson, C.; Chisholm, B. *Ceram. Trans.* **2009**, *206*, 143–149.

(287) Ye, S.; McClelland, A.; Majumdar, P.; Stafslien, S.; Daniels, J.; Chisholm, B.; C., Z. *Langmuir* **2008**, *24*, 9686–9694.

(288) Majumdar, P.; Lee, E.; Patel, N.; Stafslien, S.; Daniels, J.; Chisholm, B. *J. Coat. Technol. Res.* **2008**, *5*, 405–417.

(289) Games, L. M.; King, J. E.; Larson, R. *Environ. Sci. Technol.* **1982**, *16*, 483–488.

(290) van Ginkel, C. G. *Chemosphere* **1991**, *23*, 281–289.

(291) Gottenbos, B.; Busscher, H. J.; van der Mei, H. C.; Nieuwenhuis, P. *J. Mater. Sci.: Mater. Med.* **2002**, *13*, 717–722.

(292) Nishihara, T.; Okamoto, T.; Nishiyama, N. *J. Appl. Microbiol.* **2000**, *88*, 641–647.

(293) Laopaiboon, L.; Hall, S. J.; Smith, R. N. *J. Appl. Microbiol.* **2002**, *93*, 1051–1058.

(294) Davies, A.; Bentley, M.; Field, B. S. *J. Appl. Bacteriol.* **1968**, *31*, 448–461.

(295) Juergensen, L.; Busnarda, J.; Caux, P.-Y.; Kent, R. A. *Environ. Toxicol.* **2000**, *15*, 174–200.

(296) Voulvoulis, N.; Scrimshaw, M.; Lester, J. *Chemosphere* **2002**, *47*, 789–785.

(297) Newby, B.-M. Z.; Chaudhury, M. K.; Brown, H. R. *Science* **1995**, *269*, 1407–1409.

(298) Moss, H.; Tebbs, S.; Faroqui, M.; Herbst, T.; Isaac, J.; Brown, J.; Elliott, T. J. *Eur. J. Anaesthesiol.* **2000**, *17*, 680–687.

(299) Stafslien, S.; Chishom, B.; Majumdar, P.; Bahr, J.; Daniels, J. *Ceram. Trans.* **2009**, *206*, 151–158.

(300) Majumdar, P.; Stafslien, S.; Daniels, J.; Lee, E.; Patel, N.; Gubbins, N.; Thorson, C.; Chishom, B. *Ceram. Trans.* **2009**, *206*, 143–149.

(301) Gottenbos, B.; Busscher, H.; van der Mei, H.; Nieuwenhuis, P. *J. Mater. Sci.: Mater. Med.* **2002**, *13*, 717–722.

(302) Majumdar, P.; Lee, E.; Gubbins, N.; Christianson, D.; Stafslien, S.; Daniels, J.; VanderWal, L.; Bahr, J.; Chisholm, B. *J. Comb. Chem.* **2009**, *11*, 1115–1127.

(303) Choi, S.; Jepperson, J.; Jarabek, L.; Thomas, J.; Chisholm, B.; Boudjouk, P. *Macromol. Symp.* **2007**, *249/250*, 660–667.

(304) Thomas, J.; Choi, S.; Fjeldheim, R.; Boudjouk, P. *Biofouling* **2004**, *20*, 227–236.

(305) Chisholm, B.; Christianson, D.; Stafslien, S.; Gubbins, N.; Daniels, J. *FutureCoat Proc.* **2006**, 006/001–006/026.

(306) Choi, S.; Jarabek, L.; Chisholm, B.; Boudjouk, P. *Polym. Preprints (Am. Chem. Soc., Div. Polym. Chem.)* **2007**, *48* (1), 141–142.

(307) Alam, S.; Chisholm, B. *Polym. Preprints (Am. Chem. Soc., Div. Polym. Chem.)* **2008**, *49* (1), 100–101.

(308) Chisholm, B.; Christianson, D.; Stafslien, S.; Gallaher-Lein, C.; Daniels, J. *ACS Symp. Ser.* **2009**, *1002*, 127–141.

(309) Schweizer, H. *FEMS Microbiol. Lett.* **2001**, *202*, 1–7.

(310) Kugel, A.; Jarabek, L.; Daniels, J.; Vander Wal, L.; Ebert, S.; Jepperson, M.; Stafslien, S.; Pieper, R.; Webster, D.; Bahr, J.; Chisholm, B. *J. Coat. Technol. Res.* **2009**, *6*, 107–121.

(311) Uhl, F.; Gallagher-Lein, C.; Christianson, D.; Bahr, J.; Chisholm, B.; Gubbins, N.; Webster, D. In *Combinatorial and High-Throughput Discovery and Optimization of Catalysts and Materials*; Potyrailo, R. A., Maier, W. F., Eds.; CRC Press: Boca Raton, FL, 2006, pp 221–238.

(312) Boey, F.; Rath, S.; Ng, A.; Abadie, M. *J. Appl. Polym. Sci.* **2002**, *86*, 518–525.

(313) Potyrailo, R. A.; Olson, D. R.; Medford, G. F.; Brennan, M. J. *Anal. Chem.* **2002**, *74*, 5676–5680.

(314) Chisholm, B.; Berry, M.; Bahr, J.; He, J.; Li, J.; Balbyshev, S.; Bierwagen, G. *J. Coat. Technol. Res.* **2010**, *7*, 23–37.

(315) Loy, D. *MRS Bull.* **2001**, *26*, 364–365.

(316) Lemmo, A. V.; Fisher, J. T.; Geysen, H. M.; Rose, D. J. *Anal. Chem.* **1997**, *69*, 543–551.

(317) Calvert, P. *Chem. Mater.* **2001**, *13*, 3299–3305.

(318) de Gans, B.-J.; Schubert, U. S. *Langmuir* **2004**, *20*, 7789–7793.

(319) Apostolidis, A.; Klimant, I.; Andrzejewski, D.; Wolfbeis, O. S. *J. Comb. Chem.* **2004**, *6*, 325–331.

(320) Hassib, L.; Potyrailo, R. A. *Polym. Prepr.* **2004**, *45*, 211–212.

(321) Scheidtmann, J.; Frantzen, A.; Frenzer, G.; Maier, W. F. *Meas. Sci. Technol.* **2005**, *16*, 119–127.

(322) Schena, M. *Microarray Analysis*; Wiley: Hoboken, NJ, 2003.

(323) Potyrailo, R. A.; Morris, W. G.; Wroczynski, R. J.; McCloskey, P. J. *J. Comb. Chem.* **2004**, *6*, 869–873.

(324) Mirsky, V. M.; Kulikov, V. In *High Throughput Analysis: A Tool for Combinatorial Materials Science*; Potyrailo, R. A., Amis, E. J., Eds.; Kluwer Academic/Plenum Publishers: New York, NY, 2003; Chapter 20, pp 431–446.

(325) Mirsky, V. M.; Kulikov, V.; Hao, Q.; Wolfbeis, O. S. *Macromol. Rapid Commun.* **2004**, *25*, 253–258.

(326) Taylor, C. J.; Semancik, S. *Chem. Mater.* **2002**, *14*, 1671–1677.

(327) Aronova, M. A.; Chang, K. S.; Takeuchi, I.; Jabs, H.; Westerheim, D.; Gonzalez-Martin, A.; Kim, J.; Lewis, B. *Appl. Phys. Lett.* **2003**, *83*, 1255–1257.

(328) Cawse, J. N.; Olson, D.; Chisholm, B. J.; Brennan, M.; Sun, T.; Flanagan, W.; Akhave, J.; Mehrabi, A.; Saunders, D. *Prog. Org. Coat.* **2003**, *47*, 128–135.

(329) Amis, E. J. *Nat. Mater.* **2004**, *3*, 83–85.

(330) Potyrailo, R. A.; Morris, W. G.; Leach, A. M.; Hassib, L.; Krishnan, K.; Surman, C.; Wroczynski, R.; Boyette, S.; Xiao, C.; Shrikhande, P.; Agree, A.; Cecconie, T. *Appl. Opt.* **2007**, *46*, 7007–7017.

(331) Yoon, J.; Jung, Y.-S.; Kim, J.-M. *Adv. Funct. Mater.* **2009**, *19*, 209–214.

(332) Dickinson, T. A.; Walt, D. R.; White, J.; Kauer, J. S. *Anal. Chem.* **1997**, *69*, 3413–3418.

(333) Potyrailo, R. A.; Wroczynski, R. J.; Pickett, J. E.; Rubinsztajn, M. *Macromol. Rapid Commun.* **2003**, *24*, 123–130.

(334) Potyrailo, R. A.; Szumlas, A. W.; Danielson, T. L.; Johnson, M.; Hieftje, G. M. *Meas. Sci. Technol.* **2005**, *16*, 235–241.

(335) Potyrailo, R. A.; Wroczynski, R. J. *Rev. Sci. Instrum.* **2005**, *76*, 062222.

(336) Potyrailo, R. A.; Olson, D. R.; Brennan, M. J.; Akhave, J. R.; Licon, M. A.; Mehrabi, A. R.; Saunders, D. L.; Chisholm, B. J. Systems and methods for the deposition and curing of coating compositions. U.S. Patent 6,544,334 B1, 2003.

(337) Potyrailo, R. A. *Polym. Mater. Sci. Eng., Polym. Prepr.* **2004**, *90*, 797–798.

(338) Potyrailo, R. A.; Hassib, L. *Rev. Sci. Instrum.* **2005**, *76*, 062225.

(339) Potyrailo, R. A.; Ding, Z.; Butts, M. D.; Genovese, S. E.; Deng, T. *IEEE Sensors J.* **2008**, *8*, 815–822.

(340) Bhat, R. R.; Tomlinson, M. R.; Genzer, J. *Macromol. Rapid Commun.* **2004**, *25*, 270–274.

(341) Turcu, F.; Hartwich, G.; Schäfer, D.; Schuhmann, W. *Macromol. Rapid Commun.* **2005**, *26*, 325–330.

(342) Sysoev, V. V.; Kiselev, I.; Frietsch, M.; Goschnick, J. *Sensors* **2004**, *4*, 37–46.

(343) Klingvall, R.; Lundström, I.; Löfdahl, M.; Eriksson, M. *IEEE Sensors J.* **2005**, *5*, 995–1003.

(344) Baker, B. E.; Kline, N. J.; Treado, P. J.; Natan, M. J. *J. Am. Chem. Soc.* **1996**, *118*, 8721–8722.

(345) Mills, A.; Lepre, A.; Wild, L. *Anal. Chim. Acta* **1998**, *362*, 193–202.

(346) Bedlek-Anslow, J. M.; Hubner, J. P.; Carroll, B. F.; Schanze, K. S. *Langmuir* **2000**, *16*, 9137–9141.

(347) Wang, J.; Musameh, M.; Lin, Y. *J. Am. Chem. Soc.* **2003**, *125*, 2408–2409.

(348) Potyrailo, R. A. Devices and methods for simultaneous measurement of transmission of vapors through a plurality of sheet materials. U.S. Patent 6,567,753 B2, 2003.

(349) Potyrailo, R. A.; Brennan, M. J. Method and apparatus for characterizing the barrier properties of members of combinatorial libraries. U.S. Patent 6,684,683(B2), 2004.

(350) Potyrailo, R. A. *Combinatorial Development and Accelerated Performance Testing of Polymers*; Second Dutch Polymer Institute workshop "High Throughput Experimentation/Combinatorial Material Research", May 15–16 2003; Eindhoven University of Technology: Eindhoven, the Netherlands, 2003.

(351) Chojnacki, P.; Werner, T.; Wolfbeis, O. S. *Microchim. Acta* **2004**, *147*, 87–92.

(352) Leclerc, M. *Adv. Mater.* **1999**, *11*, 1491–1498.

(353) McQuade, D. T.; Pullen, A. E.; Swager, T. M. *Chem. Rev.* **2000**, *100*, 2537–2574.

(354) Janata, J.; Josowicz, M. *Nat. Mater.* **2002**, *2*, 19–24.

(355) Dai, L.; Soundarrajan, P.; Kim, T. *Pure Appl. Chem.* **2002**, *74*, 1753–1772.

(356) Bobacka, J.; Ivaska, A.; Lewenstam, A. *Electroanalysis* **2003**, *15*, 366–374.

(357) Bidan, G. *Sens. Actuators B* **1992**, *6*, 45–56.

(358) Albert, K. J.; Lewis, N. S.; Schauer, C. L.; Sotzing, G. A.; Stitzel, S. E.; Vaid, T. P.; Walt, D. R. *Chem. Rev.* **2000**, *100*, 2595–2626.

(359) Gomez-Romero, P. *Adv. Mater.* **2001**, *13*, 163–174.

(360) Gill, I.; Ballesteros, A. *J. Am. Chem. Soc.* **1998**, *120*, 8587–8598.

(361) Gill, I. *Chem. Mater.* **2001**, *13*, 3404–3421.

(362) Barbero, C.; Acevedo, D. F.; Salavagione, H. J.; Miras, M. C. *Jornadas Sam/Conamet/Simposio Materia* **2003**, *2003*, C–12.

(363) Collaudin, A. B.; Blum, L. J. *Sens. Actuators B* **1997**, *38−39*, 189–194.

(364) Mills, A. *Sens. Actuators B* **1998**, *51*, 60–68.

(365) Eaton, K. *Sens. Actuators B* **2002**, *85*, 42–51.

(366) Papkovsky, D. B.; Ponomarev, G. V.; Trettnak, W.; O'Leary, P. *Anal. Chem.* **1995**, *67*, 4112–4117.

(367) Levitsky, I.; Krivoshlykov, S. G.; Grate, J. W. *Anal. Chem.* **2001**, *73*, 3441–3448.

(368) Florescu, M.; Katerkamp, A. *Sens. Actuators B* **2004**, *97*, 39–44.

(369) Basu, B. J.; Thirumurugan, A.; Dinesh, A. R.; Anandan, C.; Rajam, K. S. *Sens. Actuators B* **2005**, *104*, 15–22.

(370) Potyrailo, R. A.; Hassib, L. In *MACRO 2004—World Polymer Congress, the 40th IUPAC International Symposium on Macromolecules*, July 4−9; IUPAC: Paris, France, 2004.

(371) Potyrailo, R. A.; Hassib, L. In *Proceedings of TRANSDU-CERS'05, The 13th International Conference on Solid-State Sensors, Actuators and Microsystems*, Seoul, Korea, June 5−9, 2005; The Institute of Electrical and Electronics Engineers: New York, NY, 2005, pp 2099−2102.

(372) Potyrailo, R. A.; Morris, W. G.; Leach, A. M.; Sivavec, T. M.; Wisnudel, M. B.; Krishnan, K.; Surman, C.; Hassib, L.; Wroczynski, R.; Boyette, S.; Xiao, C.; Agree, A.; Cecconie, T. *Am. Lab.* **2007**, 32–35.

(373) Potyrailo, R. A.; Morris, W. G.; Wroczynski, R.; Hassib, L.; Miller, P.; Dworken, B.; Leach, A. M.; Boyette, S.; Xiao, C. *Sens. Actuators B* **2009**, *136*, 203–208.

(374) Potyrailo, R. A.; Morris, W. G.; Leach, A. M.; Sivavec, T. M.; Wisnudel, M. B.; Boyette, S. *Anal. Chem.* **2006**, *78*, 5893–5899.

(375) Hierlemann, A.; Weimar, U.; Kraus, G.; Schweizer-Berberich, M.; Göpel, W. *Sens. Actuators B* **1995**, *26*, 126–134.

(376) Potyrailo, R. A.; Sivavec, T. M. *Anal. Chem.* **2004**, *76*, 7023–7027.

(377) Wohltjen, H. In *Plenary talk at the 11th International Meeting on Chemical Sensors*, University of Brescia, Italy, July 16−19, 2006; Elsevier Science: Amsterdam, The Netherlands, 2006.

(378) Grate, J. W.; Abraham, H.; McGill, R. A. In *Handbook of Biosensors and Electronic Noses. Medicine, Food, and the Environment*; Kress-Rogers, E., Ed.; CRC Press: Boca Raton, FL, 1997, pp 593−612.

(379) Grate, J. W. *Chem. Rev.* **2000**, *100*, 2627–2648.

(380) Grate, J. W.; Abraham, M. H. *Sens. Actuators B* **1991**, *3*, 85–111.

(381) Abraham, M. H. *Chem. Soc. Rev.* **1993**, *22*, 73–83.

(382) Maranas, C. D. *Ind. Eng. Chem. Res.* **1996**, *35*, 3403–3414.

(383) Wise, B. M.; Gallagher, N. B.; Grate, J. W. *J. Chemometrics* **2003**, *17*, 463–469.

(384) Belmares, M.; Blanco, M.; Goddard, W. A., III; Ross, R. B.; Caldwell, G.; Chou, S.-H.; Pham, J.; Olofson, P. M.; Thomas, C. *J. Comput. Chem.* **2004**, *25*, 1814–1826.

(385) Potyrailo, R. A.; May, R. J.; Sivavec, T. M. *Sensor Lett.* **2004**, *2*, 31–36.

(386) Potyrailo, R. A.; Sivavec, T. M.; Bracco, A. A. In *Internal Standardization and Calibration Architectures for Chemical Sensors*, Proceedings of SPIE-Int. Soc. Opt. Eng; Shaffer, R. E., Potyrailo, R. A., Eds.; SPIE − The International Society for Optical Engineering: Bellingham, WA, 1999; Vol. 3856, pp 140−147.

(387) Sivavec, T. M.; Potyrailo, R. A. Polymer coatings for chemical sensors. U.S. Patent 6,357,278 B1, 2002.

(388) Potyrailo, R. A.; Morris, W. G.; Wroczynski, R. J. In *High Throughput Analysis: A Tool for Combinatorial Materials Science*; Potyrailo, R. A., Amis, E. J., Eds.; Kluwer Academic/Plenum Publishers: New York, NY, 2003; Chapter 11.

(389) Potyrailo, R. A.; Morris, W. G.; Wroczynski, R. J. *Rev. Sci. Instrum.* **2004**, *75*, 2177–2186.

(390) Ulmer, C. W., II; Smith, D. A.; Sumpter, B. G.; Noid, D. I. *Comput. Theor. Polym. Sci.* **1998**, *8*, 311–321.

(391) Potyrailo, R. A.; McCloskey, P. J.; Ramesh, N.; Surman, C. M. Sensor devices containing co-polymer substrates for analysis of chemical and biological species in water and air. U.S. Patent Application 2005133697, 2005.

(392) Potyrailo, R. A.; Morris, W. G. *Rev. Sci. Instrum.* **2007**, *78*, 072214.

(393) Lim, S.-H.; Raorane, D.; Satyanarayana, S.; Majumdar, A. *Sens. Actuators B* **2006**, *119*, 466–474.

(394) Raorane, D.; Lim, S.-H.; Majumdar, A. *Nano Lett.* **2008**, *8*, 2229–2235.

(395) Zemel, J. N. *Rev. Sci. Instrum.* **1990**, *61*, 1579–1606.

(396) Suzuki, H. *Electroanalysis* **2000**, *12*, 703–715.

(397) Wang, J. *Talanta* **2002**, *56*, 223–231.

(398) Hagleitner, C.; Hierlemann, A.; Brand, O.; Baltes, H. In *Sensors Update*, Vol. 11; Baltes, H., Göpel, W., Hesse, J., Eds.; VCH: Weinheim, Germany, 2002; pp 101−155.

(399) Hagleitner, C.; Hierlemann, A.; Brand, O.; Baltes, H. In *Sensors Update*, Vol. 12; Baltes, H., Göpel, W., Hesse, J., Eds.; VCH: Weinheim, Germany, 2003; pp 51−120.

(400) Kulikov, V.; Mirsky, V. M. *Meas. Sci. Technol.* **2004**, *15*, 49–54.

(401) Franke, M. E.; Koplin, T. J.; Simon, U. *Small* **2006**, *2*, 36–50.

(402) Korotcenkov, G. *Sens. Actuators B* **2005**, *107*, 209–232.

(403) Barsan, N.; Koziej, D.; Weimar, U. *Sens. Actuators B* **2007**, *121*, 18–35.

(404) Semancik, S. *Correlation of Chemisorption and Electronic Effects for Metal Oxide Interfaces: Transducing Principles for Temperature Programmed Gas Microsensors*; Final Technical Report Project Number: EMSP 65421, Grant Number: 07−98ER62709; U.S. Department of Energy Information Bridge: http://cfpub.epa.gov/si/si_public_record_Report.cfm?dirEntryID=25597, 2002 (accessed August 14, 2011).

(405) Semancik, S. In *Combinatorial Materials Synthesis*; Xiang, X.-D., Takeuchi, I., Eds.; Marcel Dekker: New York, NY, 2003; pp 263−295.

(406) Barsoukov, E.; Macdonald, J. R., Eds. *Impedance Spectroscopy: Theory, Experiment, and Applications*; 2 ed.; Wiley: Hoboken, NJ, 2005.

(407) Simon, U.; Sanders, D.; Jockel, J.; Heppel, C.; Brinz, T. *J. Comb. Chem.* **2002**, *4*, 511–515.

(408) Simon, U.; Sanders, D.; Jockel, J.; Brinz, T. *J. Comb. Chem.* **2005**, *7*, 682–687.

(409) Sanders, D.; Simon, U. *J. Comb. Chem.* **2007**, *9*, 53–61.

(410) Feldmann, C. *Scr. Materialia* **2001**, *44*, 2193–2196.

(411) Siemons, M.; Simon, U. *Sens. Actuators B* **2006**, *120*, 110–118.

(412) Siemons, M.; Simon, U. *Sens. Actuators B* **2007**, *126*, 595–603.

(413) Frantzen, A.; Sanders, D.; Scheidtmann, J.; Simon, U.; Maier, W. F. *QSAR Comb. Sci.* **2005**, *24*, 22–28.

(414) Potyrailo, R. A.; Surman, C.; Morris, W. G. *J. Comb. Chem.* **2009**, *11*, 598–603.

(415) Potyrailo, R. A.; Morris, W. G. *Anal. Chem.* **2007**, *79*, 45–51.

(416) Potyrailo, R. A.; Morris, W. G.; Sivavec, T.; Tomlinson, H. W.; Klensmeden, S.; Lindh, K. *Wireless Commun. Mobile Comput.* **2009**, *9*, 1318–1330.

(417) Potyrailo, R. A.; Surman, C.; Go, S.; Lee, Y.; Sivavec, T.; Morris, W. G. *J. Appl. Phys.* **2009**, *106*, 124902.

(418) Lundström, I.; Shivaraman, S.; Svensson, C.; Lundkvist, L. *Appl. Phys. Lett.* **1975**, *26*, 55–57.

(419) Lundström, I.; Svensson, C.; Spetz, A.; Sundgren, H.; Winquist, F. *Sens. Actuators B* **1993**, *13−14*, 16–23.

(420) Eriksson, M.; Klingvall, R.; Lundström, I. In *Combinatorial and High-Throughput Discovery and Optimization of Catalysts and Materials*; Potyrailo, R. A., Maier, W. F., Eds.; CRC Press: Boca Raton, FL, 2006; pp 85−95.

(421) Lundström, I.; Erlandsson, R.; Frykman, U.; Hedborg, E.; Spetz, A.; Sundgren, H.; Welin, S.; Winquist, F. *Nature* **1991**, *352*, 47–50.

(422) Löfdahl, M.; Eriksson, M.; Lundström, I. *Sens. Actuators B* **2000**, *70*, 77–82.

(423) Lundström, I.; Sundgren, H.; Winquist, F.; Eriksson, M.; Krantz-Rülcker, C.; Lloyd-Spetz, A. *Sens. Actuators B* **2007**, *121*, 247–262.

(424) Klingvall, R.; Lundstrom, I.; Lofdahl, M.; Eriksson, M. *Proc. IEEE Sensors* **2003**, *2*, 1114–1115.

(425) Eriksson, M.; Salomonsson, A.; Lundström, I.; Briand, D.; Åbom, A. E. *J. Appl. Phys.* **2005**, *98*, 034903.

(426) Park, J. B.; Bronzino, J. D. *Biomaterials: Principles and Applications*; CRC Press: Boca Raton, FL, 2003.

(427) Ratner, B. D. *Polym. Int.* **2007**, *56*, 1183–1185.

(428) Ratner, B. D.; Hoffman, A. S.; Schoen, F. J.; Lemons, J. E. *Biomaterials Science. An Introduction to Materials*; Elsevier: San Diego, CA, 2004.

(429) Fisher, O. Z.; Khademhosseini, A.; Langer, R.; Peppas, N. *Acc. Chem. Res.* **2010**, *43*, 419–428.

(430) Peng, H. T.; Shek, P. N. *Expert Rev. Med. Devices* **2010**, *7*, 639–659.

(431) International Organization for Standardization, www.iso.org. (accessed August 14, 2011)

(432) Inayat-Hussain, S.; Rajab, N. F.; Siew, E. L. In *Cellular Response to Biomaterials*; Di Silvio, L., Ed.; CRC Press & Woodhead Publishing: Cambridge, U.K., 2008; pp 508–557.

(433) ASTM F748-06 Standard Practice for Selecting Generic Biological Test Methods for Materials and Devices; http://www.fda.gov/MedicalDevices/DeviceRegulationandGuidance/GuidanceDocuments/ucm080735.htm http://www.astm.org/Standards/F748.htm, 2010.

(434) Biological Evaluation of Medical Devices Part 1: Evaluation and Testing; http://www.fda.gov/MedicalDevices/DeviceRegulationand Guidance/GuidanceDocuments/ucm080735.htm (accessed August 14, 2011).

(435) Meredith, J. C. *J. Mater. Chem.* **2009**, *19*, 34–45.

(436) Simon, C. G., Jr.; Yang, Y.; Thomas, V.; Dorsey, S. M.; Morgan, A. W. *Comb. Chem. High Throughput Screen.* **2009**, *12*, 544–553.

(437) Su, J.; Meredith, J. C. *Comb. Chem. High Throughput Screen.* **2009**, *12*, 626–633.

(438) Di Silvio, L., Ed. *Cellular Response to Biomaterials*; CRC Press & Woodhead Publishing: Cambridge, U.K., 2008.

(439) Mudera, V.; Cheema, U.; Shah, R.; Lewis, M. In *Cellular Response to Biomaterials*; Di Silvio, L., Ed.; CRC Press & Woodhead Publishing: Cambridge, U.K., 2008; pp 252–290.

(440) Scotchford, C. A. In *Cellular Response to Biomaterials*; Di Silvio, L., Ed.; CRC Press & Woodhead Publishing: Cambridge, U.K., 2008; pp 252–290.

(441) Wu, X.; Schultz, P. G. *J. Am. Chem. Soc.* **2009**, *131*, 12497–12515.

(442) Dolle, R. E.; Le Bourdonnec, B.; Goodman, A. J.; Morales, G. A.; Thomas, C. J.; Zhang, W. *J. Comb. Chem.* **2008**, *10*, 739–790.

(443) Dolle, R. E.; Le Bourdonnec, B.; Goodman, A. J.; Morales, G. A.; Thomas, C. J.; Zhang, W. *J. Comb. Chem.* **2009**, 739–790.

(444) Fernandes, T. G.; M., M. D.; Clark, D. S.; Dordick, J. S.; Cabral, J. M. S. *Trends Biotechnol.* **2009**, *27*, 343–346.

(445) Heinis, C.; Rutherford, T.; Freund, S.; Winter, G. *Nat. Chem. Biol.* **2009**, *5*, 502–507.

(446) Guo, P.; Coban, O.; Snead, N. M.; Trebley, J.; Hoeprich, S.; Guo, S.; Shu, Y. *Adv. Drug Delivery Rev.* **2010**, *62*, 650–666.

(447) Campolongo, M. J.; Tan, S. J.; Xu, J.; Luo, D. *Adv. Drug Delivery Rev.* **2010**, *62*, 606–616.

(448) Zelikin, A. N. *ACS Nano* **2010**, *4*, 2494–2509.

(449) Thorstenson, J. B.; Petersen, L. K.; Narasimhan, B. *J. Comb. Chem.* **2009**, *11*, 820–828.

(450) Conix, A. J. *Macromol. Syn.* **1966**, *2*, 95–99.

(451) Domb, A. J.; Langer, R. *J. Polym. Sci. A: Polym. Chem.* **1987**, *25*, 3373–3386.

(452) Kipper, M. J.; Shen, E.; Determan, A.; Narasimhan, B. *Biomaterials* **2002**, *23*, 4405–4412.

(453) Shen, E.; Pizsczek, R.; Dziadul, B.; Narasimhan, B. *Biomaterials* **2001**, *22*, 201–210.

(454) Meredith, J. C.; Karim, A.; Amis, E. J. *Macromolecules* **2000**, *33*, 5760–5762.

(455) Lin, N. J.; S., L.-G. *Biomaterials* **2009**, *30*, 4480–4487.

(456) Adler, A. F.; Petersen, L. K.; Wilson, J. H.; Torres, M. P.; Thorstenson, J. B.; Gardner, S. W.; Mallapragada, S. K.; Wannemuehler, M. J.; Narasimhan, B. *Comb. Chem. High Throughput Screen.* **2009**, *12*, 634–645.

(457) Hiemstra, C. A.; Zhong, L. J.; Dijkstra, Z.; Feijen, P. J. *Biomacromolecules* **2007**, *8*, 1548–1556.

(458) Hiemstra, C.; Zhong, Z.; van Steenbergen, M. J.; Hennink, W. E.; Feijen, J. *J. Controlled Release* **2007**, *122*, 71–78.

(459) Singh, A.; Suri, S.; Roy, K. *Biomaterials* **2009**, *30*, 5187–5200.

(460) Liu, E.; Treiser, M. D.; Patel, H.; Sung, H.; Roskov, K. E.; Kohn, J.; Becker, M. L.; Moghe, P. V. *Comb. Chem. High Throughput Screen.* **2009**, *12*, 646–655.

(461) Yang, F.; Mei, Y.; Langer, R.; Anderson, D. G. *Comb. Chem. High Throughput Screen.* **2009**, *12*, 554–561.

(462) Mei, Y.; Gerecht, S.; Taylor, M.; Urquhart, A. J.; Bogatyrev, S. R.; Cho, S.-W.; Davies, M. C.; Alexander, M. R.; Langer, R. S.; Anderson, D. G. *Adv. Mater.* **2009**, *21*, 2781–2786.

(463) Lovman, J.; Justesen, J.; Lauridsen, R. H.; Lovman, M.; Modin, C.; Bessenbacher, F.; Pedersen, F. S.; Duch, M. *Biomaterials* **2009**, *30*, 2015–2022.

(464) Ertl, G. *Angew. Chem., Int. Ed.* **1990**, *29*, 1219–1227.

(465) Li, G. Y. Highly active, air-stable combinatorial catalysts for the cross-coupling of aryl chlorides: the first homogeneous combinatorial catalysts for industrial applications. Presented at COMBI 2002—The 4th Annual International Symposium on Combinatorial Approaches for New Materials Discovery, January 23–25, 2002.

(466) Bricker, M. L.; Gillespie, R. D.; Holmgren, J. S.; Sachtler, J. W. A.; Willis, R. R. In *High Throughput Analysis: A Tool for Combinatorial Materials Science*; Potyrailo, R. A., Amis, E. J., Eds.; Kluwer Academic/Plenum Publishers: New York, NY, 2003; Chapter 26, pp 581–609.

(467) Spivack, J. L.; Webb, J.; Flanagan, W. P.; Sabourin, C.; May, R.; Hassib, L. In *Combinatorial and Artificial Intelligence Methods in Materials Science II*, MRS Symposium Proceedings; Potyrailo, R. A., Karim, A., Wang, Q., Chikyow, T., Eds.; Materials Research Society: Warrendale, PA, 2004; Vol. 804, pp 199–204.

(468) Spivack, J. L.; Cawse, J. N.; Whisenhunt, D. W., Jr.; Johnson, B. F.; Shalyaev, K. V.; Male, J.; Pressman, E. J.; Ofori, J.; Soloveichik, G.; Patel, B. P.; Chuck, T. L.; Smith, D. J.; Jordan, T. M.; Brennan, M. R.; Kilmer, R. J.; Williams, E. D. *Appl. Catal., A* **2003**, *254*, 5–25.

(469) Boussie, T. R.; Diamond, G. M.; Goh, C.; Hall, K. A.; LaPointe, A. M.; Leclerc, M.; Lund, C.; Murphy, V.; Shoemaker, J. A. W.; Tracht, U.; Turner, H.; Zhang, J.; Uno, T.; Rosen, R. K.; Stevens, J. C. *J. Am. Chem. Soc.* **2003**, *125*, 4306–4317.

(470) Archibald, B.; Brümmer, O.; Devenney, M.; Giaquinta, D. M.; Jandeleit, B.; Weinberg, W. H.; Weskamp, T. In *Handbook of Combinatorial Chemistry. Drugs, Catalysts, Materials*; Nicolaou, K. C., Hanko, R., Hartwig, W., Eds.; Wiley-VCH: Weinheim, Germany, 2002; Vol. 2, pp Chapter 34 pp 1017–1062.

(471) Potyrailo, R. A. *Polym. Prepr.* **2004**, *45*, 174–175.

(472) Lam, K. S.; Salmon, S.; Hersh, E.; Hruby, V. J.; Kazmierski, W. M.; Knapp, R. J. *Nature* **1991**, *354*, 82–84.

(473) Lai, R.; Kang, B. S.; Gavalas, G. R. *Angew. Chem., Int. Ed.* **2001**, *40*, 408–411.

(474) Chang, H.; Gao, C.; Takeuchi, I.; Yoo, Y.; Wang, J.; Schultz, P. G.; Xiang, X.-D.; Sharma, R. P.; Downes, M.; Venkatesan, T. *Appl. Phys. Lett.* **1998**, *72*, 2185–2187.

(475) Brocchini, S.; James, K.; Tangpasuthadol, V.; Kohn, J. *J. Am. Chem. Soc.* **1997**, *119*, 4553–4554.

(476) Briceño, G.; Chang, H.; Sun, X.; Schultz, P. G.; Xiang, X.-D. *Science* **1995**, *270*, 273–275.

(477) Ramirez, A. G.; Saha, R. *Appl. Phys. Lett.* **2004**, *85*, 5215–5217.

(478) Danielson, E.; Devenney, M.; Giaquinta, D. M.; Golden, J. H.; Haushalter, R. C.; McFarland, E. W.; Poojary, D. M.; Reaves, C. M.; Weinberg, W. H.; Wu, X. D. *Science* **1998**, *279*, 837–839.

(479) Jiang, R.; Rong, C.; Chu, D. *J. Comb. Chem.* **2005**, *7*, 272–278.

(480) Zhao, J.-C. *Adv. Eng. Mater.* **2001**, *3*, 143–147.

(481) Lemmon, J. P.; Manivannan, V.; Jordan, T.; Hassib, L.; Siclovan, O.; Othon, M.; Pilliod, M. In *Combinatorial and Artificial Intelligence Methods in Materials Science II*, MRS Symposium Proceedings; Potyrailo, R. A., Karim, A., Wang, Q., Chikyow, T., Eds.; Materials Research Society: Warrendale, PA, 2004; Vol. 804, pp 27−32.

(482) Olk, C. H. *Meas. Sci. Technol.* **2005**, *16*, 14–20.

(483) Hänsel, H.; Zettl, H.; Krausch, G.; Schmitz, C.; Kisselev, R.; Thelakkat, M.; Schmidt, H.-W. *Appl. Phys. Lett.* **2002**, *81*, 2106–2108.

(484) Zou, L.; Savvate'ev, V.; Booher, J.; Kim, C.-H.; Shinar, J. *Appl. Phys. Lett.* **2001**, *79*, 2282–2284.

(485) Takeuchi, I.; Famodu, O. O.; Read, J. C.; Aronova, M. A.; Chang, K.-S.; Craciunescu, C.; Lofland, S. E.; Wuttig, M.; Wellstood, F. C.; Knauss, L.; Orozco, A. *Nat. Mater.* **2003**, *2*, 180–184.

(486) Wicks, D. A.; Bach, H. *Proc. 29th Int. Waterborne, High-Solids, Powder Coat. Symp.* **2002**, *29*, 1–24.

(487) Cui, J.; Chu, Y. S.; Famodu, O. O.; Furuya, Y.; Hattrick-Simpers, J.; James, R. D.; Ludwig, A.; Thienhaus, S.; Wuttig, M.; Zhang, Z.; Takeuchi, I. *Nat. Mater.* **2006**, *5*, 286–290.

(488) Holzwarth, A.; Schmidt, H.-W.; Maier, W. *Angew. Chem., Int. Ed.* **1998**, *37*, 2644–2647.

(489) Cooper, A. C.; McAlexander, L. H.; Lee, D.-H.; Torres, M. T.; Crabtree, R. H. *J. Am. Chem. Soc.* **1998**, *120*, 9971–9972.

(490) Ekin, A.; Webster, D. C. *J. Comb. Chem.* **2007**, *9*, 178–188.

(491) Lemmon, J. P.; Wroczynski, R. J.; Whisenhunt, D. W., Jr.; Flanagan, W. P. *Polym. Prepr.* **2001**, *42*, 630–631.

(492) Szurdoki, F.; Ren, D.; Walt, D. R. *Anal. Chem.* **2000**, *72*, 5250–5257.

(493) Greeley, J.; Jaramillo, T. F.; Bonde, J.; Chorkendorff, I.; Nørskov, J. K. *Nat. Mater.* **2006**, *5*, 909–913.

(494) Frantzen, A.; Scheidtmann, J.; Frenzer, G.; Maier, W. F.; Jockel, J.; Brinz, T.; Sanders, D.; Simon, U. *Angew. Chem., Int. Ed.* **2004**, *43*, 752–754.

(495) Strasser, P.; Fan, Q.; Devenney, M.; Weinberg, W. H.; Liu, P.; Norskov, J. K. *J. Phys. Chem. B* **2003**, *107*, 11013–11021.

(496) Reetz, M. T.; Becker, M. H.; Kuhling, K. M.; Holzwarth, A. *Angew. Chem., Int. Ed.* **1998**, *37*, 2647–2650.

(497) Wong, D. W.; Robertson, G. H. *Adv. Exp. Med. Biol.* **1999**, *464*, 91–105.

(498) Luo, Y.; Ouyang, X.; Armstrong, R. W.; Murphy, M. M. *J. Org. Chem.* **1998**, *63*, 8719–8722.

(499) Cong, P.; Doolen, R. D.; Fan, Q.; Giaquinta, D. M.; Guan, S.; McFarland, E. W.; Poojary, D. M.; Self, K. W.; Turner, H. W.; Weinberg, W. H. *Angew. Chem. Int. Ed.* **1999**, *38*, 484–488.

(500) Lauterbach, J.; Snively, C. M.; Oskarsdottir, G. In *Combinatorial Approaches to Materials Development*; Malhotra, R., Ed.; American Chemical Society: Washington, DC, 2002; Vol. 814, pp 65−85.

(501) Fischer, M.; Tran, C. D. *Anal. Chem.* **1999**, *71*, 2255–2261.

(502) Senkan, S. M. *Nature* **1998**, *394*, 350–353.

(503) Taylor, S. J.; Morken, J. P. *Science* **1998**, *280*, 267–270.

(504) McFarland, E. W.; Weinberg, W. H. *Trends Biotechnol.* **1999**, *17*, 107–115.

(505) Su, H.; Yeung, E. S. *J. Am. Chem. Soc.* **2000**, *122*, 7422–7423.

(506) Stirn, P. J.; Hofelich, T. C.; Tamilarasan, R. R. In *Combinatorial and Artificial Intelligence Methods in Materials Science*, MRS Symposium Proceedings; Takeuchi, I., Newsam, J. M., Wille, L. T., Koinuma, H., Amis, E. J., Eds.; Materials Research Society: Warrendale, PA, 2002; Vol. 700, pp 145−150.

(507) Takahashi, R.; Matsumoto, Y.; Koinuma, H.; Lippmaa, M.; Kawasaki, M. In *Combinatorial and Artificial Intelligence Methods in Materials Science*, MRS Symposium Proceedings; Takeuchi, I., Newsam, J. M., Wille, L. T., Koinuma, H., Amis, E. J., Eds.; Materials Research Society: Warrendale, PA, 2002; Vol. 700, pp 13−18.

(508) Jaramillo, T. F.; Ivanovskaya, A.; McFarland, E. W. *J. Comb. Chem.* **2002**, *4*, 17–22.

(509) Potyrailo, R. A. Development of high throughput analysis infrastructure for combinatorial materials science applications. Presented at the Pittsburgh Conference on Analytical Chemistry and Applied Spectroscopy, March 17−22, 2002.

(510) Connolly, A. R.; Sutherland, J. D. *Angew. Chem., Int. Ed.* **2000**, *39*, 4268–4271.

(511) Potyrailo, R. A.; Pickett, J. E. *Angew. Chem., Int. Ed.* **2002**, *41*, 4230–4233.

(512) de Bellefon, C.; Tanchoux, N.; Caravieilhes, S.; Grenouillet, H., V. *Angew. Chem., Int. Ed.* **2000**, *39*, 3442–3445.

(513) Hoogenboom, R.; Fijten, M. W. M.; Brändli, C.; Schroer, J.; Schubert, U. S. *Macromol. Rapid Commun.* **2003**, *24*, 98–103.

(514) Neffati, R.; Alexeev, A.; Saunin, S.; Brokken-Zijp, J. C. M.; Wouters, D.; Schmatloch, S.; Schubert, U. S.; Loos, J. *Macromol. Rapid Commun.* **2003**, *24*, 113–117.

(515) Breit, B.; Seiche, W. *Angew. Chem., Int. Ed.* **2005**, *44*, 1640–1643.

(516) Debe, M. K. *NanoStructured Thin Film Catalysts (NSTFC) for Next Generation PEM Fuel Cells*; Northern Nano Workshop, November 9, 2006; University of Minnesota: Minneapolis, MN, 2006.

633

dx.doi.org/10.1021/co200007w |*ACS Comb. Sci.* 2011, 13, 579–633